

6-12-2019

# Environment Chamber for Shape-Memory Alloy Testing

Luis Acevedo

Joseph Bodo

Nicholas Fernandes

Follow this and additional works at: [https://scholarcommons.scu.edu/mech\\_senior](https://scholarcommons.scu.edu/mech_senior)

 Part of the [Mechanical Engineering Commons](#)

---

# SANTA CLARA UNIVERSITY

Department of Mechanical Engineering

Date: June 12, 2019

I HEREBY RECOMMEND THAT THE THESIS PREPARED  
UNDER MY SUPERVISION BY

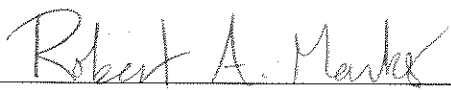
Luis Acevedo, Joseph Bodo, and Nicholas Fernandes

ENTITLED

## Environment Chamber for Shape-Memory Alloy Testing

BE ACCEPTED IN PARTIAL FULFILLMENT OF THE REQUIREMENTS  
FOR THE DEGREE OF

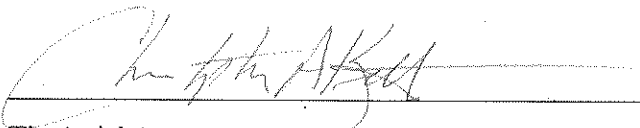
## BACHELOR OF SCIENCE IN MECHANICAL ENGINEERING



Thesis Advisor

6/12/19


Date



Thesis Advisor

6/12/19

Date



Department Chair

6/12/19

Date

ENVIRONMENT CHAMBER FOR SHAPE MEMORY  
ALLOY TESTING

By

Luis Acevedo, Joseph Bodo, and Nicholas Fernandes

**SENIOR THESIS**

Submitted in Partial Fulfillment of the Requirements for the  
Bachelor of Science Degree in  
Mechanical Engineering in the School of Engineering  
Santa Clara University, 2019

Santa Clara, California

## Abstract

The purpose of this project is to design, test, and build a temperature-controlled environment chamber to enable tensile testing of shape memory alloy (SMA) wire specimens at a temperatures ranging from 80-200°C. The most important design specifications were a maximum exterior wall temperature of 40°C and a maximum temperature variation along the specimen length of  $\pm 5^\circ\text{C}$ , with end users' ease-of-use considered. Hand calculations and iterative finite element analysis (FEA) simulations in SolidWorks were used to verify design choices before proceeding with sourcing parts and materials, and assembly. Real-world implementation of the system showed a heat-up time of roughly 25 minutes to 200°C (maximum operating temperature), with a maximum power consumption of 800 W, and with a wall temperature exceeding the safe threshold of 40°C only after 2 hours of continuous operation. The environment chamber and its accompanying hardware can be installed on a tensile testing machine and set up for use in under 10 minutes. Future work should entail heating wire specimens within the chamber and measuring the temperature variation along the specimen length, with the goal of achieving a maximum variation of  $\pm 5^\circ\text{C}$ . If this criterion is met, then the environment chamber can be used to proceed with tensile testing of the SMA specimens.

# Contents

<b>1</b>	<b>Introduction</b>	<b>1</b>
1.1	Background and Motivation . . . . .	1
1.2	Project Objective . . . . .	1
1.3	Review of Field and Academic Literature . . . . .	2
<b>2</b>	<b>Systems Level Overview</b>	<b>7</b>
2.1	Customer Needs . . . . .	7
2.2	System Sketches . . . . .	9
2.3	Functional Analysis . . . . .	12
2.4	Benchmarking . . . . .	14
2.5	Team and Project Management . . . . .	15
2.5.1	Design Process Organization and Timelines . . . . .	15
2.5.2	Challenges and Constraints . . . . .	16
2.5.3	Risks and Mitigation . . . . .	18
2.5.4	Budget and Expenditures . . . . .	19
2.6	Main Subsystems . . . . .	20
<b>3</b>	<b>Subsystem 1: Chamber Structure</b>	<b>21</b>
3.1	Finite Element Analysis . . . . .	21
3.1.1	First Design Iteration Simulations . . . . .	21
3.1.2	Unused Design Choices . . . . .	26
3.1.3	Final Design Iteration Simulations . . . . .	29
3.2	Manufacturing and Assembly . . . . .	37
<b>4</b>	<b>Subsystem 2: Mounting Hardware</b>	<b>42</b>
4.1	Base . . . . .	42
4.2	Grips and Fixturing . . . . .	45
<b>5</b>	<b>Subsystem 3: Thermal Control System</b>	<b>51</b>
<b>6</b>	<b>System Integration, Tests, and Results</b>	<b>54</b>
<b>7</b>	<b>Cost Analysis</b>	<b>59</b>

<b>8 Business Plan</b>	<b>61</b>
8.1 Introduction . . . . .	61
8.2 The Company . . . . .	61
8.3 Services . . . . .	61
8.4 Market Analysis/Competition . . . . .	62
8.5 Manufacturing Plans . . . . .	62
8.6 Cost and Price . . . . .	63
8.7 Service or Warranties . . . . .	63
8.8 Conclusion . . . . .	63
<b>9 Engineering Standards and Realistic Constraints</b>	<b>64</b>
9.1 Economic . . . . .	64
9.2 Environmental . . . . .	64
9.3 Sustainability . . . . .	64
9.4 Health and Safety . . . . .	65
9.5 Manufacturability . . . . .	65
<b>10 Summary and Conclusions</b>	<b>67</b>
10.1 Overall Evaluation of Design . . . . .	67
10.2 Future Work . . . . .	67
10.3 Lessons Learned . . . . .	68
<b>References</b>	<b>69</b>
<b>Appendix A: Hand Calculations</b>	<b>74</b>
<b>Appendix B: Parts and Assembly Drawings</b>	<b>80</b>
<b>Appendix C: Thermal Simulations</b>	<b>102</b>
<b>Appendix D: SMA Compositional Analysis</b>	<b>106</b>
<b>Appendix E: Subsystem Concept Scoring</b>	<b>108</b>
<b>Appendix F: Project Timelines</b>	<b>111</b>
<b>Appendix G: SMA Tensile Testing</b>	<b>114</b>

Appendix H: Using the Controller	116
Appendix I: Design Conference Presentation Slides	119

# List of Figures

1	Optical micrographs of a Cu-Al-Ni shape memory alloy: (a) as-cast, (b) solution annealed, (c) tempered at 150°C and at (d) 300°C. Produced by Ivanić et al. [4]. Reproduced without permission. . . . .	2
2	Illustration of microstructure change associated with the shape memory effect. Reproduced from ASTM Standard E3098-17 [5] without permission.	3
3	Optical micrographs of a Cu-Al-Ni shape memory allow showing (a) large grains and (b) precipitate formation. Produced by Suru et al. [3]. Reproduced without permission. . . . .	5
4	Concept sketch of top-down cross-section view of the tube chamber. . . .	10
5	Concept sketch of side cross-section view of chamber. . . . .	11
6	First design iteration of environment chamber, conceptual model. Quarter-section cut-out, with grips and specimen shown. . . . .	12
7	Final design iteration of environment chamber. Shown in full view with a hinge, and half-section with grips and specimen. . . . .	12
8	Temperature distribution along cross-section of chamber, before iteration. Temperature ranged from 63-368°C. . . . .	22
9	Temperature distribution along cross-section of chamber. Temperature ranged from 33-382°C. . . . .	23
10	Temperature distribution along length of specimen. Temperature ranged from 33-388°C. . . . .	24
11	Close-up of temperature distribution in insulation. Temperature ranged from 33-388°C. . . . .	24
12	Cross-section view showing mesh elements. Temperature ranged from 33-388°C. . . . .	25
13	Mesh refinement along specimen and heating elements. Temperature ranged from 33-388°C. . . . .	25
14	Cross-section view from above of temperature distribution. Temperature ranged from 33-388°C. . . . .	26
15	Temperature distribution of all components of the box design. Temperature ranged from 54-432°C. . . . .	27



16	CAD model of a double-pane ceramic glass window, to permit optical extensometry. Not included in final design due to high cost, poor manufacturability, and safety concerns. . . . .	28
17	Top-down view of temperature distribution with a window included (left side). Unsafe peak wall temperature of approximately 150°C. Temperature ranged from about 87-251°C. . . . .	29
18	Half of chamber CAD model, with silicone rubber seal shown, insulation underneath (not visible). . . . .	30
19	Half of chamber CAD model, insulation and silicone rubber hidden, stand-offs shown. . . . .	30
20	Power resistor mounts. Nuts and washers support resistors. . . . .	31
21	Fully assembled environment chamber. . . . .	31
22	Expected temperature distribution of the chamber. Temperatures range from 28-249°C. . . . .	33
23	Expected temperature distribution from the inner to outer walls of the chamber. Temperatures range from 28-249°C. . . . .	34
24	Expected temperature distribution of the specimen. Temperatures range from 28-249°C. . . . .	35
25	Expected temperature distribution of the grips. Temperatures range from 28-249°C. . . . .	36
26	Chamber structure before insulation was inserted. Silicone rubber washers (made with a punch) were placed between ceramic standoffs and aluminum end caps to allow for some compression due to thermal expansion. . . . .	38
27	Chamber structure with insulation inserted and silicone rubber seals being applied. . . . .	39
28	Silicone rubber sheets compressed with the latches to provide a tight seal. . . . .	40
29	Completed environment chamber hooked up to the controller and power supply. . . . .	40
30	CAD model for the chamber base. . . . .	42
31	Final base assembly. . . . .	43

32	Expected displacement in the base due to carrying the weight of the chamber (43 lb). Displacement ranged from the order of $10^{-32}$ in. to 0.02856 in. . . . .	44
33	Expected strains in the base due to carrying the weight of the chamber (43 lb). Strain ranged from the order of $10^{-13}$ to 0.0002243. . . . .	44
34	Expected von Mises stresses in the base due to carrying the weight of the chamber (43 lb). Stress ranged from the order of $10^{-6}$ psi to 4,320 psi. . .	45
35	Instron machine mount point. Cylindrical grips are inserted and pinned into place. . . . .	46
36	MTS machine mount point. Cylindrical threaded grips are screwed into place. . . . .	46
37	Prototype collet grip - disassembled. . . . .	46
38	Prototype collet grip - assembled. . . . .	47
39	Large tool holders for 2 mm and 5 mm wires. . . . .	47
40	Machined adapters for large tool holders, prior to welding and finishing. Work was performed by our sponsor Digital Loggers, Inc. . . . .	48
41	Completed specimen fixturing for the Instron machine. An adapter, tool holder, and collet are used to grip narrow wire specimens of 2 mm or 5 mm diameter. . . . .	48
42	CAD model for the threaded grip. Full model (top) and cross section view showing depth of UNF 10-32 threaded hole (bottom) . . . . .	49
43	Grip fitment with specimen. . . . .	49
44	Grip fitment with the Instron mount (upper mount point, connected to the load cell). . . . .	50
45	Grips and specimen installed with the environment chamber. . . . .	50
46	Basic system diagram. . . . .	52
47	Diagram of control system. . . . .	53
48	Experimental protocol used to organize and plan out all performance and safety validation tests to be conducted. . . . .	54
49	Summary of measurements and test results compared against all design specifications. The only criterion not tested for, due to time limitations, was the temperature variation along the length of a specimen. . . . .	55

50	Gain iteration plots of the PID tuning tests. . . . .	57
51	Sketch of furnace for hand calculations. . . . .	74
52	Sketch of control volume calculation for heat loss from escaping air. . . .	78
53	Spreadsheet used for natural convection coefficient calculations [29]. . . .	79
54	Drawing of a chamber assembly half. . . . .	80
55	Drawing of the inner chamber frame. . . . .	81
56	Drawing of the outer chamber frame. . . . .	84
57	Drawing of the 10 in. OD pipe split in half. . . . .	85
58	Drawing of aluminum end cap for the outer wall. . . . .	86
59	Drawing of the end cap for the inner wall. . . . .	87
60	Drawing of the 6 in. OD pipe split in half. . . . .	88
61	Drawing of base assembly. . . . .	89
62	Drawing of the leg assembly. . . . .	92
63	Drawing of the base plate assembly. . . . .	94
64	Drawing of the brackets used to fix the chamber. . . . .	97
65	Drawing of tube used for the base legs. . . . .	98
66	Drawing of the plates used at the ends of the legs. . . . .	99
67	Drawing of the gusset used for the legs. . . . .	100
68	Drawing of the threaded grip. . . . .	101
69	Plot of temperature distribution along specimen length, from the mid-length (Location 0) to one end (Location 3). . . . .	102
70	Insulation temperature variation. Probed from the heating element contact point (Location 0) to the outer wall contact point (Location 20). . . . .	103
71	Temperature variation from heating element (Location 0) to outside edge of chamber (Location 52). . . . .	103
72	Temperature distribution plot from the inner wall (Location 0) to the outer wall (Location 7) of the chamber. . . . .	104
73	Temperature distribution plot of the specimen from mid-length (Location 0) to one end (Location 6). . . . .	104
74	Temperature distribution plot along the length of the grip. Probed from the specimen contact point (Location 0) to the protruding end (Location 15). . . . .	105

75	EDS spectrum showing composition (by weight percent) of the Cu-Al-Ni SMA. Provided by A. Kim, S. Snyder, R. Marks, J. Taylor, and R. Konrath. Reproduced with permission. . . . .	107
76	Detailed scoring matrix showing the considered options for the chamber geometry. . . . .	108
77	Detailed scoring matrix showing the considered options for insulation materials. . . . .	109
78	Detailed scoring matrix showing the considered options for the heating elements. . . . .	109
79	Detailed scoring matrix showing the considered options for the specimen fixturing. . . . .	110
80	Initial Gantt chart showing project timeline and tasks for the duration of the project. . . . .	111
81	Revised Gantt chart for the winter quarter. . . . .	112
82	Revised Gantt chart for the spring quarter, also showing key assignments and Senior Design course-related deadlines. . . . .	112
83	Task dependency flowchart used to aid in organizing order and progression of tasks for the project. . . . .	113
84	$\frac{L_o}{A_o}$ vs. $\frac{1}{m}$ plot of the refined data from room temperature tensile testing, used to determine the elastic modulus of the SMA. . . . .	115
85	Controller and power supply switched on but not supplying power to the chamber. . . . .	118

## List of Tables

1	Summary of key end user needs for the design of the environment chamber.	7
2	Summary of key specifications and proposed design solutions. . . . .	8
3	Comparison of environment chambers and tube furnaces currently on the market [16, 17, 18, 19]. . . . .	14
4	Breakdown of all project expenditures (including parts/components that did not make it into the final implementation of the environment chamber) Note: oil bath materials were used to heat up SMA specimens to test for transition temperatures. . . . .	19
5	Convection coefficients used in updated model. . . . .	32
6	Radiation parameters used in updated model. . . . .	32
7	PID tuning test data. Note: Test 1 was conducted with a setpoint of 100°C, all other test setpoints were 200°C. . . . .	57
8	Performance validation test data. Note: Test 1 was conducted without access to the grips and load cell in the Materials Laboratory. . . . .	58
9	Breakdown of costs of purchased parts and materials that went into the finished environment chamber. . . . .	59
10	Breakdown of costs of sponsored parts and materials. . . . .	59
11	Heater power and resultant estimated heating element temperature. . . .	77

# Acknowledgements

## **Project Advisors**

Dr. Robert Marks, Department of Mechanical Engineering

Dr. Christopher Kitts, Department of Mechanical Engineering, Robotics Systems  
Laboratory - Director

## **Deep Sea Research Project**

Dr. C. Geoffrey Wheat, University of Alaska Fairbanks & Monterey Bay Aquarium  
Research Institute

Camden Webb, Rachel Stolzman, Ann McGuire

## **Shape Memory Alloy Compositional Analysis**

Dr. Ashley Kim, Santa Clara University Center for Nanostructures - Director

Shaun Snyder, Santa Clara University Center for Nanostructures - Laboratory Manager

Jake Taylor, Ryan Konrath

## **Santa Clara University School of Engineering**

Dr. Panthea Sepehrband, Department of Mechanical Engineering

Dr. Timothy Hight, Department of Mechanical Engineering

Dr. Gaetano Restivo, Department of Mechanical Engineering

## **Santa Clara University Machine Shop**

Don MacCubbin, Calvin Sellers

Emily Takimoto, Bethany Hsu

## **Project Sponsor**

Digital Loggers, Inc.

# 1 Introduction

## 1.1 Background and Motivation

The purpose of this project is to assist the joint research venture between marine geochemist Dr. C. Geoffrey Wheat and Dr. Christopher Kitts — the director of the Robotics Systems Laboratory here at Santa Clara University — in their efforts to study life at the seafloor. Of chief interest to them are boreholes drilled into the seafloor off the coast of Chile, where temperatures can range from 60-200°C, due to natural geothermal temperature gradients, and there exists the potential for life to survive in these conditions [1]. Dr. Wheat is interested in collecting water samples within Borehole 504B, specifically. One major challenge that water sampling devices would face under the high temperatures and pressures found in such boreholes is failure of conventional electronics. In order to actuate a sampling mechanism reliably, a solid-state actuator is ideal; this can be accomplished by using shape memory alloys (SMA). They have found that commonly available SMA are not suitable for this application, and thus there exists a need for testing to be performed on novel SMA blends at elevated temperatures, in order to identify suitable options for the design of an actuator for this application. The properties to be considered for SMA in this application are yield strength, maximum recoverable strain, transition temperature, and force exerted during shape recovery.

## 1.2 Project Objective

The Santa Clara University Materials Laboratory is well-equipped to perform all but the latter of these tests; Instron 4502 and MTS Landmark testing machines provide capability for tensile and compressive tests governed by displacement rate or stress rate, as well as hysteresis tests. A simple oil bath and hot plate can be used to determine the transition temperatures of SMA. However, measurement of the force exerted during transformation is currently not possible with the existing equipment in the Materials Laboratory; in order to conduct these tests, an environment chamber is required. Our objective for this project is to satisfy that need, by constructing an environment chamber to allow for materials testing to be conducted at elevated temperatures on the Instron and MTS

machines, with particular focus on enabling further research of SMA blends to assist Dr. Wheat and Dr. Kitts' project.

### 1.3 Review of Field and Academic Literature

Shape memory alloys are alloys that “remember” the shape they held prior to experiencing deformation. This is possible due to a reversible martensitic phase transformation, wherein deformation distorts the twinned martensite phase that is dominant at relatively low temperatures, along the twin boundaries [2, 3]. When the SMA is heated up to a critical temperature, commonly referred to as the “transition” temperature, its microstructure transforms to austenite while reverting back to the original shape, thus achieving full recovery of inelastic strain [2, 3]. Following shape recovery and upon cooling down, the microstructure reverts back to the twinned martensite seen prior to deformation. Ivanić et al. [4] produced optical micrographs (see Figure 1) showing this twinned martensite arrangement, which manifests as needle-like regions of differing orientations, during their study of a Cu-Al-Ni SMA.

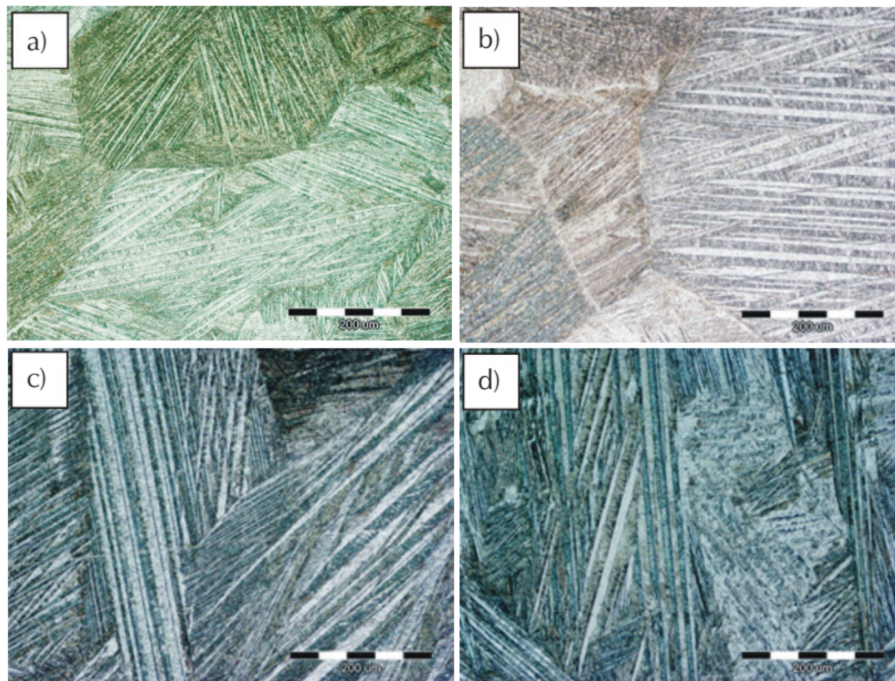


Figure 1: Optical micrographs of a Cu-Al-Ni shape memory alloy: (a) as-cast, (b) solution annealed, (c) tempered at 150°C and at (d) 300°C. Produced by Ivanić et al. [4]. Reproduced without permission.



Figure 2 illustrates this relationship between temperature and strain. Start and finish temperatures denote, respectively, the temperatures at which the alloy microstructure initiates and completes a transformation into a different phase. The austenite start temperature is  $A_s$ , and the finish temperature is  $A_f$ . The martensite start temperature is denoted by  $M_s$ , and the finish temperature by  $M_f$ . Of primary concern for our application is the range between  $A_s$  and  $A_f$ , henceforth referred to as the transition temperature of the SMA; it is at this point during the heating process that strain is recovered and the SMA returns to its undeformed shape.

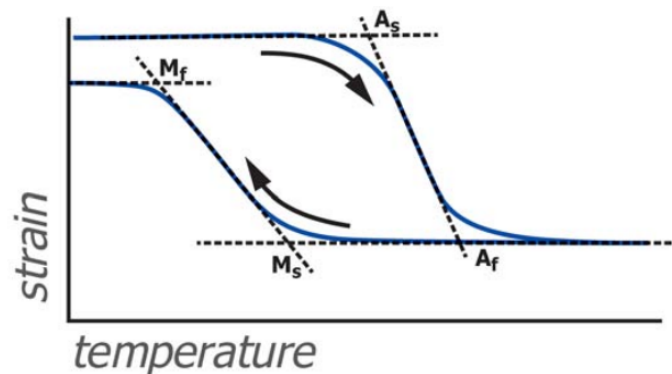


Figure 2: Illustration of microstructure change associated with the shape memory effect. Reproduced from ASTM Standard E3098-17 [5] without permission.

This mode of shape recovery described thus far is known as the “shape memory effect” (SME) [2]. When inelastic strain is recovered by unloading the SMA at isothermal condition (at a temperature above  $A_f$ ), this phenomenon is called “superelasticity” [2].

SMA are very commonly used in actuators [6], as an alternative to hydraulic, pneumatic, or motor-driven components. Typically, these alloys are used in environments in which the operating temperatures will trigger changes in their microstructures, or they are controlled using an electric current to drive temperature-influenced shape change.

SMA also see more novel use in a wide variety of areas, from “smart” building structures [7] to advanced prosthetics [2]. For instance, some of the most innovative emerging applications include using SMA plates to cushion fractured bones [2], and embedding SMA capsules in beams and support structures to induce “self-healing” of structural damage by reversing deformation [7].

The current academic literature on the subject shows a field undergoing constant growth and innovation. Some of the major recent or ongoing developments in the study of SMA include:

- Introducing additional alloying elements to develop new alloy blends, in order to modify shape memory behavior and mechanical properties [8]
- Developing modeling methods for predicting SMA behavior in underwater actuator applications [9]
- Creating intermediate activation temperatures and phase changes through thermal cycling and strain treatments [10]
- Raising alloy activation temperatures and increasing yield strength and hardness through severe plastic deformation [11]
- Designing “multiple inputs-single accumulated output” linear actuators using SMA wires [12]

SMA fall into two major categories, based on their main alloying elements: Ni-Ti and Cu-based (most commonly Cu-Al-Ni). Dr. Wheat is seeking to use Cu-based alloys because their typical activation temperatures are more in line with the expected environmental conditions the water sampling devices will be exposed to [8]. While Ni-Ti SMA see the most commercial usage, they tend to have a very limited range of transition temperatures, typically up to 120°C [11]. Further, Ni-Ti SMA are much more expensive. There is an increasing demand to develop SMA with higher transition temperatures at a lower cost, which makes Cu-based SMA more appealing.

Dr. Wheat has procured SMA specimens of 71.9 at% Cu, 23.9 at% Al, 4.2 at% Ni (see Appendix D: SMA Compositional Analysis for full details on how the alloy composition was determined) for further study, in order to evaluate their suitability for use in the water sampling device.

Cu-based SMA present their own shortcomings, however, most notably low ductility and poor mechanical strength, due to large grain sizes and high elastic anisotropy, which have been found to magnify stress concentrations at grain boundaries [11, 13]. This is especially true for Cu-Al-Ni blends, which are markedly prone to intergranular crack pro-

pogation, leading to brittle fracture during martensitic transformations [14] (i.e., during deformation). As a result, it is quite rare to see this class of SMA recover large strains via the shape memory effect or superelasticity [14]. Research has shown that grain size can be reduced, and consequently also the propensity for brittle fracture, by introducing Mn as a quaternary alloying element [13]. Another significant weakness of Cu-Al-Ni SMA is the tendency to develop Cu-rich precipitates through thermal cycling that erode martensite, harden the alloy, and ultimately hinder the martensitic transformations that are critical to the SME, thus degrading the thermoelastic properties of the SMA [3]. Analysis of a Cu-Al-Ni SMA by Suru et al. [3] produced optical micrographs (see Figure 3) showing the large grains and precipitate formation characteristic of this class of SMA.

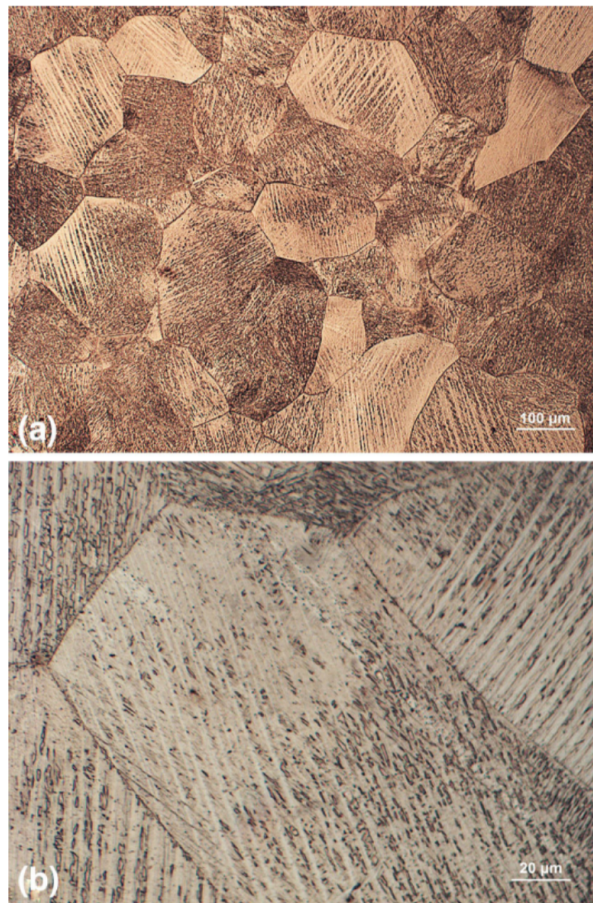


Figure 3: Optical micrographs of a Cu-Al-Ni shape memory alloy showing (a) large grains and (b) precipitate formation. Produced by Suru et al. [3]. Reproduced without permission.

Looking towards future testing of the alloys, we consulted ASTM standards for recom-

mended methods and procedures for assessing SMA characteristics. ASTM Standard E3098-17 provides a test method for heating and cooling of SMA specimens after enduring uniaxial tensile strain, which can be used to determine the residual strain after loading/unloading, the recovered strain after heating, the unrecovered strain after cooling, and the transition temperatures [5]. Consideration of ASTM E3098-17 is important to the design of our environment chamber because the standardized procedure specified will be carried out when using the finished chamber for SMA testing. Temperature uniformity is paramount, and thus the chamber must accommodate multiple temperature-sensing devices to probe for temperatures at different areas along the SMA specimen. Either crosshead position or extensometry may be used to provide strain data, as per the standard; as such, implementing a window into the final design of the chamber to allow for extensometry would be ideal, but not strictly necessary.

## 2 Systems Level Overview

### 2.1 Customer Needs

During the Fall Quarter, we met with potential end users for the environment chamber, in order to identify the key needs they wanted addressed in the design. The most important needs are summarized in Table 1 below.

Table 1: Summary of key end user needs for the design of the environment chamber.

<b>End User</b>	<b>Feedback</b>
Dr. Robert Marks	<ul style="list-style-type: none"><li>- Chamber should interface with Instron and MTS testing machines in the Materials Laboratory</li><li>- Height of the chamber should be at least 2-3x typical specimen length</li><li>- Design and fabrication of grips for 2-5 mm diameter wire specimens</li><li>- Specimens should be heated evenly and consistently</li></ul>
Dr. C. Geoffrey Wheat & Dr. Christopher Kitts	<ul style="list-style-type: none"><li>- Chamber should heat up to at least 180°C to cover range of desired SMA transition temperatures</li><li>- Testing should provide consistent and repeatable results</li></ul>
Dr. Panthea Sepehrband	<ul style="list-style-type: none"><li>- Design for ease of use, particularly for installing/removing specimens</li><li>- Minimize temperature variation along specimen length</li><li>- Chamber should be suited for smaller specimens, easier to provide even heating</li></ul>

Combining this qualitative feedback with the SMA testing objectives, we were able to organize a preliminary list of key design specifications for this project.

Table 2: Summary of key specifications and proposed design solutions.

Area of Concern	Design specifications	Solution
Chamber structure, shape, and dimensions	<ul style="list-style-type: none"> <li>- Max width = 15 in. (constrained by machine dimensions)</li> <li>- No max. height limit</li> <li>- Height must be min. 2x test specimen length</li> <li>- Must be freestanding, add no extra weight to load cell</li> </ul>	<ul style="list-style-type: none"> <li>- Cylindrical chamber with 10 in. OD and 24 in. height</li> <li>- Base to support freestanding chamber</li> <li>- Material: Aluminum (lightweight, machinable, good strength-to-weight ratio)</li> </ul>
Operating Temperature	<ul style="list-style-type: none"> <li>- Test at temp. range of 80-180°C</li> <li>- Should not operate at max. heating capacity during tests (safety, reduce power usage)</li> </ul>	<ul style="list-style-type: none"> <li>- Design for max. operating temp. of 200-250°C</li> <li>- Resistive heating elements (affordable)</li> </ul>
Insulation	<ul style="list-style-type: none"> <li>- Max. outer surface temp. of 40°C (safety)</li> </ul>	<ul style="list-style-type: none"> <li>- 2-3 in. thick ceramic fiber for insulation</li> </ul>
Temperature Regulation	<ul style="list-style-type: none"> <li>- Maintain a stable specimen temp. at desired set-point</li> <li>- Minimize temp. variation along specimen length, ensure reliable results</li> </ul>	<ul style="list-style-type: none"> <li>- PID controller for temp. and power regulation</li> <li>- Thermocouples for temp. measurements and controller input</li> <li>- Max. temp. variation along specimen length of <math>\pm 5^\circ\text{C}</math></li> </ul>
Grips/Fixturing	<ul style="list-style-type: none"> <li>- Must be compatible with Instron (pinned) and MTS (threaded) mounting hardware</li> <li>- Must secure wire specimens of 2 or 5 mm diam.</li> <li>- Must support up to 5 kN (load cell capacity)</li> </ul>	<ul style="list-style-type: none"> <li>- Purchase collets for small diam. specimens, fabricate fixtures to affix collets to testing machines</li> <li>- Fabricate threaded grips for securing specimens to testing machines</li> <li>- Material: Steel (durable, high strength, machinable)</li> </ul>

After reviewing the information provided, making the heated environment chamber as universally compatible as possible was a top priority. This would make it more broadly useful for professors and student researchers who have access to different tensile machines. Even though the focus of this project was more research-orientated (as opposed to product design-oriented), making the chamber able to interface with multiple machines at a low cost could make it appealing to potential consumers, thus giving an avenue to pursue

turning it into a product in the future.

Additionally, having a control system that maintains the chamber's inner temperature at up to 200-250°C was an equally key priority. The chamber must be able to maintain this temperature, consistently and with a high degree of accuracy. It must also heat the specimen evenly, to ensure reliable experimental data.

Designing and fabricating appropriate specimen grips was also necessary. Testing wire specimens only a few mm thick introduces complications with properly securing them during tests and with ensuring tensile failure does not occur at the point of contact with the grips. We decided to purchase and test a set of collets (and make custom adapters so they could be pinned to the Instron machines mounting points) to see if they could grip the specimens under tensile load, before proceeding with designing a custom pair of grips to address this need.

## **2.2 System Sketches**

In order to maintain as even an internal temperature distribution, we decided to design a cylindrical chamber, due to its ideal radial symmetry. As this was a key design criterion, we accepted this trade-off even though manufacturing a box-shaped chamber would have been simpler and less costly. Various concepts and component choices were considered (details in Appendix E: Subsystem Concept Scoring).

We initially planned to run thick Nichrome wires along the inner wall to heat the chamber interior (AWG 4-8, to give an approximate range). Nichrome is a commonly available and affordable choice for resistive heating wires. A concept sketch of this desired radial symmetry and the wire heating elements is shown in Figure 4.

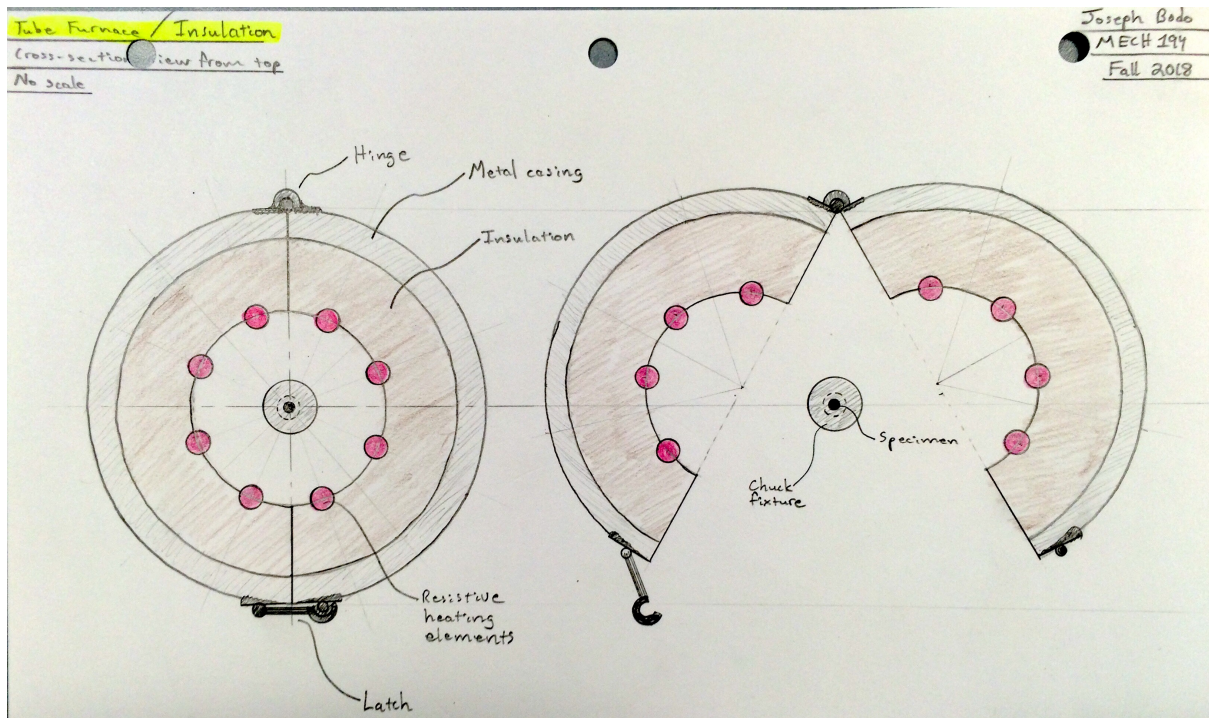


Figure 4: Concept sketch of top-down cross-section view of the tube chamber.

Figure 5 is a concept sketch depicting the setup for the environment chamber, except for the base on which it would rest. A user would be able to sit the chamber on its base, pass grips through the top and bottom (between which the specimen is affixed), and then pass thermocouples through an opening or port in the chamber in order to take temperature measurements. These thermocouples connect to a nearby user-adjustable controller, which would provide temperature and power regulation. This system-level concept served as our baseline for further developing the design of the chamber into its final iteration and implementation.



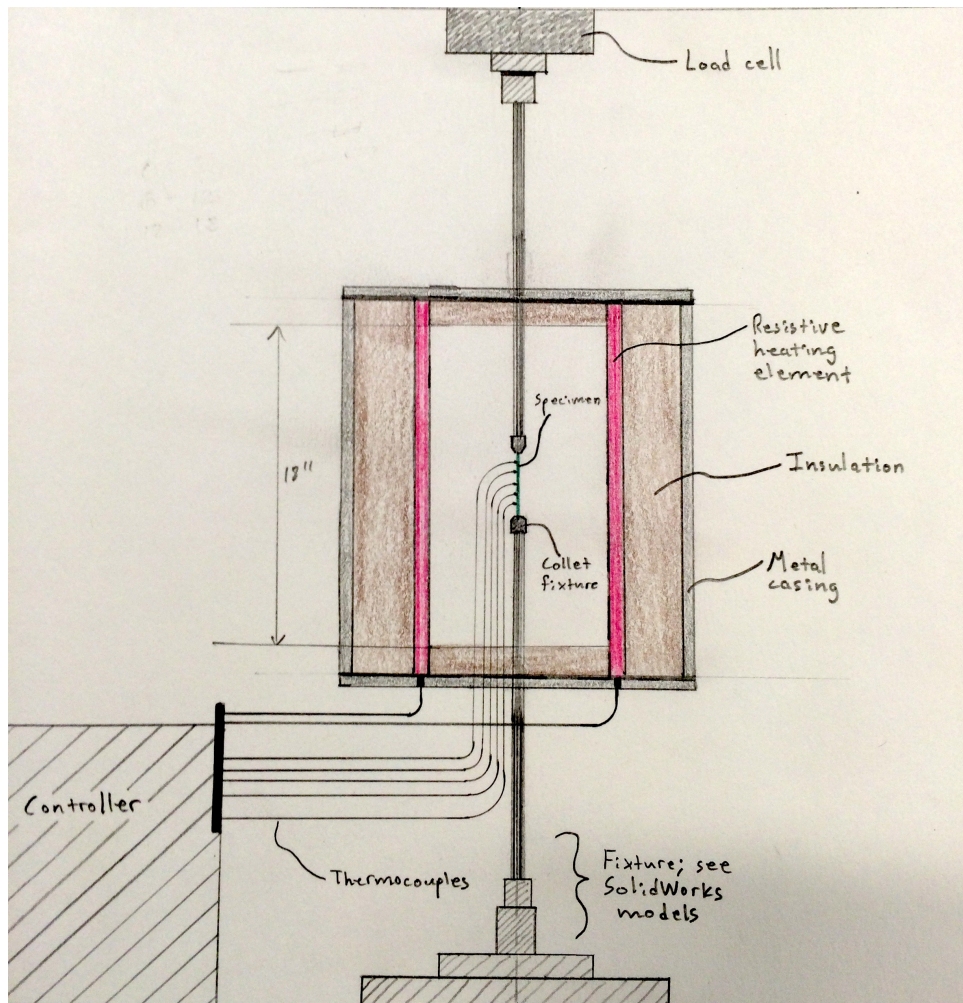


Figure 5: Concept sketch of side cross-section view of chamber.

The flat bed of the Instron 4502 testing machine provides an area of 16 in. by 8.5 in. with threaded holes for bolting down hardware, thus giving enough area to accommodate a 10 in. diameter chamber with a stand that can be bolted to the testing machine.

We then turned to computer-aided design (CAD) to develop a 3D model in SolidWorks for this initial concept review phase (see Figure 6), which was then expanded and iterated upon over the course of the Fall and Winter Quarters. We arrived at the final iteration of the chamber design, pictured in Figure 7, after a series of revisions demanded by safety requirements, production cost and time concerns, and a focus on manufacturability. Full details on thermal simulations, the manufacturing and assembly process, and performance validation of the final chamber design can be found in Section 3: Subsystem 1: Chamber Structure and Section 6: System Integration, Tests, and Results.

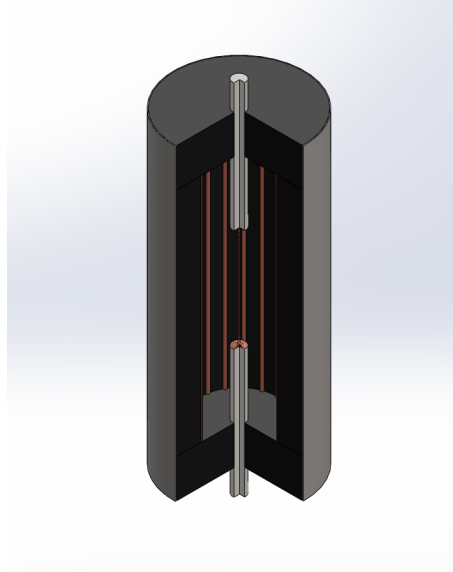


Figure 6: First design iteration of environment chamber, conceptual model. Quarter-section cut-out, with grips and specimen shown.

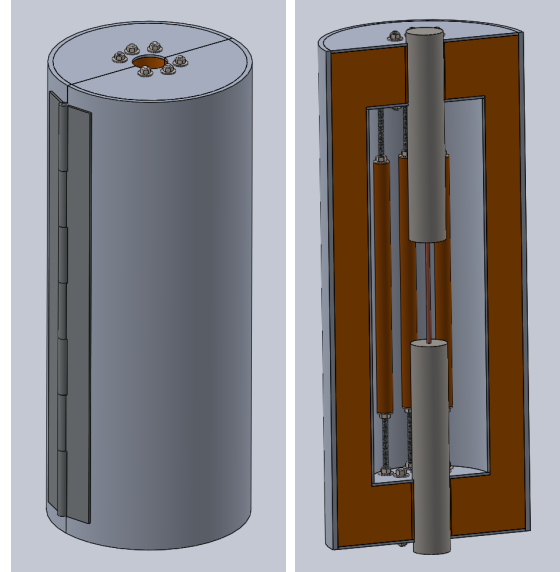


Figure 7: Final design iteration of environment chamber. Shown in full view with a hinge, and half-section with grips and specimen.

## 2.3 Functional Analysis

Looking now at the finalized design of the environment chamber, the walls are 6061 Al, chosen for its favorable strength-to-weight ratio and the ease with which it can be machined. It houses aluminosilicate ceramic fiber insulation of varying thickness — 2 in. between the inner and outer side walls, and 3 in. between the inner and outer top/bottom walls. This insulation material is commonly used in ovens, furnaces, and fire doors.

Design constraints for the structure of the chamber were governed by size and weight restrictions, in particular that the chamber must fit within the load frames of the tensile testing machines and that it must be light enough for an able-bodied user to reasonably be able to carry it:

- Maximum outer diameter of 10 in., so that it fits between the columns of the load frames on the testing machines in the Materials Laboratory
- Ideal weight of 40 lb, maximum weight of 60 lb

A base was constructed to support the chamber and keep it securely held to the testing

machine. The design constraints for the base were:

- It must support the weight of the chamber, with a safety factor of at least 2-3
- Its geometry must allow for it to be bolted to the bed of the Instron machine (since this is the machine with which the environment chamber will be used for the foreseeable future)

A pair of grips had to be obtained in order to secure specimens during testing. Initially, we purchased a pair of 5 mm collets — a type of chuck well-suited to hold long, narrow objects — but found that specimens slipped out of them when subjected to tensile load (see Section 4.2 for more information). We then designed a pair of threaded grips so that specimens could be screwed into them.

The chamber operates by using 6 vitreous-enameled power resistors with a power input regulated by a user-adjustable PID controller. These heating elements are fixed within the interior of the chamber, and heat the specimen via convection and radiation. An external DC power supply provides power to the controller and heating elements. The design constraints for this heating subsystem were governed by project safety policies, end user safety and environmental impact considerations:

- Power input  $< 1000$  W, reduce power usage and stay under 1000 W limit mandated by project safety guidelines
- Maximum 50 Vdc through circuits we assembled, mandated by project safety guidelines
- Maximum outer wall temperature of  $40^{\circ}\text{C}$  [15]
- Wiring must be shielded or otherwise contained in order to protect end users

Full details on the function, design, and implementation of each of these subsystems can be found in the subsystem-specific chapters (Section 3-5).

To determine the safe threshold for the outer wall temperature, in order to mitigate burn risks, we consulted a study on safe temperature limits for human touch [15]. At temperatures below  $45^{\circ}\text{C}$ , an object is safe to touch with no risk of developing a burn [15]. To try and account for imperfect sealing and conduction through the grips that would allow for heat to escape to the exterior, we shot for a more conservative maximum

outer wall temperature of 40°C.

## 2.4 Benchmarking

Table 2.4 below details some commercially available chambers, along with their operating temperatures, insulation materials, heating and cooling methods, and compatibility with test machines [16, 17, 18, 19]. Although we did not design and build our own chamber with the intent of taking it to market, this was still a useful exercise in reviewing industry preferred chamber geometry, heating and cooling methods, and insulation materials.

Table 3: Comparison of environment chambers and tube furnaces currently on the market [16, 17, 18, 19].

Environment Chamber or Furnace	Operating Temperature Ranges	Structure & Insulation	Heating and Cooling Methods	Compatibility
<i>Instron 3119-600 Series</i>	-150°C to 600°C	Details on structure not given, interlocks keep heat inside chamber	Forced convection, cooling not mentioned	Instron dual column load frames
<i>MTS Series 651 Environmental Chambers</i>	-150°C to 540°C	Welded metal body, fiberglass insulation	Forced convection, liquid nitrogen coolant	Various MTS load frames
<i>MTS Series 651.04 Furnace</i>	Ambient to 1000°C	Stainless steel clamshell, proprietary insulation	Resistive heating, passive convection	MTS Landmark Machines
<i>Thermcraft 114-12-1ZH 13326 Tube Furnace</i>	Ambient to 1010°C	Hinged, 18" length, 12" heating element with 1" diameter	Resistive heating, passive convection	Universal
<i>SATEC SSI-F7 Tube Furnace</i>	Varies	Stainless steel clamshell, proprietary insulation	Hoskins 875 resistive heater, passive convection	Universal
<i>Netzsch 6.225.6-03 Tube Furnace</i>	Ambient to 1550°C	Various materials, solid tube design	Proprietary "all-in-one" shell, passive convection	Universal
<i>RI Research Model E4</i>	Ambient to 1100°C	Aluminum reflectors, aluminum clam shell	Infrared radiation, water cooling	Universal

Many of these chambers can reach temperatures in excess of 1000°C, with the trade-off of high cost and complexity, and limited compatibility with testing machines. Our design considerations focus less on maximum operating temperature, and more on minimizing the temperature variation along the specimens in order to provide a high level of reliability

for temperature measurements and data to be collected during tests. Furthermore, a liquid cooling system was not deemed strictly necessary by our end users, reducing the time and cost to build the chamber. The system should be compatible with any testing machines whose load columns are at least 18 in. apart, and that have a flat bed or deck with an area of 12 in. by 12 in. on which to rest the chamber and base.

## **2.5 Team and Project Management**

### **2.5.1 Design Process Organization and Timelines**

The two most time-consuming stages of this process were the design and construction stages, and each subsequent stage required the prior one to be completed. Our approach to this design project was fairly standard, laid out by the following steps:

- Review commercially-available products which accomplish similar tasks, to become familiar with existing implementations
- Brainstorm viable concepts for different subsystems and components (chamber geometry, insulation materials, fixturing options, etc.)
- Evaluate advantages and drawbacks of each concept (Appendix E: Subsystem Concept Scoring provides details on our process for concept evaluation), decide on options for the initial design
- Iterate and further refine the design, taking into account manufacturability, production costs, safety, and time-constraints
- Verify with hand calculations, FEA simulations, and qualitative consideration of hardware features
- Finalize the design, and begin ordering necessary parts and materials
- Construct the environment chamber, making changes to assembly as necessary when challenges arise
- Fine-tune the final hardware for real-world implementation
- Evaluate the performance of the final hardware

In order to give enough time for testing and analysis, finalization of the design, CAD drawings, and necessary calculations was completed by the end of Winter Quarter. This process involved making decisions on the following items:

- Chamber dimensions and material
- Insulation material and thickness
- Base design
- Design and fabrication of threaded grips
- Heating elements, temperature controller, thermocouples

This allowed for the group to purchase materials in advance, so that potentially slow delivery times of materials purchased online or lead times of outside shops would not become problematic.

The Gantt charts in Appendix F: Project Timelines provide a more detailed overview of the tasks to be accomplished throughout the academic year in accordance with the above processes, as well as ideal completion deadlines.

### **2.5.2 Challenges and Constraints**

A number of challenges arose during the design and construction of the environment chamber. The first was funding; the team received \$1500 from the university, but unfortunately did not receive an additional \$4500 from a desired Xilinx grant. Consequently, we could not purchase an appropriate load cell for the MTS machine. While the resolution provided by the load cell on the Instron machine is adequate, the servohydraulic MTS machine provides additional capabilities, such as allowing the user to specify a constant load rate, as opposed to the Instron's constant displacement rate. While the additional functionality is not strictly necessary for the SMA testing, having the environment chamber interface with the MTS machine with an appropriate capacity load cell could allow future users to further enhance the scope of SMA testing in the Materials Laboratory beyond what we considered for this project.

The challenges encountered were not only limited to funding; a number of logistical challenges arose throughout the academic year, all of which were addressed and mitigated.

For example, local shop rates and lead times for welding aluminum components were untenable for this project (we were quoted in excess of \$1300 to perform all necessary machining and welding of components, with lead times of 3-4 weeks). We contacted a third-party certified welder, and he offered to perform the welding free of charge. He welded the walls of the furnace; however, he was out of town for the latter half of the Spring Quarter, and thus the furnace base had to be constructed with bolted joints instead of welds. The protrusion of bolts and machine screws was mitigated by using flat-head bolts, counter-sunk into flat components, which were made thicker to accommodate the reduced contact area.

We designed and fabricated threaded grips early in the Winter Quarter. However, the SMA specimens provided to us were not straight wires (most likely due to being subjected to repeated compression tests [1]), thus making it difficult to turn down the diameters of the specimens' test sections and thread their ends to interface with the grips. Additionally, we were not provided with and could not obtain a safety data sheet or other manufacturer information on the SMA specimens, which by School of Engineering Machine Shop policy prevented us from being able to machine the specimens in the shop. Digital Loggers, Inc. performed this work for us.

Safety restrictions imposed significant limitations on the selection of a power supply, which was absolutely necessary to convert gridded AC power to comparatively safer DC power. To achieve the fastest heat-up times possible with a 50 V limit, an uncommon power supply was needed. Our sponsor Digital Loggers, Inc. provided us with second-hand power supplies to try out. The first two 1/4-rack-mount power supplies failed to work, so a larger, more reliable 3/4-rack power supply was then used to avoid further failures.

A number of unexpected hardware-related challenges were encountered, all of which were resolved in time. We found that constructing resistive heating elements from scratch was not feasible, as small inconsistencies would lead to hot spots. Instead, large DC power resistors were used as heating elements. Digikey's selection of over 10,000 chassis-mount power resistors was refined based on criteria defined in Section 5: Thermal Control System. Additionally, we had to reduce the maximum allowable operating temperature for the chamber (i.e., the setpoint entered into the controller) due to temperature limita-

tions with certain components. The RTV silicone used as a sealant and adhesive, and the Teflon coating on the thermocouples and wires begin to smoke, melt, or otherwise degrade at approximately 260°C. We deemed an operating temperature of 250°C to be dangerously close to this point, and decided to restrict users to a maximum temperature of 200°C, in order to avoid any such issues of heat-induced degradation.

Another challenge encountered during implementation involved properly sealing the top end of the chamber against the grip fixtures (as the top grip is connected to the testing machine's load cell and crosshead, which move during tests). While achieving an air-tight seal was simple, accomplishing this without introducing significant friction on the grips was difficult. Friction between the seals and grips is problematic because it causes the load cell to report a higher value than is being applied to the specimen, which consequently makes data inaccurate. This ultimately resulted in a trade-off between sealing and friction; it is nearly impossible to have one without the other, so a balance between the two was reached where a tiny amount of space was left between the grips and the silicone rubber seal.

### **2.5.3 Risks and Mitigation**

We had to take steps throughout the assembly process to mitigate safety risks. For example cutting the ceramic fiber insulation releases small, abrasive particles from it that cause skin, eye, and respiratory irritation if contact is made. In order to prevent exposure to these particles while installing the insulation in the chamber, we followed the recommended guidelines in the manufacturer's safety data sheet [20], and wore goggles, gloves, face masks, and long sleeves. To protect users, we thoroughly sealed the insulation within the chamber so that no particles could escape, using silicone rubber sheets and RTV silicone.

While working in the School of Engineering Machine Shop, we followed all shop safety rules and consulted with the shop managers and/or shop assistants prior to operating any machinery or working with delicate materials (such as ceramics). Soldering was performed either under a fume hood or in an open, well-ventilated space. We reviewed our circuit diagrams with our advisor Dr. Robert Marks and the shop manager Don MacCubbin prior to wiring up the controller, power supply, and heating elements.



## 2.5.4 Budget and Expenditures

Table 4: Breakdown of all project expenditures (including parts/components that did not make it into the final implementation of the environment chamber) Note: oil bath materials were used to heat up SMA specimens to test for transition temperatures.

Material/Manufacturing	Material	Vendor	Cost (\$)
10" OD Pipe	6061 Aluminum	Tube Service Co.	245.00
6" OD Pipe	6061 Aluminum	Tube Service Co.	155.00
12"x12"x0.125" Sheet (x2)	6061 Aluminum	Metal-Werx	29.49
6"x12"x0.250" Plate	6061 Aluminum	Metal-Werx	12.44
2"OD 0.125" Wall, 24" Len. Round Tube	6061 Aluminum	Metal-Werx	10.56
Temperature Controller	PID Controller	Omega (via eBay)	217.95
1.50"x1.50" 0.125" Wall, 24" Len. Box Tube	6061 Aluminum	Metal-Werx	9.60
1/4-20 Threaded Rod (x6)	Stainless Steel	Home Depot	30.54
Thermocouple (x2)	K-Type	Fry's Electronics	80.00
24"x54"x2" Insulation Blanket	Aluminosilicate	UniTherm	64.20
1/2" OD x 1/4" Tube (12" Length)	Alumina Ceramic	McMaster-Carr	46.50
Adhesive/Sealant	RTV Silicone	O'Reilly Auto Parts	9.80
Waterjet-Cut & Machined Parts	6061 Aluminum	Rustworks	386.75
1.50"x1.50" 0.125" Wall, 24" Len. Box Tube	6061 Aluminum	Metal-Werx	9.60
Grommet (x4)	Rubber	Home Depot	6.16
Oil Bath Materials	Dish and Canola Oil	Target	23.48
1"x1", 24" Len., Square Bar	6061 Aluminum	Metal-Werx	11.52
2.50"x5"x0.1875" Window (x2)	Ceramic Glass	Peninsula Glass Co.	56.00
<b>Total spent: \$1,404.56</b>			

Ideally, construction of the environment chamber should have begun midway through the Winter Quarter and completed before Spring Break. Ultimately we could not begin purchasing parts until late in the Winter Quarter, and did not begin manufacturing and assembly until Spring Break. This was due to encountering a series of errors and challenges with thermal simulations and proper meshing of CAD models; we delayed manufacture as we wanted to be sure our models, simulations, and calculations were correct and properly predictive of the behavior of the environment chamber first. Also, the team encountered issues with finding local shops that would perform necessary work within our budget, causing us to fall behind in the construction of the furnace (Appendix F: Project Timelines shows these changes to the project schedule).

Ultimately, the amount spent on our end was kept within the given budget of \$1500. We did rely on contributions from our sponsor in order to complete the environment chamber, as the given budget was not sufficient. More details on the value of parts and materials provided by our sponsor can be found in Table 7.

## 2.6 Main Subsystems

The main subsystems are:

- Chamber structure
- Mounting hardware (base and grips)
- Thermal control system

The chamber structure was made from 6061 Al, with the inner and outer walls being large, extruded tubes that were split in half with a table saw. The material was carefully considered since the user will need to be able to lift the chamber to install it on test machines or to put it away in storage. Although steel (with the exception of stainless steel) is machinable and generally easier to weld than aluminum, we determined that a steel chamber would be too heavy, and elected to make one from aluminum instead. In addition, a cylindrical chamber geometry was chosen, so as to allow radially symmetric positioning of the heating elements for as even a temperature distribution on the specimen as possible.

Resistive heating elements were used in the inner chamber and were long enough to cover nearly half of the inner chambers height, 10.5 in. These were readily available and easily incorporated into the electric circuit (see Section 5 for more information on the heating elements).

The insulation was critical to preserving a high and even interior air temperature, while also trapping heat within and keeping the exterior chamber surface temperature below a safe threshold of 40°C. The grip fixture was custom-designed to be compatible with the Instron machine in the Materials Laboratory.

## 3 Subsystem 1: Chamber Structure

As previously mentioned, the chamber structure needed to meet the following criteria:

- Effectively seal where each half interfaces, to prevent heat loss
- Minimize heat loss through the top and bottom holes where the grips pass through
- Provide a uniform temperature distribution along the length of the specimen
- Weigh less than 60 lb, ideally about 40 lb
- Heat inner chamber to 200°C

With these requirements set into place, a design matrix (Figure 76) that considered different chamber geometries was created to aid in deciding which design was most appropriate. The box design ranked highest due to its lower manufacturing cost and ease of installation. However, the team opted for a tube chamber since its ease of incorporating resistive heating elements in a radial pattern to provide uniform heating took priority over cost. With this decision made, steady-state thermal simulations were performed in SolidWorks.

### 3.1 Finite Element Analysis

#### 3.1.1 First Design Iteration Simulations

The first FEA study was run towards the end of the Fall Quarter, after a detailed first design iteration had been developed from initial concepts, with a power input of 30 W per heating element. The convection coefficient along the outer surface of the chamber was estimated to be  $7.0 \frac{W}{m^2K}$ , and the convection coefficient along the inner surfaces of the chamber was estimated to be  $4 \frac{W}{m^2K}$  using the spreadsheet in Figure 53, found in Appendix A: Hand Calculations. The external air temperature was assumed to be 20°C, and the inner air temperature was assumed to be 200°C. Conductive, convective, and radiative modes of heat transfer were considered as follows:

- Conduction from the heating elements through the insulation out to the chamber wall

- Conduction between the grips and the specimen
- Convection from the outer surfaces of the chamber to the environment
- Convection from the inner surfaces to the air inside the chamber
- Convection between the specimen and air inside the chamber
- Radiation from the heating elements to the specimen
- Radiation from the outer surfaces of the chamber to the environment

Temperature distributions inside the chamber, as determined by the steady-state thermal study in SolidWorks, are provided below.

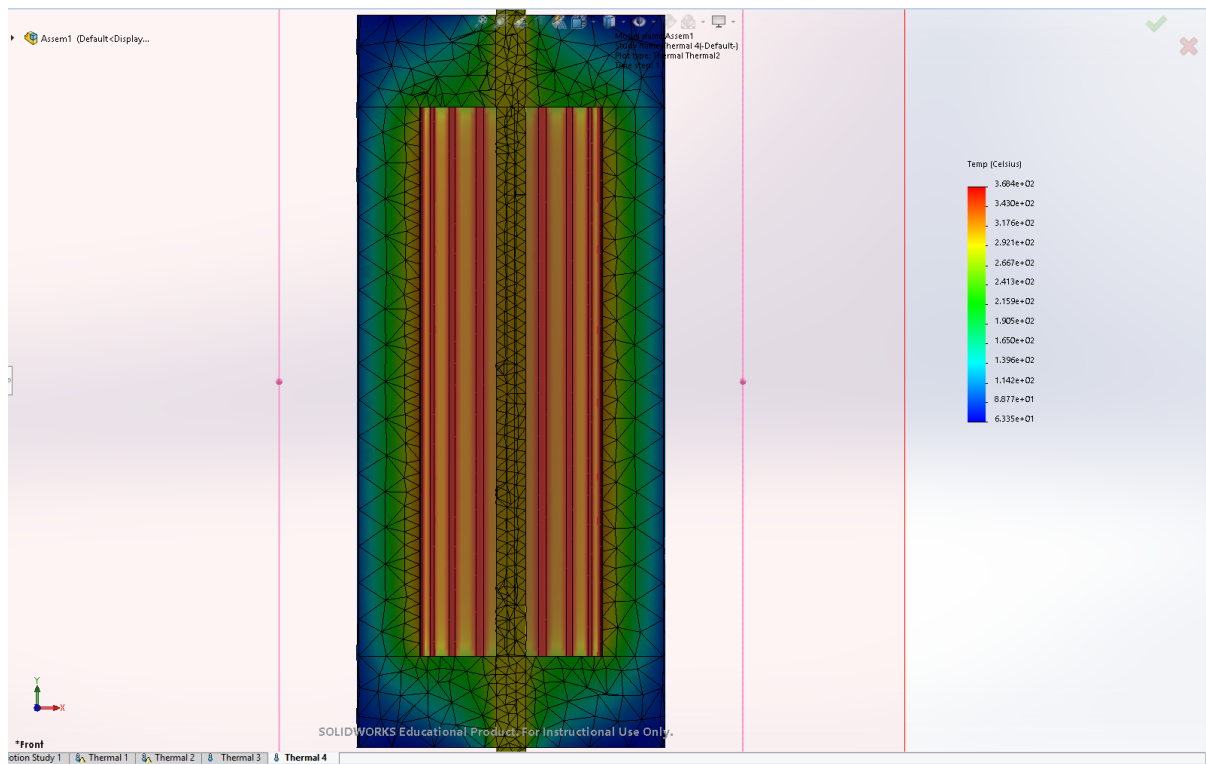


Figure 8: Temperature distribution along cross-section of chamber, before iteration. Temperature ranged from 63-368°C.

The heating elements have a surface temperature of 368°C, the specimen has a temperature of roughly 300°C, and the outer surface of the chamber has a temperature of 63°C.

However, the natural convection coefficients used for the inner surface of the chamber assumed an air temperature of 200°C. Thus the study was iterated with new values, and

a more realistic specimen model (made of pure Cu, since this was all the information we had been given about the SMA composition at the time):

- Power per element = 20 W
- $T_{surf,outer} = 60^{\circ}\text{C}$
- $T_{\infty} = 20^{\circ}\text{C}$
- $T_{air,inner} = 230^{\circ}\text{C}$

The results of this iterative process are shown below.

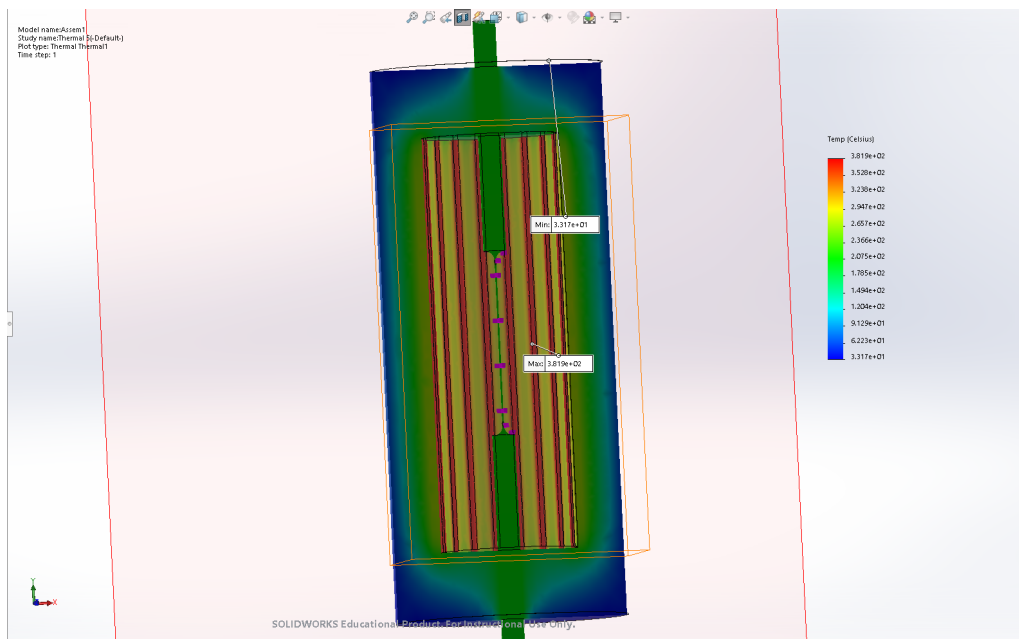


Figure 9: Temperature distribution along cross-section of chamber. Temperature ranged from 33-382°C.

The temperature of the specimen is roughly 213°C. The temperature at a few points along the length of the specimen is shown below.

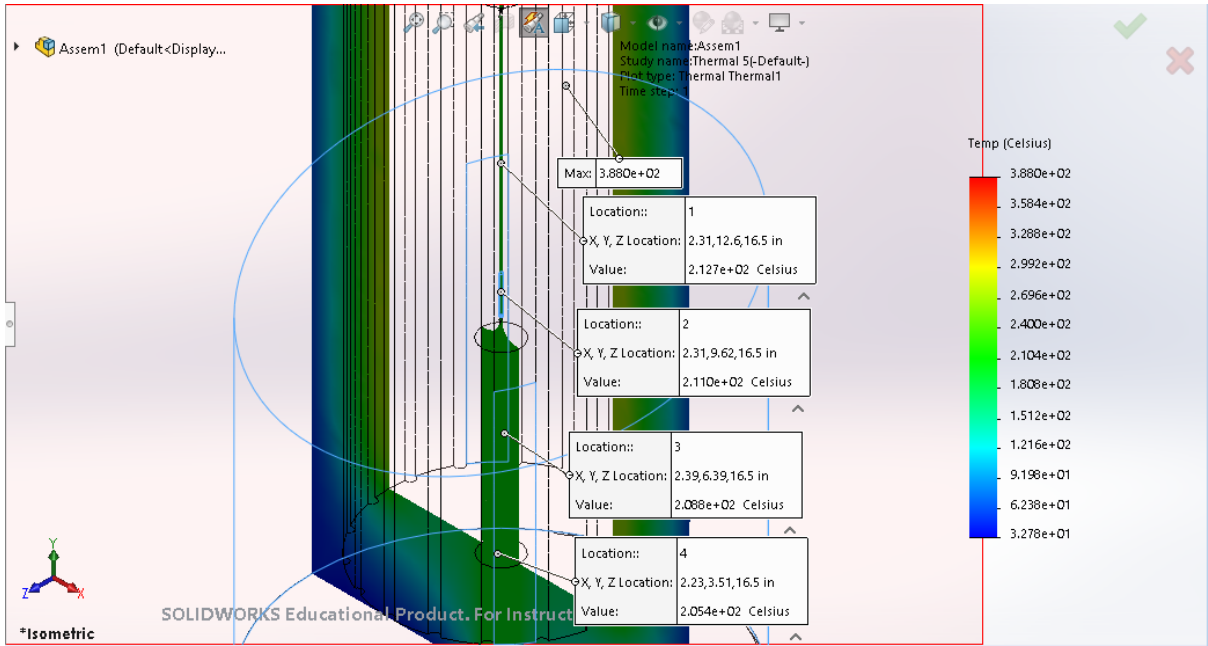


Figure 10: Temperature distribution along length of specimen. Temperature ranged from 33-388°C.

The probed values in the above figures are plotted to show the temperature of the specimen from its mid-length (hottest part) to gripped end (coldest part) and can be found in Appendix C: Thermal Simulations, Figure 69.

A close-up view of the chamber cross-section provides a clearer sense of the temperature distribution through the solid insulation and walls.

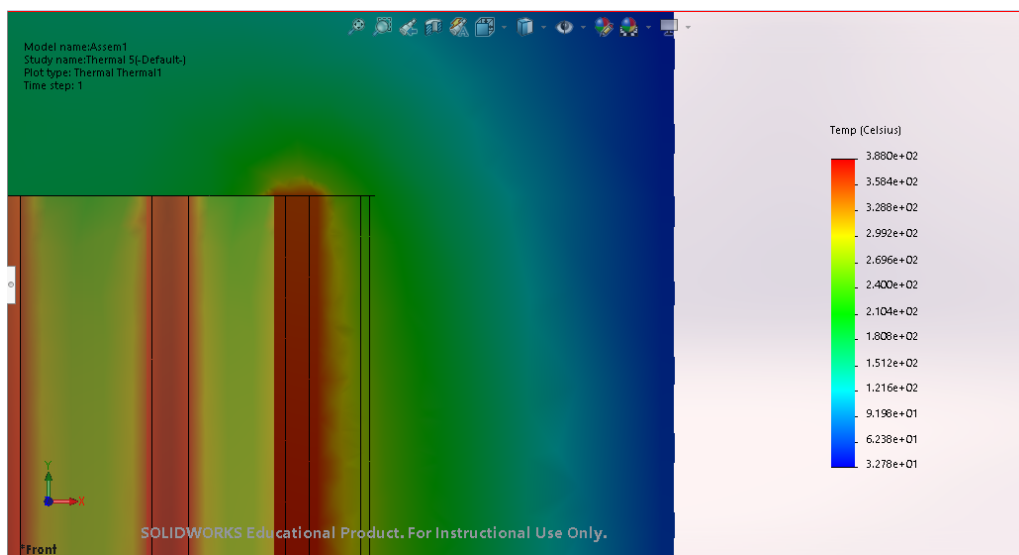


Figure 11: Close-up of temperature distribution in insulation. Temperature ranged from 33-388°C.

The mesh elements are shown alongside the results to illustrate the mesh controls used.

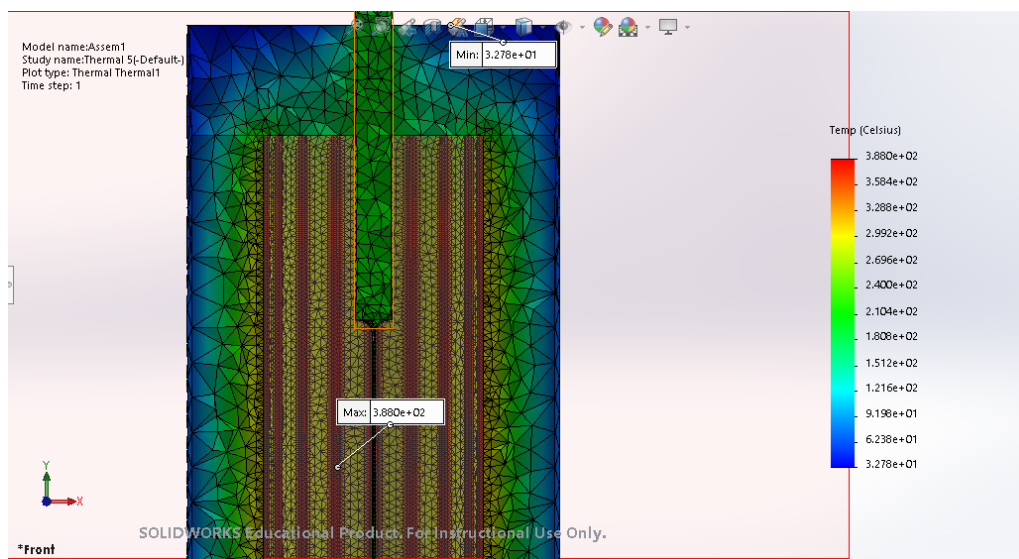


Figure 12: Cross-section view showing mesh elements. Temperature ranged from 33-388°C.

The mesh elements are much finer near the inner edge of the insulation. The mesh elements are also relatively finer near the resistive heating elements and specimen, especially where the specimen cross-section shrinks. A close-up of this is shown below.

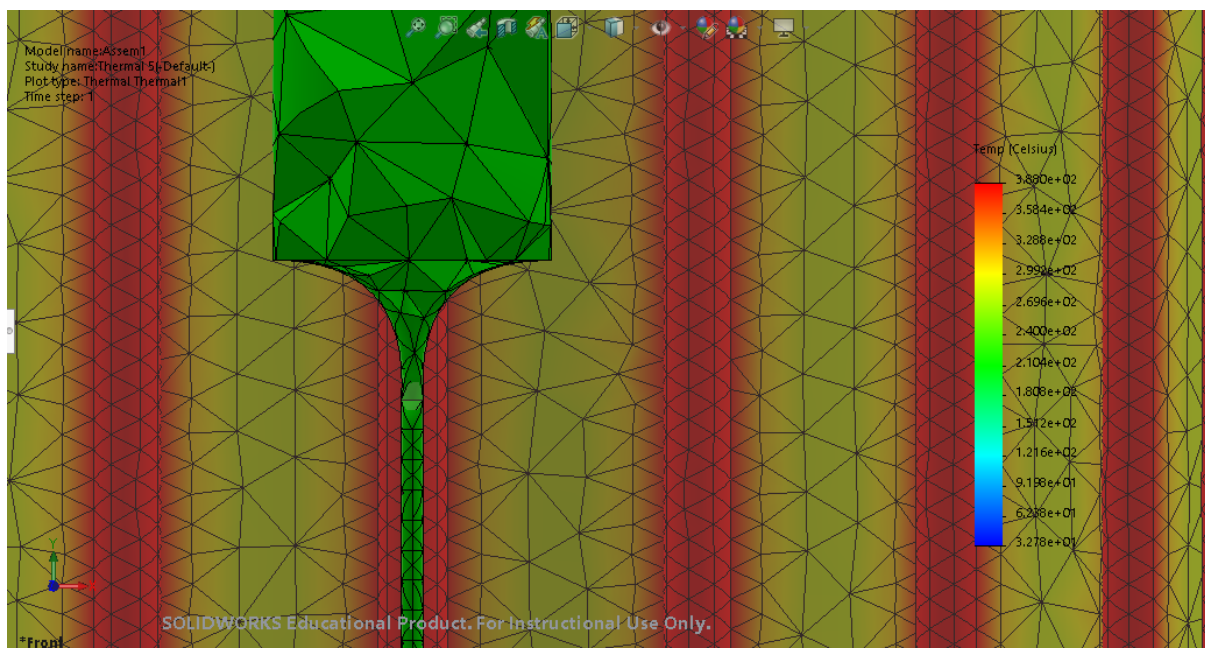


Figure 13: Mesh refinement along specimen and heating elements. Temperature ranged from 33-388°C.

The mesh aspect ratio peaks at 58. Finally, a top-down cross-section view is shown, to illustrate the temperature distribution in the insulation near the heating elements:

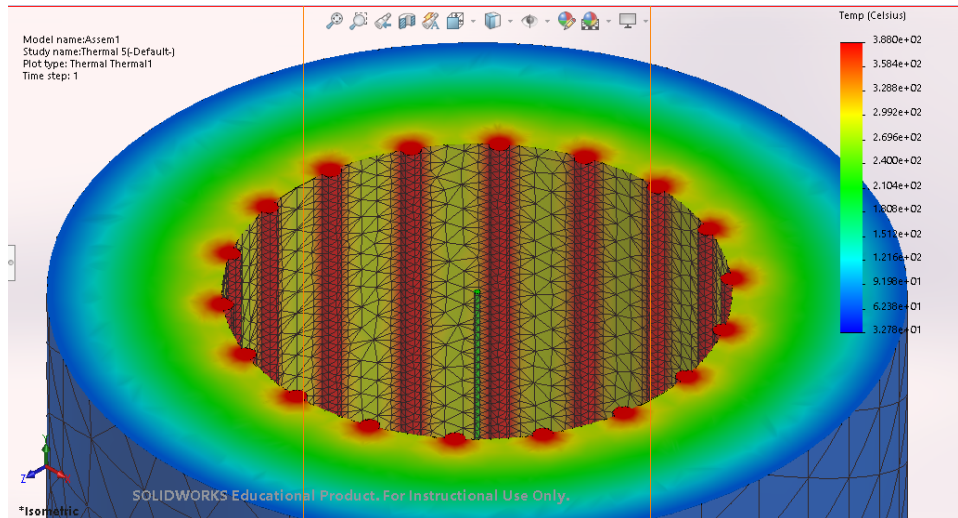


Figure 14: Cross-section view from above of temperature distribution. Temperature ranged from 33-388°C.

### 3.1.2 Unused Design Choices

Similar to the tube chamber previously shown, a thermal analysis was conducted for a box design. Since the number of resistive heating elements doubled to 36 for this design, a power output of 10 W per heating element was assumed. All other thermal loads and material properties remained the same as with the previous simulation.



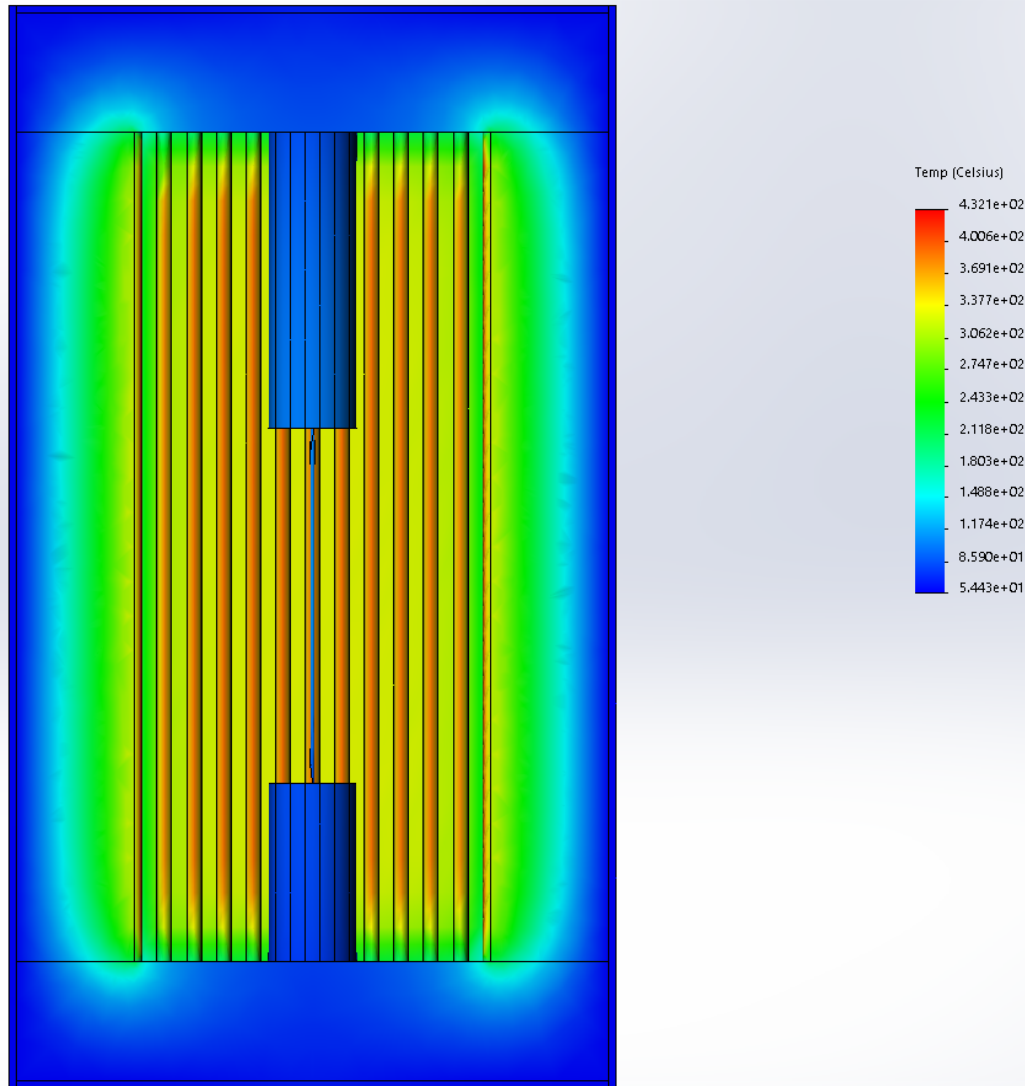


Figure 15: Temperature distribution of all components of the box design. Temperature ranged from 54-432°C.

The unsafe exterior wall temperature of 54°C for the box design further showed that it would not satisfy safety requirements.

Additionally, we attempted to implement a window into the chamber design, in order to permit optical extensometry so that future users could gain a higher degree of accuracy from measurements. The window was double-pane ceramic glass, rated up to 700°C, encased in an aluminum housing (see Figure 3.1.2), so that it could be welded into a cutout section of the chamber walls.

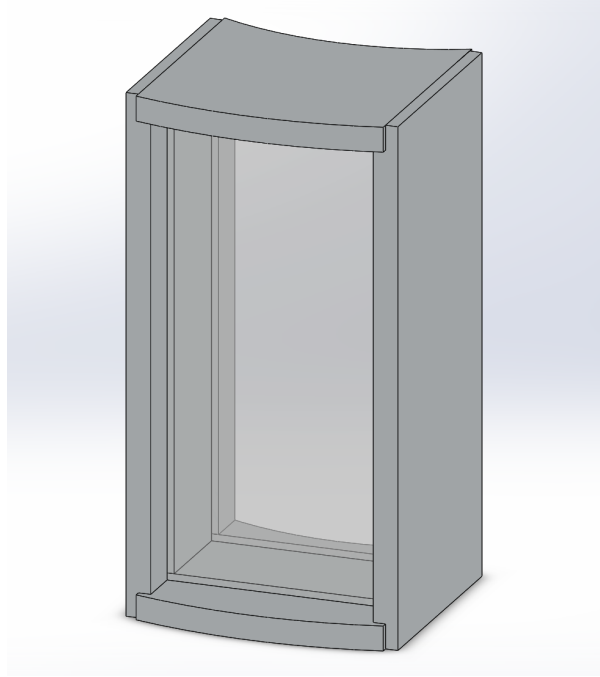


Figure 16: CAD model of a double-pane ceramic glass window, to permit optical extensometry. Not included in final design due to high cost, poor manufacturability, and safety concerns.

Unfortunately, the process of machining this aluminum housing, welding it together, and integrating it into the chamber was too expensive (we were quoted a shop rate in excess of \$300) for us to justify the inclusion of a window in the chamber, as it was not a strictly necessary component. The process to cut out a section of the chamber to accommodate the window was even more fraught with challenges, as the shops we contacted were unable or unwilling to do this. The only quote we received came from the vendor of the extruded aluminum tubes, who offered to laser cut this feature for over \$2,000 (including the \$400 cost of the tubes themselves).

A steady-state thermal study was conducted on the first iteration of the chamber model, with this window included, with the same inputs and conditions as in Section 3.1.1. The result was a severely skewed internal temperature distribution and a totally unsafe peak exterior wall temperature of around 150°C.

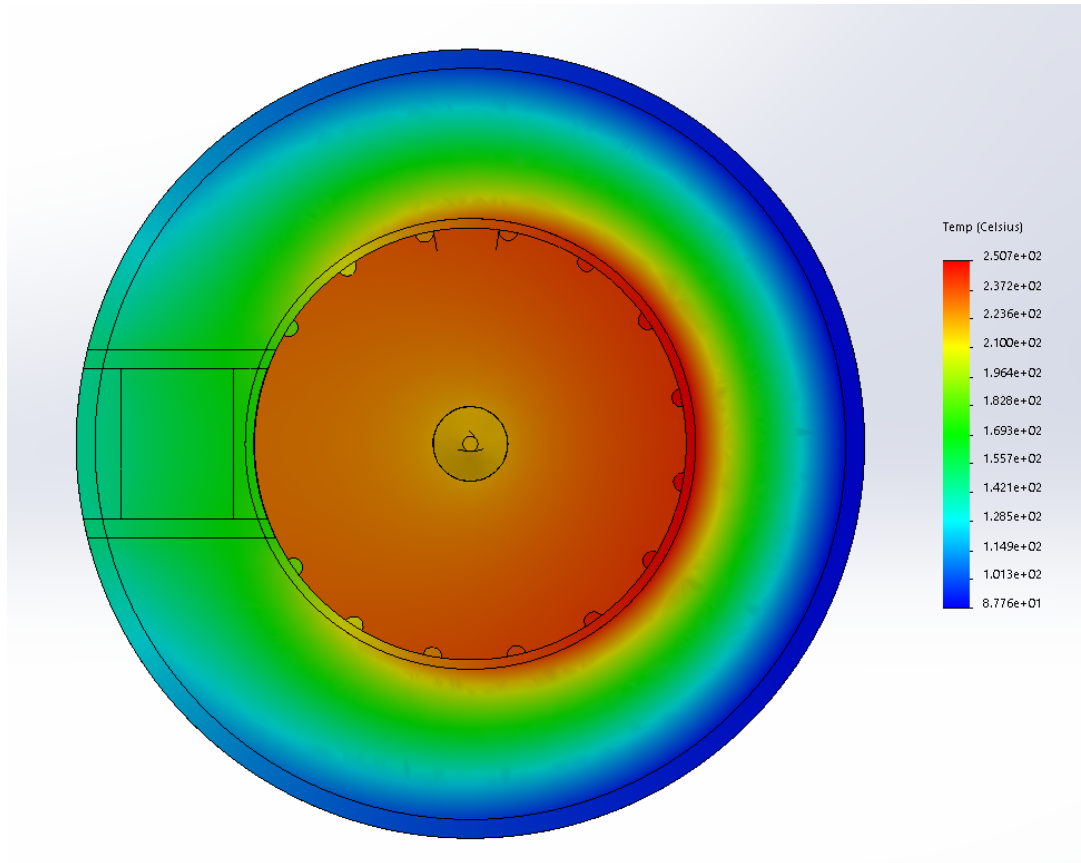


Figure 17: Top-down view of temperature distribution with a window included (left side). Unsafe peak wall temperature of approximately 150°C. Temperature ranged from about 87-251°C.

Considering the startling production costs and safety concerns associated with the window, we had to omit it from further design iterations. It would be possible to devise a better plan for implementation of a window in the future, but this consideration was beyond the scope of our project.

### 3.1.3 Final Design Iteration Simulations

The initial concept of the chamber had resistive heating elements being fixed to the inner chamber wall with high-temperature adhesive. However, this design was revised due to the high cost to obtain high-temperature polymer thick-film heaters that could be fixed along the curvature of the inner wall. Creating our own coils and arrays from resistance wires, such as Nichrome, was deemed to be too tricky and imprecise to be practical for our application and timelines. So instead, stainless steel threaded rods with nuts and

washers were used to hold power resistors within the furnace. Figures 18-21 show the final design and how the resistors were fixed. This is a comparatively much simpler design to implement, and required less time and money spent to put it together.

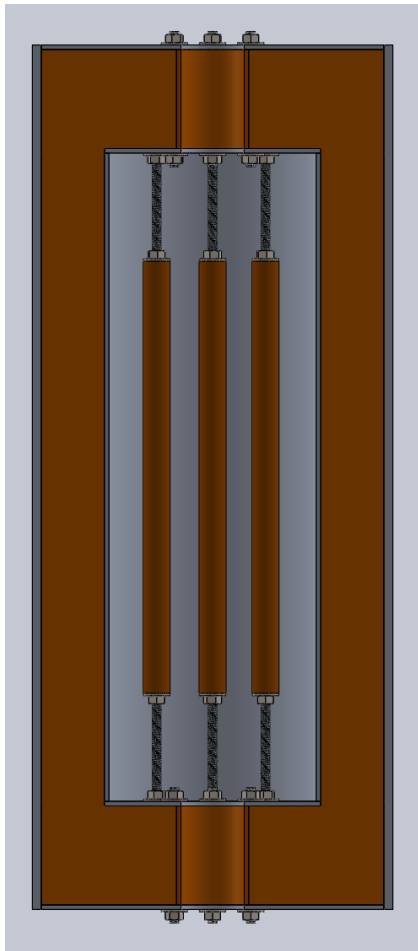


Figure 18: Half of chamber CAD model, with silicone rubber seal shown, insulation underneath (not visible).

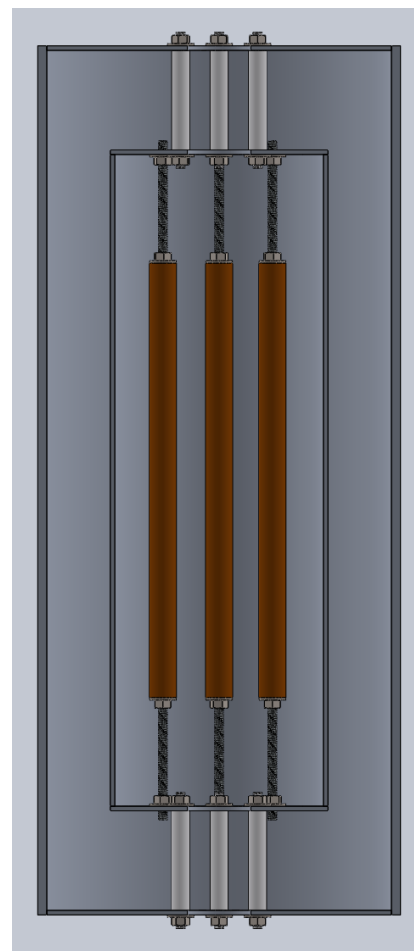


Figure 19: Half of chamber CAD model, insulation and silicone rubber hidden, standoffs shown.

Figures 20-21 also illustrates how the power resistors were fixed using the threaded rods, nuts, and washers to allow users to adjust the height of the heaters to accommodate specimens of various lengths. The nuts that lie within the length of the power resistors (Figure 20) keep the inner diameter concentric with the rod while the nuts and washers at each end hold them at a specified height. These can be tightened and loosened with a crescent wrench to adjust the height of the power resistors as desired.



Figure 20: Power resistor mounts.  
Nuts and washers support resistors.



Figure 21: Fully assembled environment chamber.

Thermal simulations were performed on the final model so that the expected temperature distribution of the specimen and grips could be observed and compared to real-world test data. The interior and exterior bulk air temperatures of the previous simulation were used. However, the convection heat transfer coefficients used in the previous simulation were not permitting heat transfer from the new resistors. Live tests had been performed on the chamber and the temperature distribution of the chamber itself was known. As a result, the convection coefficients were increased through iteration (see Table 5) so that heat transfer could take place and the team could gain some insight on the temperature distributions of the specimen and grips.

Additionally, the material of the heating elements in the model was changed to reflect the now-used power resistors made of ceramic tubes. Power input was adjusted to 115 W per heating element to give a total power input of 690 W, because this was the power consumption observed in live tests conducted prior to this thermal study. The material of the test specimen remained as pure Cu. In addition, to improve sealing of the chamber and to hold the insulation in place, silicone rubber sheets were added to each chamber half. Radiation was included and Tables 5-6 show the final convection coefficients and emissivity values used.

Table 5: Convection coefficients used in updated model.

Air	Convection Coefficient ( $\frac{W}{m^2K}$ )
Inner Bulk Ambient Air	100
Outer Bulk Ambient Air	103

The final convection coefficients in Table 5 were two orders of magnitude higher than those used in the previous simulations. However, the convection coefficient of air can range from 10-100  $\frac{W}{m^2K}$  [21] (albeit the higher end of the range applies to forced convection, rather than free convection as with this simulation), so these values are not entirely unreasonable. Nevertheless, these final design iteration simulation results should be taken with a grain of salt, as the temperature measurements taken during live-tests present a more accurate sense of the heating performance of the environment chamber.

Table 6: Radiation parameters used in updated model.

Material	Emissivity	View Factor
Vitreous-Enamel (Power Resistors)	0.9 [22]	0.5
6061 Al (Chamber Walls)	0.09 [23]	1.0

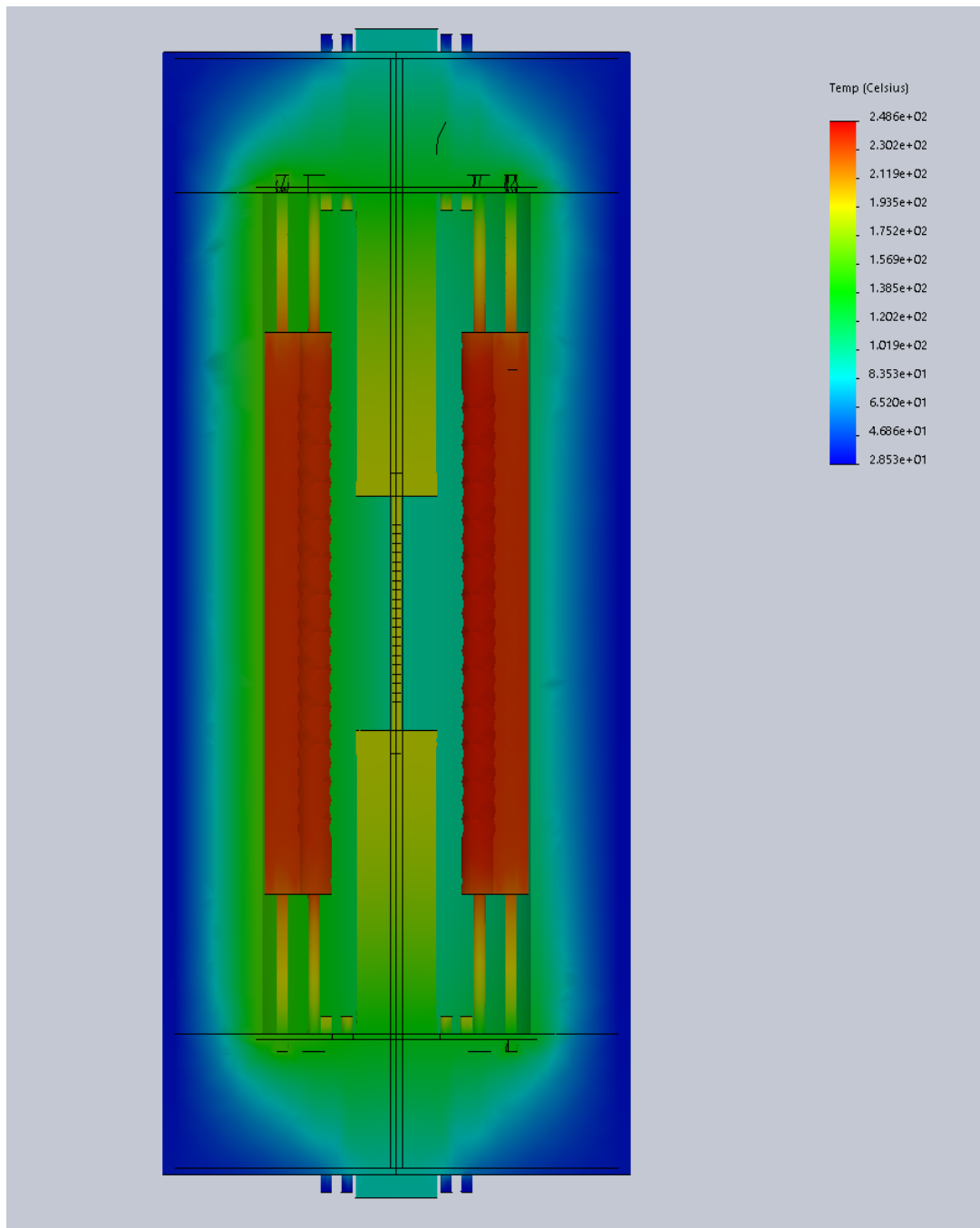


Figure 22: Expected temperature distribution of the chamber. Temperatures range from 28-249°C.

The predicted exterior wall temperature was 30°C, under the maximum temperature of 40°C.

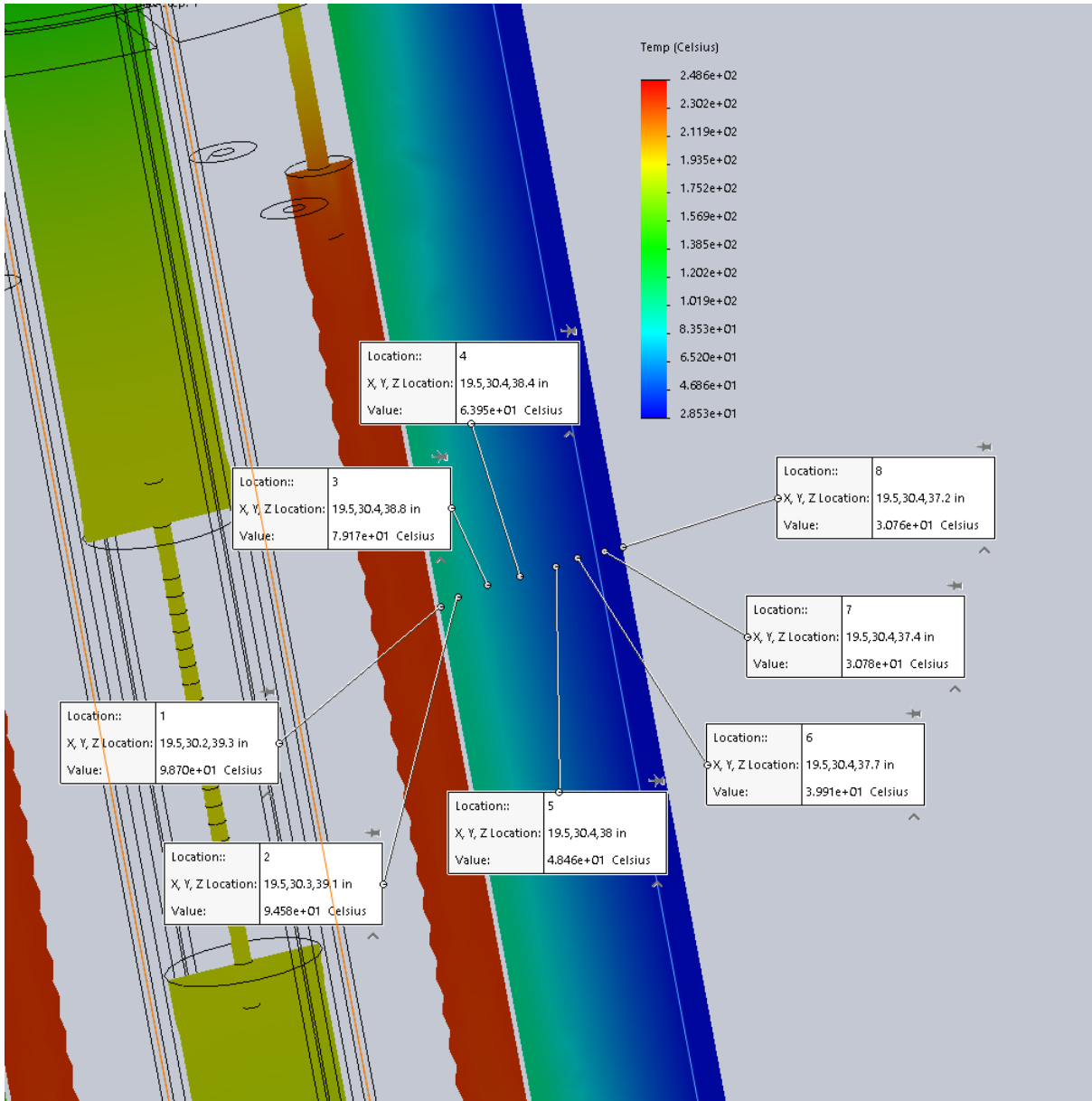


Figure 23: Expected temperature distribution from the inner to outer walls of the chamber. Temperatures range from 28-249°C.

Additionally, the temperature was probed from the inner wall, through the insulation, to the outer wall in order to gain better insight on the temperature distribution. The silicone rubber and RTV sealant used at the interface of the two halves have a maximum continuous operating temperature of 260°C. Upon creating the plot in Appendix C Figure 72, it was verified that the temperatures of the silicone and RTV would not be a concern at the maximum ambient air temperature of 200°C.



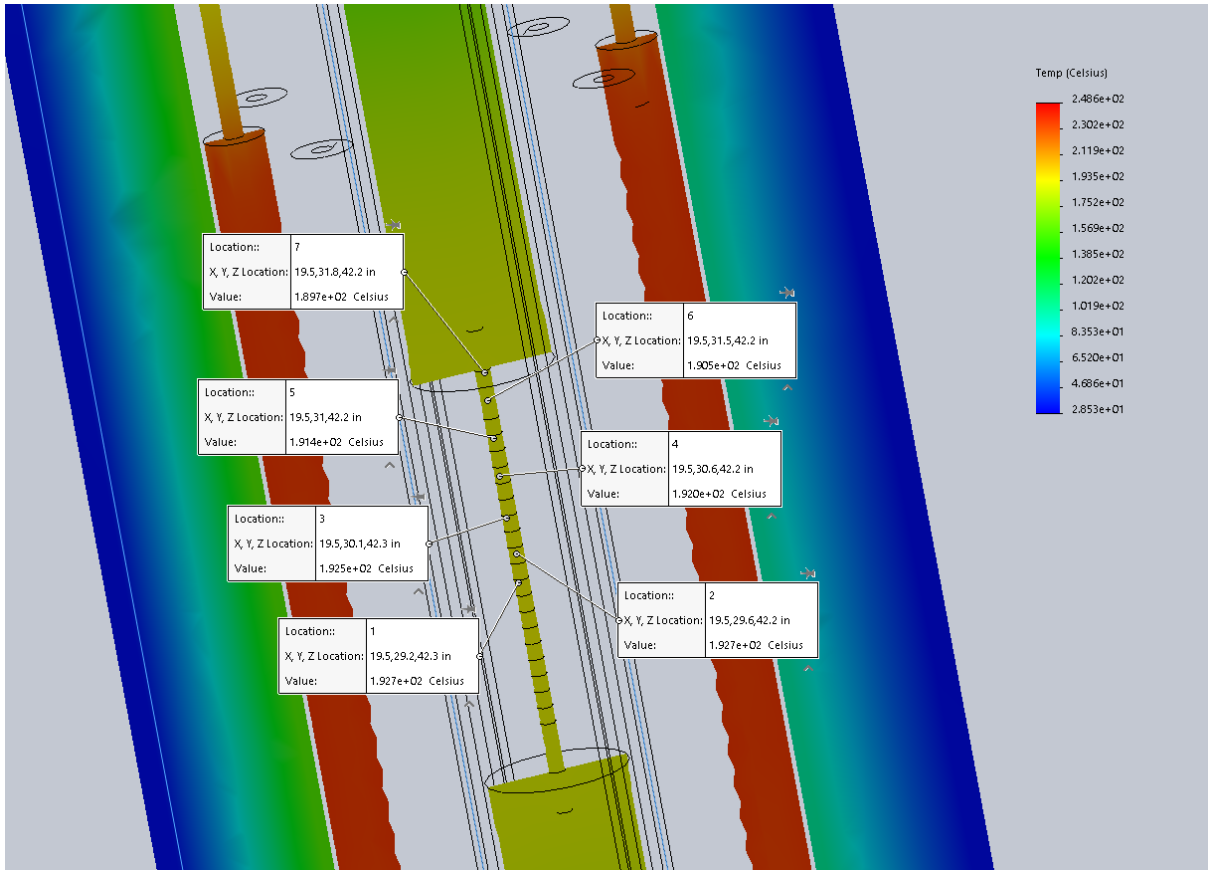


Figure 24: Expected temperature distribution of the specimen. Temperatures range from 28-249°C.

Figure 24 depicts the temperature distribution of the specimen from probing the specimen from midlength to one end. Its maximum temperature at the midlength reached 192.5°C and dropped to 189.5°C, giving a temperature variation of  $\pm 2.5^\circ\text{C}$ . This also full-filled the design specification that was set for the maximum specimen temperature variation of  $\pm 5^\circ\text{C}$ .

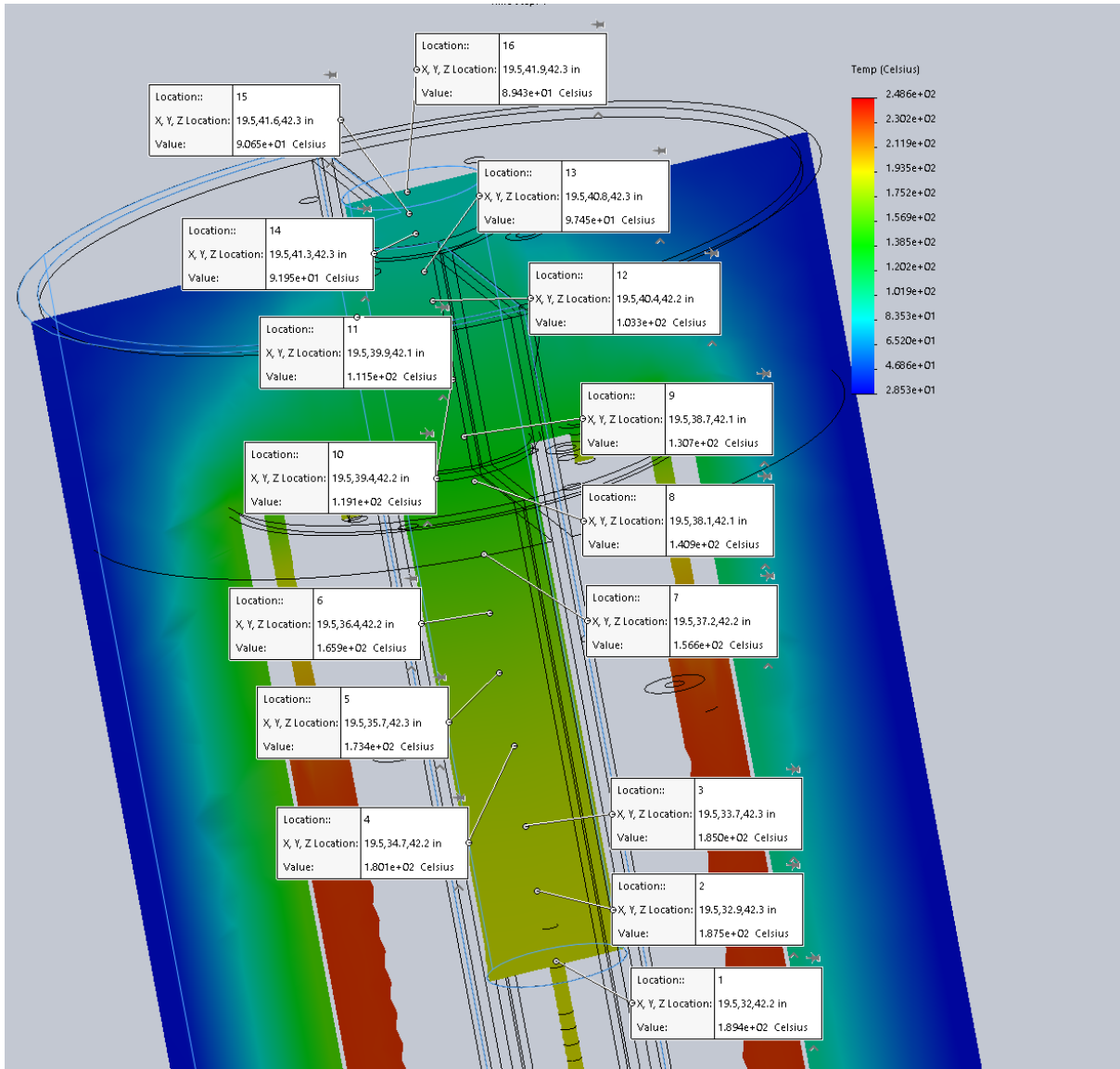


Figure 25: Expected temperature distribution of the grips. Temperatures range from 28-249°C.

A grip was also probed in order to assess the safety of the user when concluding a test and the specimen's removal is necessary. The grips were made from a precision-ground steel rod. The simulation revealed that the temperature at the end of the grip that makes contact with the grip fixture and load cell of the Instron was 88°C. This raised concerns because it would result in an instant burn if it came into contact with the user's bare hand. The team intends to assess this issue by machining down the diameter of the grip with a lathe so that it can be coated with silicone rubber to reduce heat transfer to the user's hand.

## 3.2 Manufacturing and Assembly

Manufacturing the inner and outer chamber walls required splitting tubes in half. A local tubing company called Tube Service Co. quoted \$3,500 for the doing the job precisely with a laser cutter. Due to this high cost, we reached out to our sponsor, Digital Loggers Inc., and they were able to split the tubes on their table saw. While the cuts were not as precise, they were within our design tolerances (refer to Appendix B: Parts and Assembly Drawings). In addition, the flat plate end caps for each half-tube were cut with a waterjet at a local shop called Rustworks. We had initially intended for all flat parts to be machined from 6061 Al plates using a milling machine, however, Rustworks recommended using their waterjet to reduce costs, the amount of material used, and lead time (from 2 weeks to 2-3 days after expediting), while also improving the precision of the cuts. Also, a welder from Hogue Inc. in San Luis Obispo agreed to weld the chamber wall components for us, as a donation to the project. Furthermore, threaded ceramic standoffs were used to separate the inner and outer walls, because:

- Ceramic, unlike metal, standoffs prevent conductive heat loss from the inner wall to the outer wall
- Threaded holes on the ends of the standoffs allowed us to secured them tightly with machine screws
- Having some solid standoffs or spacers prevents the inner wall from sinking due to gravity and compressing the soft insulation

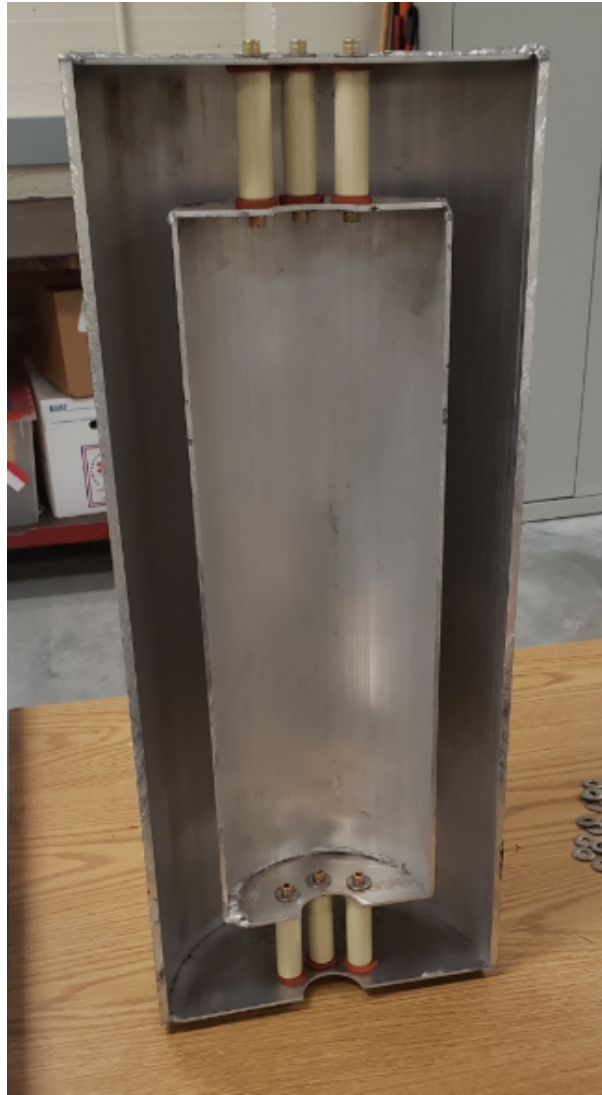


Figure 26: Chamber structure before insulation was inserted. Silicone rubber washers (made with a punch) were placed between ceramic standoffs and aluminum end caps to allow for some compression due to thermal expansion.

In Figure 27, a layer of orange silicone rubber can be seen sealing in the aluminosilicate ceramic fiber. Custom-made silicone rubber washers were punched out of a rubber sheet and placed between the standoffs and the walls. The compressibility of the material accommodates thermal expansion and prevents the standoffs from cracking under compression.

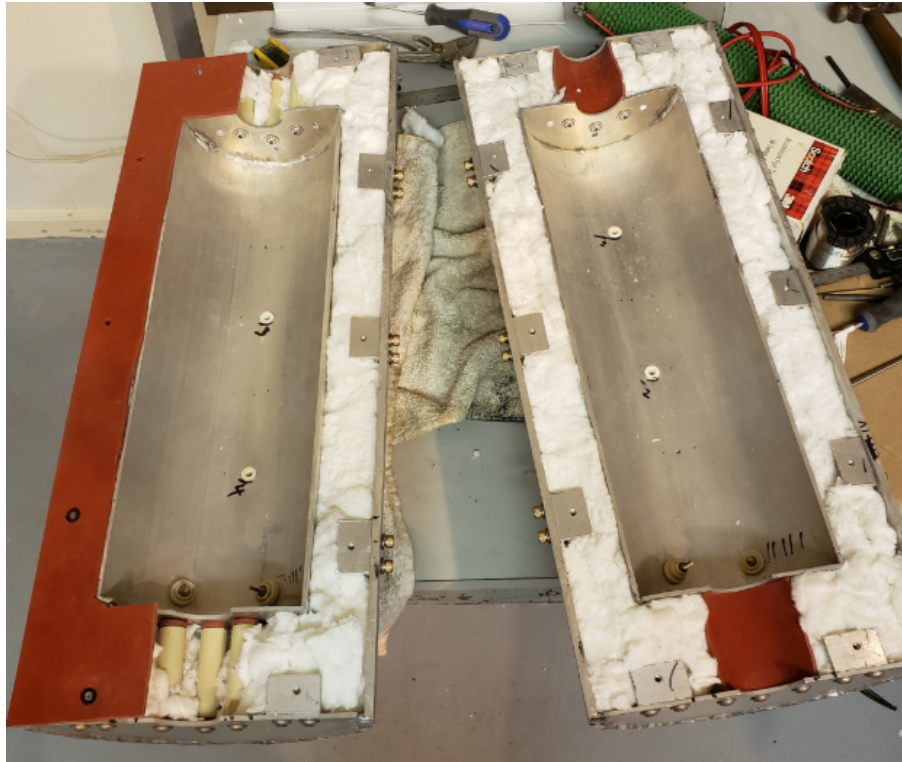


Figure 27: Chamber structure with insulation inserted and silicone rubber seals being applied.

The insulation was ordered as an aluminosilicate ceramic fiber blanket, which was easily cut with shears into the appropriate lengths for packing in-between the inner and outer chamber walls. It was imperative that the insulation could not escape from the chamber, due to the irritation risk it poses with skin contact and to the respiratory system if inhaled. To properly house the insulation, we cut angle iron into 1.5 in. sections and drilled holes into them to permit press-fitting a self-clinching onto the side facing the insulation. Afterwards, a slightly compressible 0.125 in. thick silicone rubber sheet was cut to size to seal in the insulation and to create a tight seal when the two chamber halves close, making up for imperfect splitting of the tubes. The sheets were fixed to the angle iron by using bolts, washers, and the self-clinching nuts. Lastly, RTV silicone was used to adhere the edges of the silicone rubber sheets to the walls. Figures 28-29 provide a close-up view of how the chamber halves seal together on the finished assembly.



Figure 28: Silicone rubber sheets compressed with the latches to provide a tight seal.

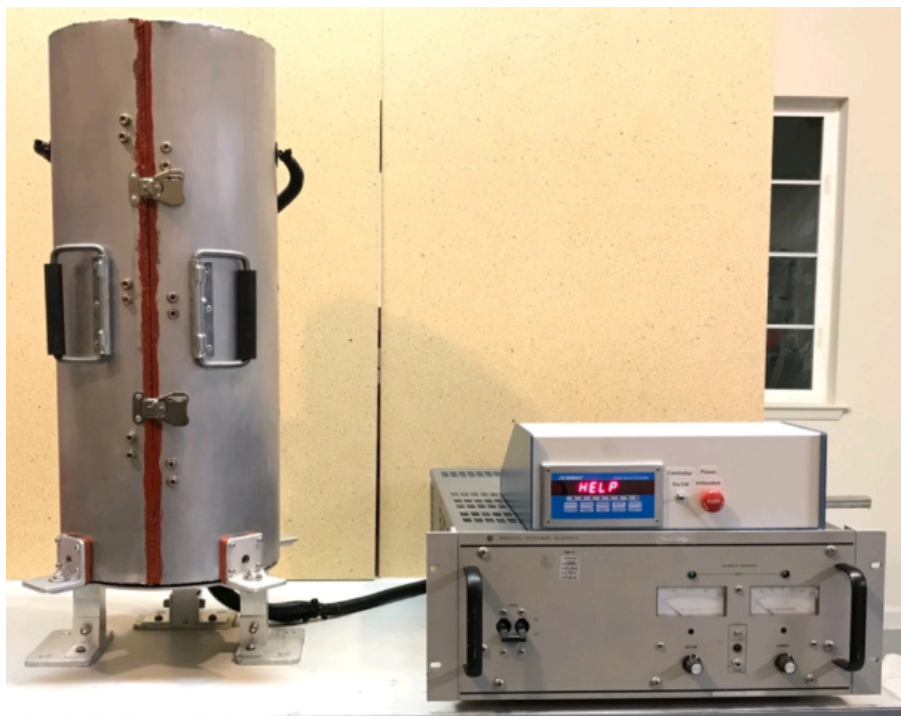


Figure 29: Completed environment chamber hooked up to the controller and power supply.

A stainless steel hinge was provided by Digital Loggers, Inc., which we riveted to the chamber body, to allow it to open and close easily. As can be seen in Figure 28, latches

and handles were bolted to outer wall (again provided by Digital Loggers, Inc). The latches ensure the chamber will remain tightly shut during tests or when kept in storage, and the handles — which have rubber sleeves — give users an easy way to lift and carry the chamber.

## 4 Subsystem 2: Mounting Hardware

### 4.1 Base

In order to make the chamber free-standing, so that its weight would not be supported by the load cell, we constructed a base. The base is made of 6061 Al plates and box tube. Four brackets are affixed to the circular plate, with holes through them, so that the chamber (containing four brackets along its bottom edge that line up) can be pinned to the base. Holes in the bottom plates on the legs of the base allow for it to be bolted to the deck of the Instron testing machine. Originally, we planned to have all these parts machined on a milling machine and the entire assembly welded together, but due to high costs (about \$400 for machining and welding, not including expedite fees) and a lead time over two weeks, we had to rethink and simplify the assembly.

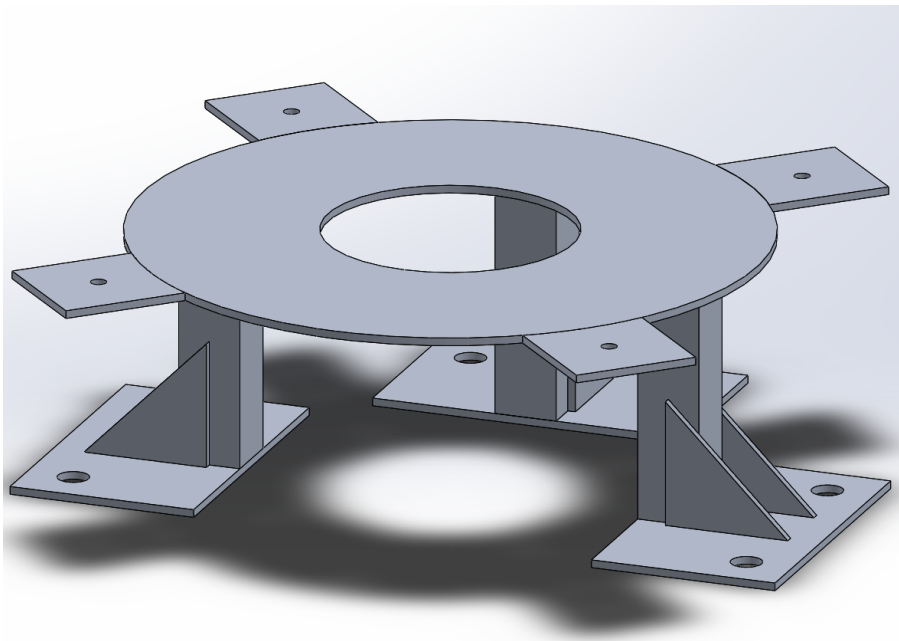


Figure 30: CAD model for the chamber base.

The circular plate and brackets were instead cut as one continuous part, and the bottom plates and triangular gussets were also cut, all by waterjet. This process was around \$200 cheaper (including expedite fees, but not assembly) and was completed in two days. We then cut angle iron sections to assist with bolting the pieces together, omitting the triangular gussets in the process. Instead of putting pins through the brackets, we decided



to bolt angle iron sections with pieces of compressible silicone rubber to the brackets, to press against and more securely hold the chamber when it is resting on the base. The compressible pads were included to accommodate the curvature of the chamber walls, and to increase the contact area of the flange pressing against the chamber.

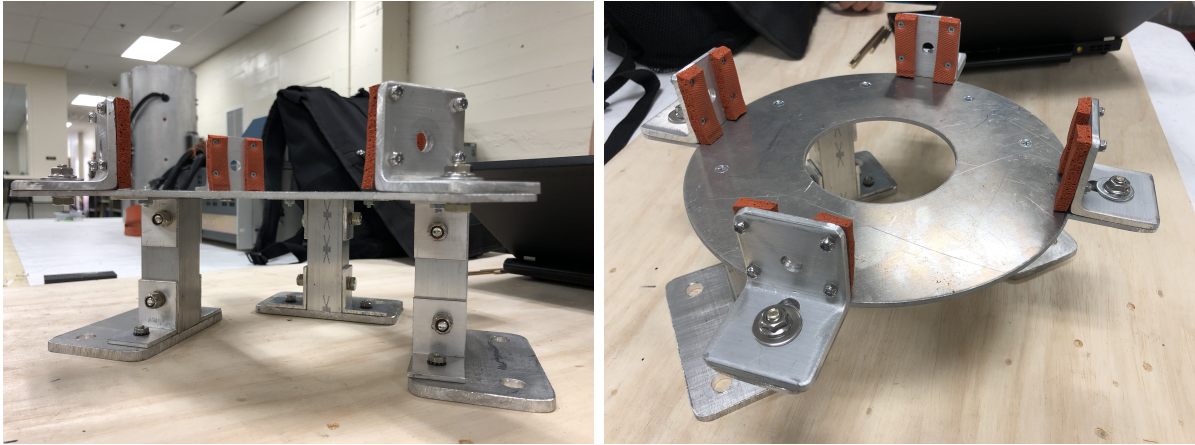


Figure 31: Final base assembly.

The model for the base was run through static load simulations in SolidWorks. It was fixed on its bottom plates and a 43 lb load was applied on its top circular plate, to replicate the weight of the environment chamber. Displacement, strain, and von Mises stress were tested for in the simulation (Figures 32-34), and for all three criteria the base showed no areas for concern. As neither the originally intended fillet welds nor the angle iron sections would be load-bearing components, they were not considered as important from a design safety standpoint as the circular plate and the box tube legs.

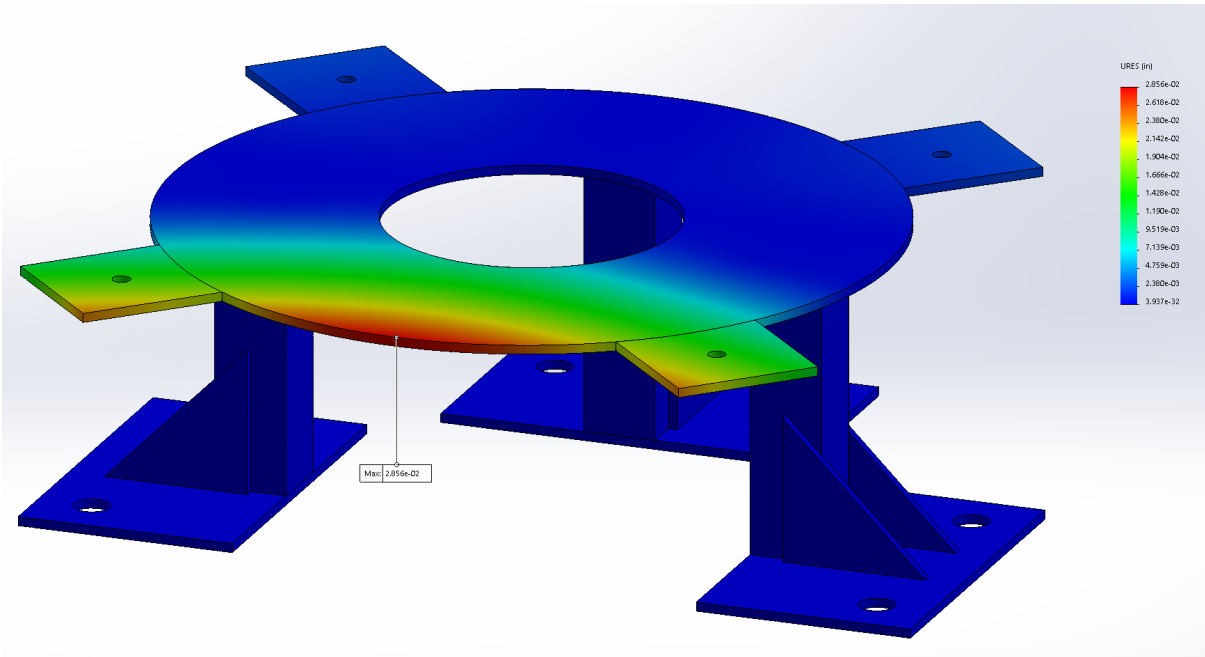


Figure 32: Expected displacement in the base due to carrying the weight of the chamber (43 lb). Displacement ranged from the order of  $10^{-32}$  in. to 0.02856 in.

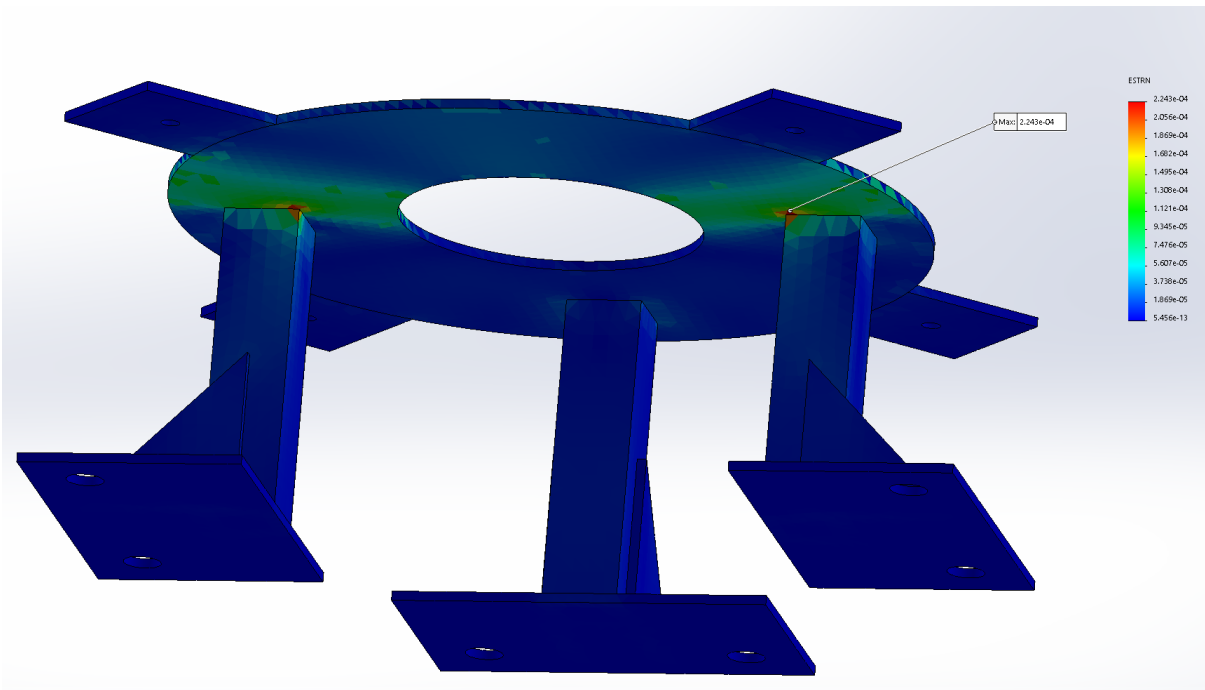


Figure 33: Expected strains in the base due to carrying the weight of the chamber (43 lb). Strain ranged from the order of  $10^{-13}$  to 0.0002243.

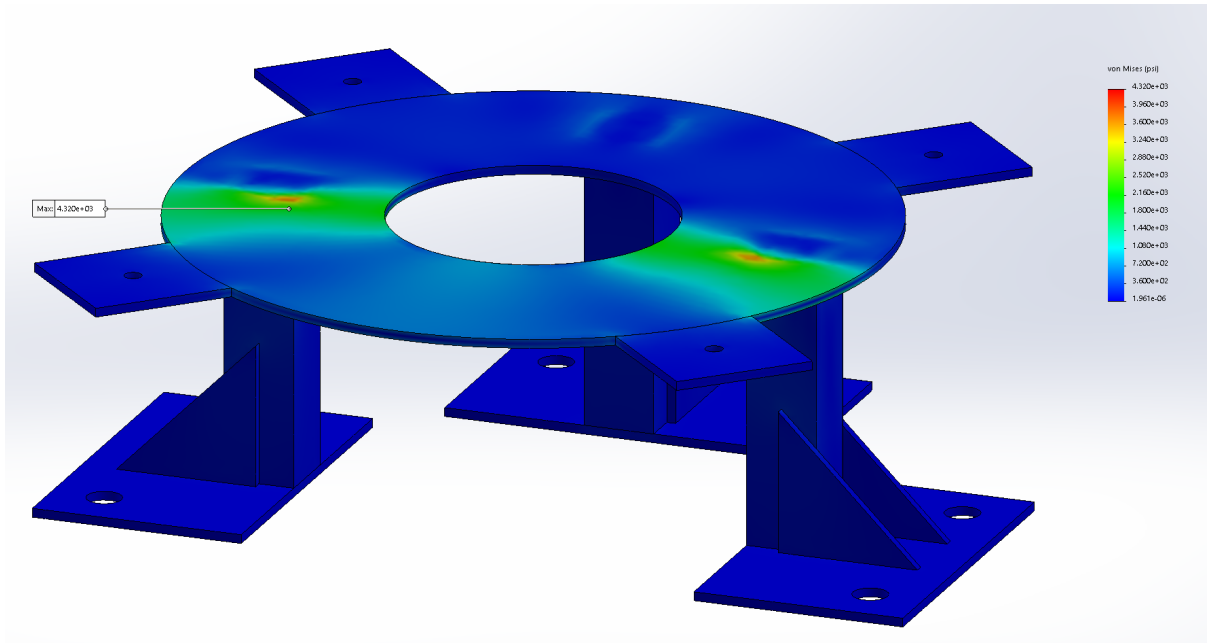


Figure 34: Expected von Mises stresses in the base due to carrying the weight of the chamber (43 lb). Stress ranged from the order of  $10^{-6}$  psi to 4,320 psi.

The largest deflection is seen at the front of the circular plate (Figure 32), where it is not supported by a leg; this decision was made to allow room for an operator to access the mounting hardware on the Instron machine in order to install grips. Nevertheless, the highest expected deflection is under 0.028 in, which we found to be a negligible amount when loading the chamber onto the base in real life. As the yield strength of 6061 Al is typically around 40,000 psi [24], and the highest expected stress in the assembly is 4320 psi (Figure 34), this gives a safety factor over 9. In practice, we expect the base to be able to easily support the chamber, and to handle impacts from a user accidentally dropping the chamber on top of it without buckling or falling apart.

## 4.2 Grips and Fixturing

The mount points for specimen grips on both the Instron and MTS machines are shown in Figures 35-36 below. For the purposes of our work, we focused on just the Instron 4502 testing machine, and designed grips that are compatible with it. Another set of grips compatible with the MTS Landmark machine would need to be machined in order to use the chamber with it, but this could be easily accomplished within a day or two, as

future work.



Figure 35: Instron machine mount point. Cylindrical grips are inserted and pinned into place.



Figure 36: MTS machine mount point. Cylindrical threaded grips are screwed into place.

The lowest-capacity load cell in the Materials Laboratory compatible with the MTS machine is 50 kN; the specific SMA samples which will be tested with the chamber should not require a load greater than roughly 5 kN. For this reason, the Instron machine will be used to test the SMA specimens, with its 5 kN load cell. The 50 kN MTS counterpart would offer comparatively poor resolution. We fabricated a prototype grip fixture accommodating a 5 mm collet, to test fitment with the Instron machine.



Figure 37: Prototype collet grip - disassembled.



Figure 38: Prototype collet grip - assembled.

Threaded portions are used to allow the end user to swap collets without removing the entire grip fixture from the Instron machine. Unfortunately, the collets used in the prototype do not provide enough gripping force to prevent a test specimen from slipping out during tensile tests. Larger collets, traditionally used as tool holders for CNC machining processes, were loaned to us by Digital Loggers, Inc.



Figure 39: Large tool holders for 2 mm and 5 mm wires.

An adapter was needed to interface these tool holders with the Instron machine's mount point. This was accomplished by welding portions of tool holder adapters to steel rods, machined to fit the mount points of the Instron machine. The parts are depicted below

in Figure 40, prior to welding and finishing, which were performed by Digital Loggers, Inc.



Figure 40: Machined adapters for large tool holders, prior to welding and finishing. Work was performed by our sponsor Digital Loggers, Inc.

Once finished, the adapters were tested (refer to Figure 41 below) to fit with both the mounting hardware that connects to the test machine's load cell (left end) and the tool holder (right end).



Figure 41: Completed specimen fixturing for the Instron machine. An adapter, tool holder, and collet are used to grip narrow wire specimens of 2 mm or 5 mm diameter.

Three tensile tests were performed at room temperature, the results of which can be found in Appendix G: SMA Tensile Testing. During the testing, the 5 mm diameter specimens

began to slip out of the collets at roughly 2-4 kN applied tensile load. As a result, we had to rethink our plans for securing specimens during testing, and decided instead on threading the ends of the specimens and fabricating threaded grips to accommodate them.

We used precision-ground cold-rolled steel rods for the new grips, to ensure tight tolerances and very good fitment with the specimens. For the threads, we used a UNF 10-32 tapping tool to cut threads in a 5 mm wide hole in the grip. Digital Loggers, Inc. then used a UNF 10-32 die to cut threads on the ends of the SMA specimens. We elected to use fine-pitch threads to maximize the number of threads bearing tensile stress in the specimens. The secure fitment between the two can be seen in Figure 43 below.

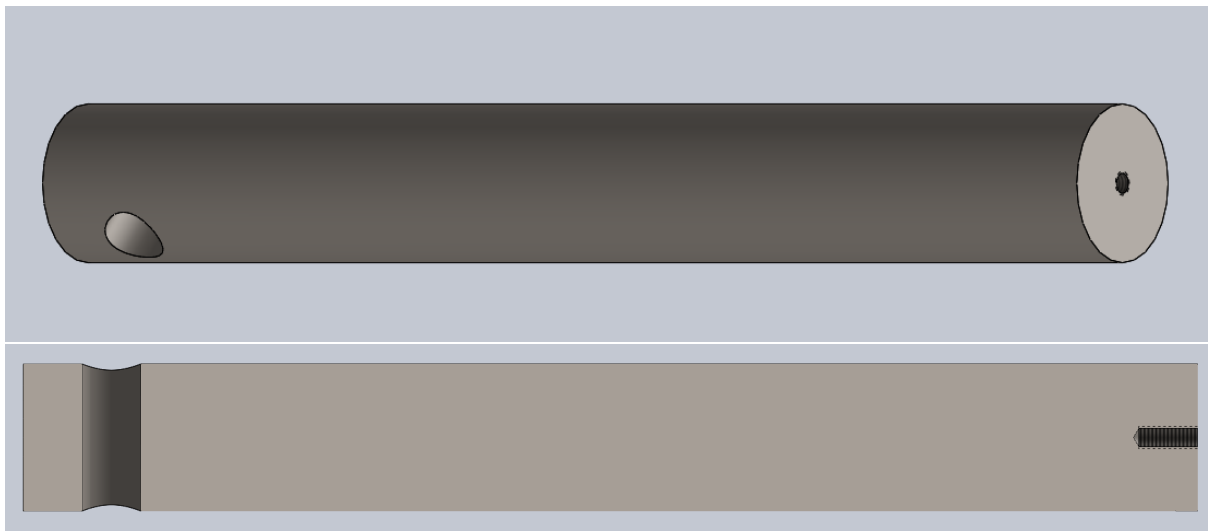


Figure 42: CAD model for the threaded grip. Full model (top) and cross section view showing depth of UNF 10-32 threaded hole (bottom)



Figure 43: Grip fitment with specimen.

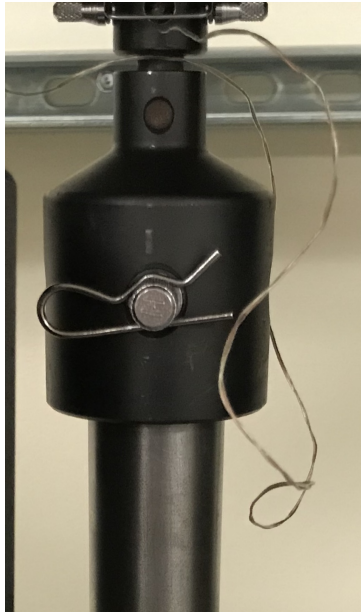


Figure 44: Grip fitment with the Instron mount (upper mount point, connected to the load cell).



Figure 45: Grips and specimen installed with the environment chamber.



## 5 Subsystem 3: Thermal Control System

The purpose of the thermal control system is to modulate power input to the heating elements, in order to regulate the temperature within the chamber. The thermal control system consists of:

- Omega CN1500-Series multi-channel PID temperature controller (specifically 4 channels for the controller used here)
- Vitreous-enameled power resistors as heating elements
- Programmable DC power supply

The temperature controller was selected due to its ability to apply PID control and take input from up to 4 temperature sensors (accepted types are: RTDs, thermocouples, thermistors, etc). Normally it would cost upwards of \$550, with options, but we were able to purchase a barely-used 4-channel model from a private seller.

See Appendix H: Using the Controller for instructions on operating the controller (a physical copy of the controller's user guide will also be provided with the environment chamber, controller, and power supply to the Materials Laboratory for future users to refer to). While multiple input channels are not strictly necessary for the SMA testing related to this project, the extra capability may be of use to future users.

A simple block diagram which governed the design of the system is shown in Figure 46 below.

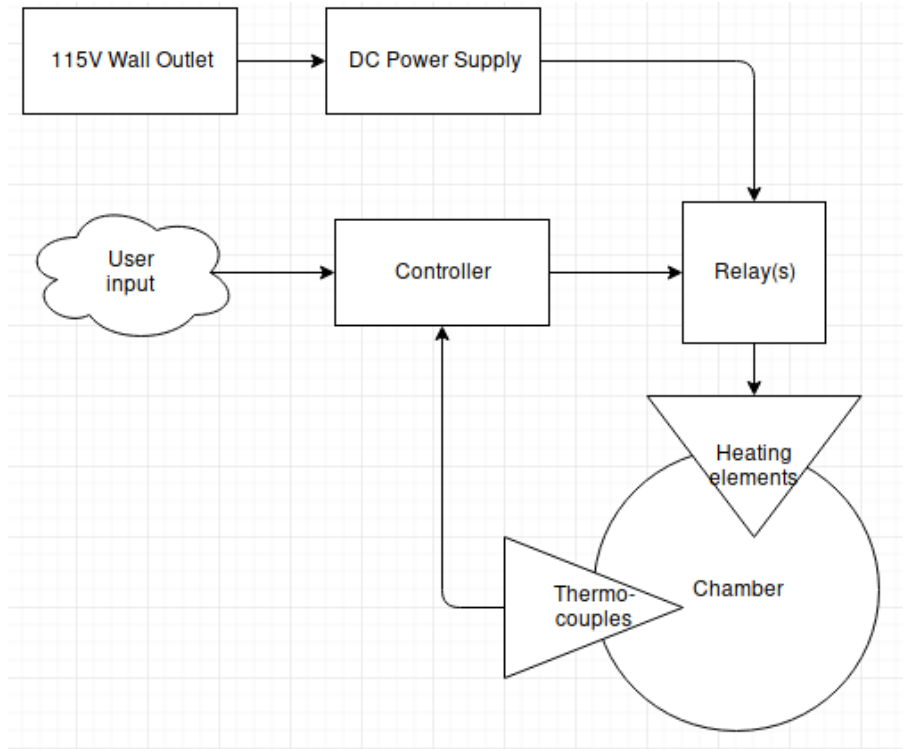


Figure 46: Basic system diagram.

Constraints governing the selecting of heating elements included:

- Safety: 50 V voltage limit, 1000 W power limit from power supply
- Geometry: width < 2 in., height as close to 18 in. as possible
- Performance: total power 2 kW at ambient, 1 kW at 200°C
- Rating: lead-free, ROHS-compliant, maximum operating temperature > 300°C
- Resistance: network the resistors for a net resistance allowing for maximum current draw at 36 V (maximum voltage output of the power supply)

With these constraints considered, 6 identical Ohmite 225 W resistors were selected and wired 2S3P (2 resistors in series per branch, 3 parallel branches), with a net resistance of 1.33  $\Omega$ , a maximum power output of 1350 W at ambient temperature, and maximum operating temperature of 450°C. A Kepco 36 V, 30 A programmable DC power supply was used to convert 110 V AC input to DC output. The power supply remote output is switched by a relay, controlled by a 5 V, 50 mA output from the controller.

K-type thermocouples were used as inputs to the temperature controller as their response

time is quicker than an RTD, they have the same resolution of 1°C as with an RTD, and they offer higher operating temperature capabilities at a lower cost. A high-level wiring diagram is shown in Figure 47.

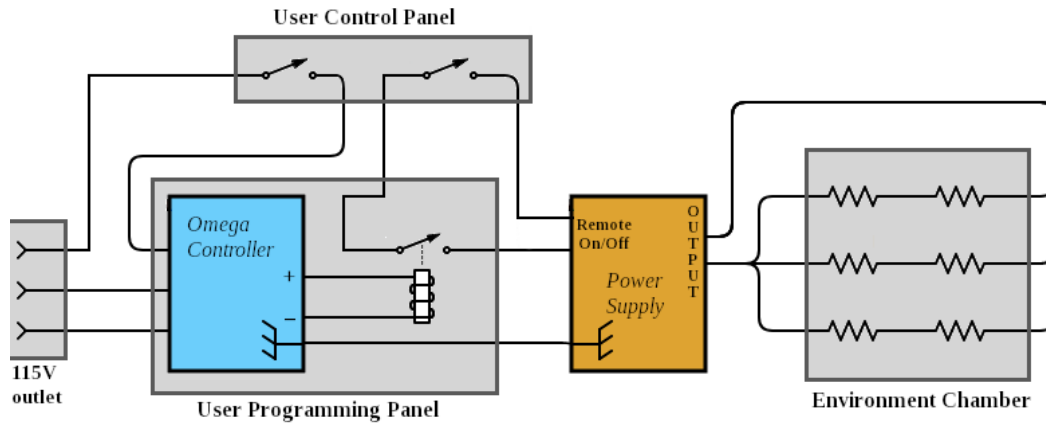


Figure 47: Diagram of control system.

## 6 System Integration, Tests, and Results

Taking into account our customer needs, design specifications, and safety considerations, we composed an experimental protocol to organize and plan out all the tests we needed to conduct to verify the performance and safety of the environment chamber (Figure 48).

### Experimental Protocol

#### Environment Chamber for Shape Memory Alloy Testing (ver. 3.0)

Evaluation	Equipment	Accuracy	Trials	Expected Outcome	Assumptions	Man-Hours
Exterior Surface Temp.	Environment Chamber, PID Controller, Thermocouples	1°C	8	< 40°C	200°C internal temperature. Steady-state.	3.0
Specimen Temp. Variation	Environment Chamber, PID Controller, Thermocouples	1°C	1	< ±5°C	200°C internal temperature. Steady-state.	7.5
Power Resistor Temp.	Environment Chamber, PID Controller, Thermocouples	1°C	4	< 250°C	200°C internal temperature. Steady-state.	1.5
Grip Temp.	Environment Chamber, PID Controller, Thermocouples	1°C	3	< 60°C	200°C internal temperature. Steady-state.	1.0
Load Cell Temp.	Environment Chamber, PID Controller, Thermocouples	1°C	3	< 40°C	200°C internal temperature. Steady-state.	1.0
Chamber Weight	Environment Chamber, Scale	0.1 lb	1	40 < 60 lb	N/A	0.1
Setup Time (install base, chamber, grips, & specimen)	Environment Chamber, Base, Grips, Specimen, Instron 4502 Testing Machine	1 sec	2	5-10	Start with Instron 4502 testing machine. Set up to working state.	0.2
Heat-up time, room temp. to 200°C	Environment Chamber, PID Controller, Thermocouples	1 sec	7	20-30 min	Start at 20°C, end at 200°C.	42.0
Steady-state error	Environment Chamber, PID Controller, Thermocouples	1°C	5	< 5%	200°C internal temperature. Steady-state.	12.0
Verify safe operation @ max. temp. (200°C)	Environment Chamber, PID Controller, Thermocouples	1°C	8	Safe operation (no materials melt/burn)	Silicone RTV, thermocouple Teflon coating begin to melt @ 260°C.	1.0

\*Most of the heating- & temperature-related trials are conducted simultaneously, with multiple thermocouples used for taking different measurements (man-hours for those tests just reflect the additional amount of time required to take those measurements and not the whole testing duration)

Figure 48: Experimental protocol used to organize and plan out all performance and safety validation tests to be conducted.

The most important results from these tests are discussed. For just a summary of measurements and test results compared against design specifications, refer to Figure 49.

### PRODUCT DESIGN SPECIFICATION

**Design Project:** Environment Chamber for Shape Memory Alloy Testing

**Team:** Environment Chamber for SMA Testing      **Date:** 7 June 2019      **Revision:** 3.0

**Datum Description:** Measurement of chamber evaluation metric

ELEMENTS/REQUIREMENTS	PARAMETERS		
	UNITS	DATUM	TARGET - RANGE
Measured specimen temp. variation @ 200°C interior temperature	°C		< ±5
Chamber Weight	lb	43	40-60
Setup time (install base, chamber, grips, & specimen on machine)	min	6.5	< 10
~Room temp. (20°C) to 200°C heat-up time	min	24-27	20-30
Max. safe operating temp.	°C	200	200-250
Steady-state error, short test (< 1 hr)	%	±3	< ±5
Steady-state error, long test (< 3 hr)	%	±1	< ±5
Max. exterior surface temp. @ 200°C interior temp., short test (< 1 hr)	°C	31	< 40
Max. exterior surface temp. @ 200°C interior temp., long test (< 3 hr)	°C	44	< 40
Max. power resistor temp. @ 200°C interior temp., short test (< 1 hr)	°C	255	250-300
Max. power resistor temp. @ 200°C interior temp., long test (< 3 hr)	°C	201	200-250
Max. grip temp. @ 200°C interior temp., short test (< 1 hr)	°C	48	< 60
Max. grip temp. @ 200°C interior temp., long test (< 3 hr)	°C	80	< 60
Max. load cell temp. @ 200°C interior temp., short test (< 1 hr)	°C	32	< 40
Max. load cell temp. @ 200°C interior temp., long test (< 3 hr)	°C	34	< 40
Power drawn during heat-up	W	< 800	< 1000

Figure 49: Summary of measurements and test results compared against all design specifications. The only criterion not tested for, due to time limitations, was the temperature variation along the length of a specimen.

To begin with testing, we focused on tuning the PID controller in order to shape the

heating response to meet the following criteria, based on the feedback and needs laid out by prospective end users:

- Minimize overshoot, response speed is not critical so long as it is reasonable (i.e., heat-up time is within 25-30 minutes)
- Avoid oscillation and instability in the response
- Prioritize consistent stabilization of the interior air temperature, minimize steady-state error

To do this, we manually adjusted the proportional, integral, and derivative gains (called proportional, reset, and rate bands in the controller) in 4 iterations. Instructions for how to do this PID tuning can be found in Appendix H: Using the Controller. Results from these tests are summarized in Table 7 and in Figure 50. The first gain iteration was run at a setpoint of 100°C due to time constraints on that day, but the other 3 thereafter were run at the maximum allowable temperature of 200°C. We conducted tests at this temperature to get a sense of a “worst-case scenario” or the longest times it would need to achieve heat-up and temperature stabilization.

Tests 2-3 were stopped before reaching steady-state as they showed significant overshoot and trended towards oscillation. Our desired response would be critically damped. As can be seen in the results of the fourth PID tuning test, we achieved what appears to be a slightly overdamped response, which was accurate enough for our purposes. With this gain setup, we achieved a heat-up time of 25 min and 40 sec, a steady-state error of 1%, and kept the power consumption well under the 1000 W limit.

Table 7: PID tuning test data. Note: Test 1 was conducted with a setpoint of 100°C, all other test setpoints were 200°C.

Test #	Prop. Gain	Integral Gain	Deriv. Gain	Settling Time (sec)	Steady-State Error (%)	Power (W)
1	5.00	0.05	0.00	550	3.0	690
2	5.00	0.50	5.00	N/A	8.5	690
3	5.00	0.50	15.00	N/A	7.0	690
4	5.00	0.05	15.00	1540	1.0	690

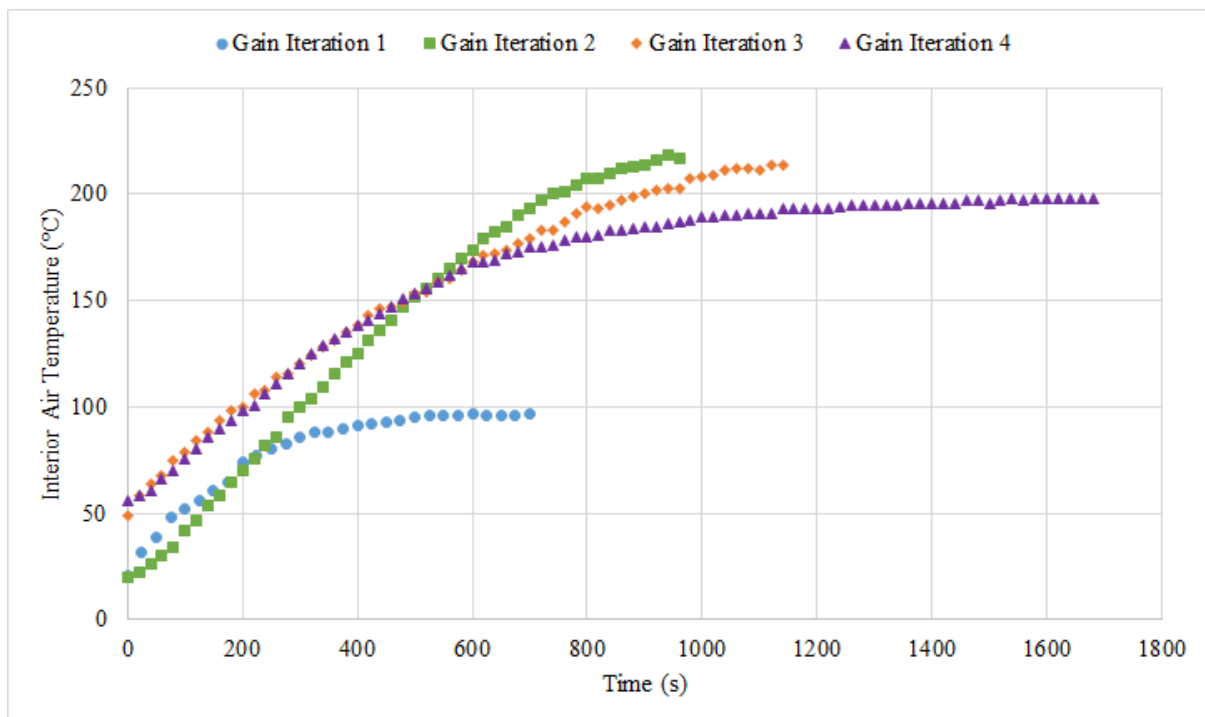


Figure 50: Gain iteration plots of the PID tuning tests.

After we were satisfied with calibration of the controller, we turned towards long-duration heating tests with the environment chamber installed on the Instron machine in the Materials Laboratory, in order to gauge how well the chamber maintains a stable temperature at the setpoint. Key results are summarized in Figure 49 and in Table 8.

Table 8: Performance validation test data. Note: Test 1 was conducted without access to the grips and load cell in the Materials Laboratory.

Test #	Duration (hr)	Steady-State Error (%)	Max. Exterior Wall Temp. (°C)	Max. Power Resistor Temp. (°C)	Max. Grip Temp. (°C)	Max. Load Cell Temp. (°C)
1	1.0	1	30	255	N/A	N/A
2	1.0	3	31	253	48	32
3	2.5	1	44	201	80	34

We found that our “worst-case scenario” (i.e., running the chamber at maximum allowable temperature for a long period of time) resulted in an exterior wall temperature of 44°C, which exceeded our conservative limit, but remained below the safe threshold of 45°C determined by Ungar and Stroud [15]. For all lower temperatures, the chamber can be run for over 2.5 hours without users having to worry about the temperature of the outer wall. The only other area in which the environment chamber failed to meet a safety specification, as can be seen in Figure 49, was the temperature of the grip. Running the chamber at maximum temperature for long time periods causes the top grip to reach a temperature of up 80°C, which is unsafe and poses a burn risk to users. Though we did not have time to implement this ourselves, we recommend machining down the diameter of the grip to accommodate placement of a silicone or rubber sleeve around the grip to protect users from inadvertently burning themselves due to accidental contact.

Load cell temperatures remained safe to the touch even in this scenario, but due to a lack of readily-available information on the load cell, we were not able to determine its sensitivity to temperature nor whether the heat of the grip could potentially influence its measurement accuracy.



## 7 Cost Analysis

The following table details the costs for the purchased components and/or manufactured parts necessary to construct the environment chamber.

Table 9: Breakdown of costs of purchased parts and materials that went into the finished environment chamber.

Component	Material	Vendor	Cost (\$)
10" OD Pipe	6061 Aluminum	Tube Service Co.	245.00
6" OD Pipe	6061 Aluminum	Tube Service Co.	155.00
12"x12"x0.125" Sheet (x2)	6061 Aluminum	Metal-Werx	29.49
6"x12"x0.250" Plate	6061 Aluminum	Metal-Werx	12.44
2"OD 0.125" Wall, 24" Len. Round Tube	6061 Aluminum	Metal-Werx	10.56
Temperature Controller	PID Controller	Omega (via eBay)	217.95
1.50"x1.50" 0.125" Wall, 24" Len. Box Tube	6061 Aluminum	Metal-Werx	9.60
1/4-20 Threaded Rod (x6)	Stainless Steel	Home Depot	30.54
Thermocouple (x2)	K-Type	Fry's Electronics	80.00
24"x54"x2" Insulation Blanket	Aluminosilicate	UniTherm	64.20
1/2" OD x 1/4" Tube (12" Length)	Alumina Ceramic	McMaster-Carr	46.50
Adhesive/Sealant	RTV Silicone	O'Reilly Auto Parts	9.80
Waterjet-Cut Plates	6061 Aluminum	Rustworks	386.75
<b>Total Cost: \$1,297.83</b>			

The following table details the components supplied to us by our sponsor Digital Loggers, Inc., and their respective costs. Please note that the precision-ground cold-rolled steel rod stock was actually provided to us by the Machine Shop manager Don MacCubbin.

Table 10: Breakdown of costs of sponsored parts and materials.

Item/Service	Material	Cost (\$)
Power Resistors ( x6)	Vitreous-enamel	200.00
Hinge (24 in. length)	Stainless Steel	60.00
Fasteners	Bolts, Nuts, Washers, Rivets, etc.	5.00
Silicone Rubber Sheets	High Temp. Silicone Rubber	47.00
Misc.	Latches & Handles	22.00
Precision-Ground Rod (24 in.)	12L14 Steel	25.00
<b>Total Cost: \$349.00</b>		

Certain manufacturing processes like splitting the pipes in half are omitted from the above table, as they were performed by the team's sponsor. A conservative estimate of manufacturing costs for welding, using typical local shop rates of \$120/hr for three hours of work, would put the total cost at roughly \$2000. If this chamber were to be mass-produced, manufacturing costs for welding, machining, and waterjet cutting would all be lower due to volume discounts offered by shops, placing the estimated production cost per chamber between \$1,600 and \$2,000.

## **8 Business Plan**

### **8.1 Introduction**

The team will provide researchers at universities and other research institutions with an environment chamber that is compatible with various tensile test machines. Doing so gives researchers flexibility with experimentation at elevated temperatures up to 200°C, since they are not limited by a chamber that is model-specific. Additionally, current model-specific chambers on the market can cost as much as \$10,000, meaning our chamber poses an appealing value-for-money proposition, especially for prospective users looking to test at relatively lower temperatures or who are working on tighter budgets.

### **8.2 The Company**

The environment chamber team consists of 3 senior Mechanical Engineering students in Santa Clara, California. Currently based at Santa Clara University. The team's primary customers will be researchers and university laboratories interested in expanding their testing capabilities at a modest price.

### **8.3 Services**

The environment chamber gives the user control over the temperatures they desire for specific experiments. Providing a service like this was broken into two subgroups that researchers will greatly appreciate, uniform temperature distribution and user-adjustable response time of the system. A key feature of this chamber is that the user has great flexibility with the PID temperature controller. If a scenario in which quick response time is desired, the proportional, integral, and derivative gains of the controller can be manually adjusted to obtain a more appropriate response time, as well as minimize steady-state error. Furthermore, the chamber comes with K-type thermocouples, however, the controller accepts other sensors like RTD's and different type thermocouples as input if the users feels a different sensor is more adequate for their purposes.

## 8.4 Market Analysis/Competition

The market for this product is limited due to the nature of this project. It is a tool for expanding research capabilities at a lower cost than other model-specific chambers in the market, like those produced by Instron. However, not all universities and research institutions will be in need of an environment chamber. Additionally, large companies that focus on environmental testing typically use chambers that whose capabilities and features far exceed those of our design. To avoid this competition, we offer a product at a much more affordable rate, suitable for small projects, relatively low-temperature applications, and for expanding the scope of student laboratory experiments. This is not a product that we expect will supplant any of the high-grade environment chambers favored by professional laboratories and industry leaders.

## 8.5 Manufacturing Plans

Low volume projects would need to be manufactured in house by the employees. The team reached out to local manufacturing shops like Bright Light Welding and Manufacturing, BTLaser, and Rustworks to obtain cost estimates for manufacturing out-of-house. All shops quoted \$1,300-\$1,600 with a minimum 2-4 week lead times, for the machining, welding, and assembly of metal components. Installation of ceramic components, insulation, and silicone rubber sheets and RTV sealant would need to be done in-house. Due to the expected low-volume demand, manufacturing of components and assembly would need to be performed in-house, as shops typically offer discounts only for large production volumes. This entails the use of a lathe, vertical mill, table saw, MIG/TIG welding equipment, soldering equipment, and other standard light fabrication and machine shop tools. After building one chamber and understanding the best way to go about this manufacturing process, the team is confident in being able to produce a completed environment chamber every 4-6 weeks (again, this is expected for very low-volume production).

## **8.6 Cost and Price**

One unit would cost between \$1,600-\$2,000, so we will assume a production cost \$1,800/unit. As there are table-top environment chambers that are priced as high as \$15,000 [25], we have significant leeway in determining a lower price than that which still grants us sufficient profits to maintain and grow the business. We would offer our environment chamber to customers at \$3,600/unit.

## **8.7 Service or Warranties**

A warranty of 2 years would be offered. The chamber was designed so that frequent services are not necessary, with many components lasting the lifetime of the chamber (barring misuse or accidental damage caused by the user). Services include replacement of faulty electrical components, such as the PID controller, power supply, relay, or power resistors. In addition, faulty hardware such as latches and other base components will be replaced at no cost to the customer throughout the 2 year warranty period.

## **8.8 Conclusion**

In conclusion, starting a business targeting the very limited market that this design addresses is not advisable. As previously mentioned, the purpose of this chamber is to aid the research of Dr. Wheat, Dr. Kitts, and other researchers at Santa Clara University. Additionally, large companies that perform high-volume, comprehensive testing for advanced engineering projects require environment chambers with far greater capabilities. The small potential market coupled with the cost of manufacturing one unit would not outweigh the startup costs required for initiating a business.

## **9 Engineering Standards and Realistic Constraints**

### **9.1 Economic**

Minimizing costs was a key consideration in every step of the design process so far; as existing environment chambers and test furnaces on the market offer far greater utility and more features, we had to focus on minimizing the cost to build ours in order to present a value-for-money advantage for prospective users who need a low-cost chamber for relatively low-temperature testing. For instance, resistive heating elements were used, as opposed to more expensive radiative heating elements and elliptical reflectors.

Another economic consideration is cross-compatibility with multiple testing machines. This means that our end users need not purchase a chamber for each testing machine in the Materials Laboratory, as our environment chamber is compatible with the Instron and MTS models currently in use.

### **9.2 Environmental**

The primary environmental concern was the power used to heat the furnace. Power is received from a 115 V, 60 Hz wall outlet, and the electric power likely originates from burning natural gas, coal, or petroleum. All of these energy sources are harmful to the environment, and thus it was necessary to keep power usage as low as was reasonably possible while still meeting performance targets. Combining this with the university's safety regulations, we decided to cap our maximum power consumption at 1000 W. This was accomplished by minimizing heat loss from the furnace to the surrounding environment, by sealing and insulating the furnace as well as possible, thereby improving the heating efficiency of the system. We were able to achieve a maximum power consumption of about 800 W as a result.

### **9.3 Sustainability**

Designing for sustainability was a consideration of the materials and components selection stage of the design process. We sought to use materials that would last for as long as

possible, thus minimizing potential waste and environmental contamination associated with replacing and/or discarding components. For instance, many insulating materials, such as asbestos, have excellent thermal properties, but do not degrade naturally, cannot be recycled, and can pose long-term health risks to people in contact with them. The use of aluminosilicate ceramic fiber eliminated the need to replace the insulation within the chamber's life-time. Additionally, the power resistors used for heating operate at temperatures up to 56% of their maximum operating temperature, further reducing the likelihood of damaging them from overuse.

## **9.4 Health and Safety**

The two largest health and safety concerns are the high temperatures produced by the heating elements, and exposure to harmful materials. To minimize the risk of burns, an appropriate amount of insulation was used to keep the chamber exterior surface temperature below 40°C (a temperature below which users will not be burned) for at least 2 hours of continuous use (measured for the maximum operating temperature). Further, the chamber is designed to seal the interior air from the surrounding environment, preventing hot air from escaping.

The aluminosilicate ceramic fiber chosen for insulation disperses small particles when cut, is very abrasive, and causes irritation if direct contact is made. In order to eliminate exposure risks, the insulation was very securely and thoroughly sealed in the chamber, and we ensured that replacement of the insulation would not be necessary throughout the chamber's lifetime, since it is rated for continuous use up to 1300°C, far greater than our maximum operating temperature of 200°C.

We also avoided the use of harmful materials such as asbestos, mercury, and beryllium, all of which pose significant health risks if inhaled or ingested.

## **9.5 Manufacturability**

Improving manufacturability allows for a lower cost of production, shorter turnover times, and may save raw materials. To accomplish this, a flexible ceramic fiber blanket was chosen for insulation, thus eliminating the need to purchase or custom order costly ceramics

that have been manufactured to a specific geometry (as would have been required for calcium silicate insulation, which we had initially planned to use).

The chamber was designed mostly from aluminum (save for a few stainless steel parts), in order to keep weight down and to ensure parts would be easily machinable. Stainless steel was largely avoided due to its poor machinability. Also, the majority of the chamber and the entirety of the base were assembled with mechanical fasteners (nuts, bolts, rivets, etc.), in order to reduce the cost and lead times for production by forgoing welding for all but the walls of the chamber.



## 10 Summary and Conclusions

### 10.1 Overall Evaluation of Design

The environment chamber heats up to the target 200°C in roughly 25 minutes and the exterior wall temperature does not exceed the safety threshold of 40°C until 2 hours of continuous use. However, the primary mode of heat transfer from the power resistors to the specimen is natural convection, thus causing steady-state to occur after 2.5 hours and an exterior wall temperature of 44°C. Additionally, the maximum grip temperature met the target range in Figure 49 after one hour of continuous use but exceeded it after 2.5 hours of continuous use. Another crucial parameter that needed to be satisfied was the weight of the chamber; a final weight of 43 lb. satisfying the target range. The power consumption of the heating elements did not exceed 800W, making it fall well below the maximum power consumption of 1000 W. Another imperative parameter was the steady-state error of the chamber, resulting  $\pm 3\%$  after a short test (<1 hr.) and  $\pm 1\%$  after a long test (<3 hr.). Further, these results come from operating the chamber at 200°C. The exterior wall and grip temperatures would not be as high if the chamber is used to test SMA's with lower transition temperatures.

### 10.2 Future Work

Future work will focus primarily on application of the chamber for SMA testing, and possibly on implementation of additional features. The objective of this project was to create an environment chamber to enable testing of SMA specimens on the Instron and MTS machines within the Materials Laboratory; Dr. Kitts has expressed his intent to use the chamber over the summer and in the coming Fall Quarter to conduct these tests. One key action that must be taken first is to run a few tests with a wire specimen installed in the chamber, in order to gauge how evenly the chamber provides heating (i.e., verify that the environment chamber meets the performance specification of a maximum temperature variation along a specimen of  $\pm 5^\circ\text{C}$ ). Should the temperature distribution be undesirably high:

- The vertical positions of the power resistors in the chamber can be adjusted with

crescent wrenches to try to eliminate cold spots (this can be done in 10-15 minutes)

- The PID controller can be tuned to adjust the heating response as desired (modifying gains can be done within 2 minutes per iteration)
- The user can wait for the interior air temperature to reach steady-state before initiating tests (takes up to 2 hours when operating at the maximum allowable set-point temperature of 200°C, and is quicker for lower set-point temperatures)

Additionally, in order to decrease the time required to conduct each test, one might investigate the digital output capabilities of the controller, so that a computer could log all of the data from the controller without requiring manual data recording by the user.

Additional features could be implemented to the chamber, such as a window to allow for optical extensometry, or a simple cooling system to allow for higher internal temperatures, and more rapid cool-down times. Furthermore, the implementation of a forced convection system would greatly reduce the time it takes to obtain a uniform temperature distribution within the chamber.

These actions would be undertaken by future users of the environment chamber in the Materials Laboratory.

### **10.3 Lessons Learned**

We learned that outsourcing manufacturing processes from machine shops is unfavorable with projects that have low quantities due to shop minimums and equipment set-up time. Due to this, it was preferable to perform most machining and assembly in the Santa Clara University Machine Shop. Additionally, obtaining quotes from local shops to come to this conclusion was time consuming, causing delays that stressed the project timelines. Also, as the manufacturing and assembly stage gained momentum, we found that welding should be avoided if time constraints and budget are a concern. For example, the base had to be converted to a bolt-on assembly due to the shortage in budget and time.

## References

- [1] C. Webb, “SMA Tests 2018,” Dept. of Mech. Eng., Santa Clara Univ., Santa Clara, CA, USA, 2018.
- [2] P. Chowdhury, “Frontiers of Theoretical Research on Shape Memory Alloys: A General Overview,” *Shape Memory and Superelasticity*, vol. 4, no. 1, pp. 26-40, Mar. 2018. Available: <https://doi.org/10.1007/s40830-018-0161-4>. [Accessed: 1 Oct. 2018].
- [3] M. Suru, N. Lohan, B. Pricop, E. Mihalache, M. Mocanu, and L. Bujoreanu, “Precipitation Effects on the Martensitic Transformation in a Cu-Al-Ni Shape Memory Alloy,” *Journal of Materials Engineering and Performance*, vol. 25, no. 4, pp. 1562-1569, Feb. 2016. doi: 10.1007/s11665-016-1981-z. [Accessed: 15 May 2019].
- [4] I. Ivanić, S. Kožuh, T. H. Grgurić, B. Kosec, M. Gojić, “The Influence of Heat Treatment on Microstructure and Phase Transformation Temperatures of Cu-Al-Ni Shape Memory Alloy,” *Kemija u Industriji, Journal of Chemists and Chemical Engineers of Croatia*, vol. 68, no. 3-4, pp. 111-118, 2019. doi: 10.15255/KUI.2018.037. [Accessed: 16 May 2019].
- [5] *Standard Test Method for Mechanical Uniaxial Pre-strain and Thermal Free Recovery of Shape Memory Alloys*, ASTM E3098-17, ASTM International, West Conshohocken, PA, USA, 2017. [Online]. Available: <https://doi-org.libproxy.scu.edu/10.1520/E3098-17>.
- [6] J. Kolansky, P. Tarazaga, and O. J. Ohanian, III, “Experimental Implementation of Opposed Shape Memory Alloy Wires for Actuator Control,” *Journal of Vibration and Acoustics*, vol. 137, no. 1, pp. 011007-1-011007-7, Nov. 2014. doi: 10.1115/1.4028831. [Accessed: 13 Oct. 2018].
- [7] Y. Jia, Z. Yu, L. Li, and Z. Wu. “A Review of Applications and Research of Shape Memory Alloys in Civil Engineering,” in *2018 IOP Conf. Ser.: Mater. Sci. Eng., 22-24 June 2018, Zhuhai, China*. [Online]. doi: 10.1088/1757-899X/392/2/022009. [Accessed: 1 Oct. 2018].
- [8] R. Dasgupta, “A look into Cu-based shape memory alloys: Present scenario and future prospects,” *Journal of Materials Research*, vol. 29, no. 16, pp. 1681-1698, July

2014. doi: 10.1557/jmr.2014.189. [Accessed: 23 Oct. 2018].
- [9] J. Ertel and S. Mascaro, “Dynamic Thermomechanical Modeling of a Wet Shape Memory Alloy Actuator,” *Journal of Dynamic Systems, Measurement, and Control*, vol. 132, no. 5, pp. 051006-1-051006-9, Aug. 2010. doi: 10.1115/1.4002067. [Accessed: 21 Oct. 2018].
- [10] C. Tang, W. M. Huang and C. C. Wang, “From Dual-Shape/Temperature Memory Effect to Triple-Shape Memory Effect in NiTi Shape Memory Alloys,” *Advances in Science and Technology*, vol. 78, pp. 1-6, Sept. 2012. doi:10.4028/www.scientific.net/AST.78.1. [Accessed: 28 Oct. 2018].
- [11] M. Bagherpour, A. Shokouhfar, A. Zolriasatein, A. F. Bahelgerdy, “Effect of Severe Plastic Deformation on Shape Memory and Mechanical Properties of Nanostructured Cu-Zn-Al Alloy,” *Journal of Nano- & Electronic Physics*, vol. 9, no. 1, pp. 01008–01008–6, Feb. 2017. doi: 10.21272/jnep.9(1).01008 [Accessed: 5 Nov. 2018].
- [12] H. C. Kyeong, H. M. Kim, Y. Kim, S. Y. Yang, and H. R. Choi, “Multiple Inputs-Single Accumulated Output Mechanism for Soft Linear Actuators,” *Journal of Mechanisms and Robotics*, vol. 11, no. 1, pp. 1-14, Oct. 2018. doi: 10.1115/1.4041632 [Accessed: 5 Nov. 2018].
- [13] S. N. Saud, E. Hamzah, T. Abubakar, H. R. Bakhsheshi-Rad, M. Zamri, and M. Tanemura, “Effects of Mn Additions on the Structure, Mechanical Properties, and Corrosion Behavior of Cu-Al-Ni Shape Memory Alloys,” *Journal of Materials Engineering and Performance*, vol. 23, no. 10, pp. 3620-3269, July 2014. doi: 10.1007/s11665-014-1134-1. [Accessed: 14 May 2019].
- [14] M. Zare and M. Ketabchi, “Effect of chromium element on transformation, mechanical and corrosion behavior of thermomechanically induced Cu–Al–Ni shape-memory alloys,” *Journal of Thermal Analysis and Calorimetry*, vol. 127, pp. 2113-2123, Mar. 2017. doi: 10.1007/s10973-016-5839-2. [Accessed: 14 May 2019].
- [15] E. Ungar and K. Stroud. “A New Approach to Defining Human Touch Temperature Standards,” in *40th Int. Conf. on Env. Stud., 11–15 July 2010, Barcelona, Spain*. [Online]. Available: <https://doi.org/10.2514/6.2010-6310>. [Accessed: 6 Nov. 2018].

- [16] “Environmental Chamber for Floor Model Systems,” *Instron Environmental Chamber for Floor Model Systems - Instron*. [Online]. Available: <http://www.instron.us/en-us/products/testing-accessories/environmental-chambers-furnaces/environmental-chambers/chambers/3119-610>. [Accessed: 16 Oct. 2018].
- [17] “Series 651 Environmental Chambers,” *MTS Systems Corporation*. 2018. [Online] Available: <https://www.mts.com/cs/groups/public/documents/library/dev003712.pdf>. [Accessed: 17 Oct. 2018].
- [18] “High-Temperature High-Cycle Fatigue (HCF) Standard Solution,” *MTS Systems Corporation*. Copyright 2012. [Online]. Available: <http://www.mts.com/cs/groups/public/documents/library/mts006632.pdf>. [Accessed: 10 Oct. 2018].
- [19] “Rhodium furnace Model 6.225.6,” *Research Equipment Database*. 2009. [Online]. Available: <http://eqdb.nrf.ac.za/equipment/thermal-analysis-system/netzsch-gmbh-rhodium-furnace-calorimetry-module-simultaneous>. [Accessed 17 Oct. 2018].
- [20] DS Industries, “Ceramic Fiber Blanket Safety Data Sheet,” CF datasheet, n.d. [Revised June 2016].
- [21] L. L. C. Engineers Edge, “Convective Heat Transfer Coefficients Table Chart,” *Engineers Edge - Engineering, Design and Manufacturing Solutions*, 11-Feb-2015. [Online]. Available: [https://www.engineersedge.com/heat\\_transfer/convective\\_heat\\_transfer\\_coefficients\\_13378.htm](https://www.engineersedge.com/heat_transfer/convective_heat_transfer_coefficients_13378.htm). [Accessed: 8 June 2019].
- [22] Optotherm Support, “Emissivity in the Infrared Emissivity Values” *Optotherm Thermal Imaging*. [Online]. Available: <https://www.optotherm.com/emiss-table.htm>. [Accessed: 4 Jan. 2019].
- [23] “Emissivity Coefficients Materials,” *Engineering ToolBox*. [Online]. Available: [https://www.engineeringtoolbox.com/emissivity-coefficients-d\\_447.html](https://www.engineeringtoolbox.com/emissivity-coefficients-d_447.html). [Accessed: 4 Jan. 2019].
- [24] “Aluminum 6061-T6; 6061-T651,” *ASM Aerospace Specification Metals Inc.* [Online]. Available: <http://asm.matweb.com/search/SpecificMaterial.asp?bassnum=MA6>

- 061T6. [Accessed: 8 Nov. 2018].
- [25] “TH-PE Temperature and Humidity Chamber,” *LabIncubators.net*. [Online]. Available: [https://labincubators.net/products/th-pe-temperature-and-humidity-chamber?variant=40430163152&utm\\_medium=cpc&utm\\_source=google&utm\\_campaign=Google Shopping&gclid=Cj0KCQjwrDjnBRDXARIsAEcE5YnBajDm2egoBDLGE6RElOOHqX1qLw-X7\\_zssUTOcvxMonhJy6FhjkaAq6TEALw\\_wcB](https://labincubators.net/products/th-pe-temperature-and-humidity-chamber?variant=40430163152&utm_medium=cpc&utm_source=google&utm_campaign=Google+Shopping&gclid=Cj0KCQjwrDjnBRDXARIsAEcE5YnBajDm2egoBDLGE6RElOOHqX1qLw-X7_zssUTOcvxMonhJy6FhjkaAq6TEALw_wcB). [Accessed: 7 June 2019].
- [26] ”Enthalpy of Moist Air,” *The Engineering Toolbox*. [Online]. Available: [https://www.engineeringtoolbox.com/enthalpy-moist-air-d\\_683.html](https://www.engineeringtoolbox.com/enthalpy-moist-air-d_683.html). [Accessed: 6 Nov. 2018].
- [27] T. L. Bergman, A. S. Lavine, F. P. Incropera, and D. P. Dewitt, *Fundamentals of Heat and Mass Transfer*, 7th ed. Hoboken, NJ: John Wiley & Sons, 2011.
- [28] “Air Properties - SI Units,” *Engineering ToolBox*. [Online]. Available: [https://www.engineeringtoolbox.com/air-properties-d\\_1257.html](https://www.engineeringtoolbox.com/air-properties-d_1257.html). [Accessed: 10 June 2019].
- [29] ”Horizontal Cylinder Natural Convection Coefficient Calculator.” *Engineers Edge*. [https://www.engineersedge.com/heat\\_transfer/horizontal\\_cylinder\\_natural\\_convection\\_13970.htm](https://www.engineersedge.com/heat_transfer/horizontal_cylinder_natural_convection_13970.htm) [Accessed: 18 Nov. 2018].
- [30] U.S. Department of Energy, National Renewable Energy Laboratory, *Scanning Electron Microscopy*. [Online]. Available: <https://www.nrel.gov/materials-science/scanning-electron.html>. [Accessed: 11 Mar. 2019].
- [31] Central Microscopy Research Facility, *Scanning Electron Microscopy*, The University of Iowa, Iowa City, IA. [Online]. Available: <https://cmrf.research.uiowa.edu/scanning-electron-microscopy>. [Accessed: 16 Mar. 2019].
- [32] J. Goodge, *Energy-Dispersive X-Ray Spectroscopy (EDS)*, Science Education Resource Center, Carlton College, 26 April 2017. [Online]. Available: [https://serc.carleton.edu/research\\_education/geochemsheets/eds.html](https://serc.carleton.edu/research_education/geochemsheets/eds.html). [Accessed: 16 Mar. 2019].

- [33] R. A. Marks, “MECH 15 Lab Manual: Exercise #3 Effects of Annealing on the Microstructure and Tensile Behavior of a Cu-Zn Alloy,” course materials for MECH 15: Introduction to Materials Science, Dept. of Mech. Eng., Santa Clara Univ., Santa Clara, CA, USA, 2016.
- [34] R. A. Marks, “MECH 15 Lab Manual: Appendix VI Refining Uniaxial Tensile Test Data when Total Load-Train Displacement is Measured,” course materials for MECH 15: Introduction to Materials Science, Dept. of Mech. Eng., Santa Clara Univ., Santa Clara, CA, USA, 2016.
- [35] “Modulus of Elasticity for Metals.” *AmesWeb*. <https://www.amesweb.info/Materials/Modulus-of-Elasticity-Metals.aspx> [Accessed: 22 May 2019].
- [36] *CN1500 Series Multi-Zone Ramp & Soak Controller User’s Guide*, Omega Engineering Inc., Norwalk, CT, USA, 1999.

## Appendix A: Hand Calculations

The tube chamber used for hand calculations is sketched below:

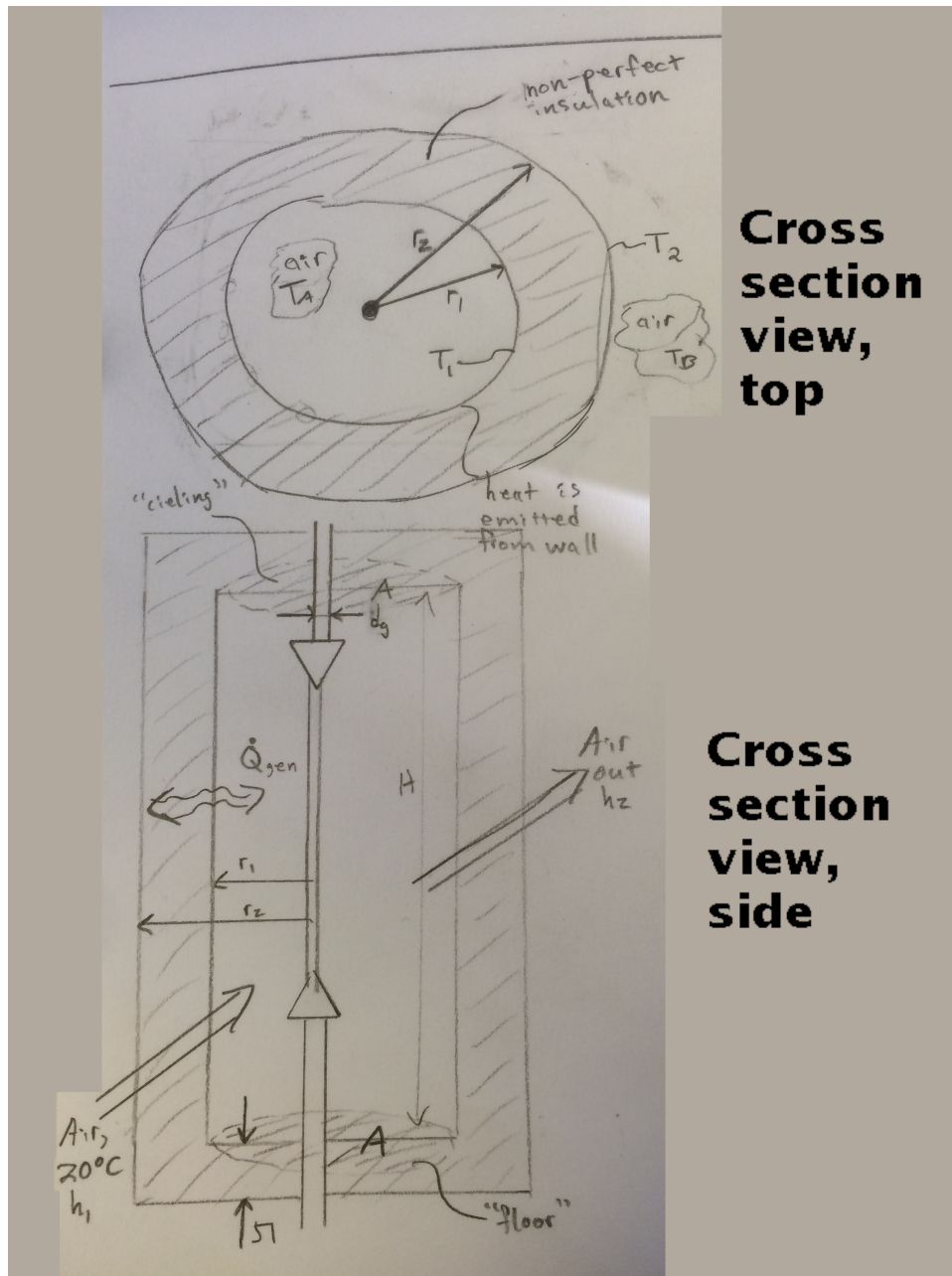


Figure 51: Sketch of furnace for hand calculations.

The assumptions have been discussed in the above Section 2: System, Environment, and Assumptions.

Values used are:

- $r_1 = 3$  in



- $r_2 = 5$  in
- $T_1 \approx T_A = 200^\circ\text{C}$
- $T_2 \approx T_2 = 20^\circ\text{C}$
- $H = 18$  in
- $t = 3$  in
- $d_g = 1$  in
- $A = \pi(3\text{in})^2 - \pi(0.5\text{in})^2 \approx 27.5$  in<sup>2</sup>
- $h_{hot} = 473 \frac{\text{kJ}}{\text{kg}}$  [26]
- $h_{cold} = 293 \frac{\text{kJ}}{\text{kg}}$  [26]
- $k = 0.072 \frac{\text{W}}{\text{m}\cdot\text{K}}$  [27]
- $\dot{V}_{air} = 1.5 \frac{\text{cm}^3}{\text{sec}}$
- $\dot{m}_{air} = 4.1\text{E-}6 \frac{\text{kg}}{\text{sec}}$
- $h_1$  and  $h_2$  are neglected
- $\dot{Q}_{gen} = 300\text{W}$
- Number of heating elements = 8
- Diameter of heating elements =  $\frac{1}{4}$  in
- $A_s = 0.0045$  m<sup>2</sup>

General equations for convective and conductive heat transfer are found in the textbook used for MECH 123: Heat Transfer and MECH 125: Thermal Systems Design [27]. Considering the system at steady-state, the energy balance for the entire system is:

$$\dot{Q}_{gen} = \dot{Q}_{loss} \quad (1)$$

Where  $\dot{Q}_{gen}$  is the heat output by the resistive heating elements, and  $\dot{Q}_{loss}$  is the heat lost to the environment. The heat output by the resistive heaters is:

$$P = IV = I^2R \quad (2)$$

The heat loss rate to the environment is simplified as consisting of heat loss through the walls of the chamber, heat loss through the ceiling and floor of the chamber, and heat loss through the grip fixture. It is also assumed that some amount of air enters the chamber at ambient temperature at a constant rate, and that an equivalent amount of hot air exits at the same rate.

$$\dot{Q}_{res} = \dot{Q}_{ins} + \dot{Q}_{grip} + \dot{Q}_{air} \quad (3)$$

Where the heat loss through insulation is:

$$\dot{Q}_{ins} = \dot{Q}_{wall} + \dot{Q}_{floor,ceiling} + \dot{Q}_{res,wall} \quad (4)$$

The heat loss through the walls of the chamber is:

$$\dot{Q}_{wall} = 2\pi r_2 h_o (T_A - T_B) H \quad (5)$$

Where the overall heat transfer coefficient  $h_o$  is found with:

$$\frac{1}{h_o} = \frac{1}{h_2} + \frac{r_2}{k} \ln\left(\frac{r_2}{r_1}\right) + \frac{r_2}{r_1 h_1} \quad (6)$$

The heat loss through the floor and ceiling of the chamber is:

$$\dot{Q}_{floor,ceiling} = \frac{T_A - T_B}{\frac{1}{h_1 A} + \frac{t}{kA} + \frac{1}{h_2 A}} \quad (7)$$

And the heat loss from the resistive heating elements through the wall is:

$$\dot{Q}_{res,wall} = \frac{HkA_s(T_w - T_2)}{t} \quad (8)$$

The heat loss through the grips is assumed to be negligible:

$$\dot{Q}_{grips} \approx 0 \quad (9)$$

The heat loss by cold air entering and hot air leaving is:

$$\dot{Q}_{air} = \dot{m}_{air}(h_{hot} - h_{cold}) \quad (10)$$

Combining the above equations yields:

$$P = IV = I^2 R = \frac{HkA_s(T_w - T_2)}{t} + \frac{2\pi r_2(T_A - T_B)H}{\frac{r_2}{r_1 h_1} + \frac{r_2}{r_1} \ln\left(\frac{r_2}{r_1}\right) + \frac{1}{h_2}} + \frac{2(T_A - T_B)}{\frac{1}{h_1 A} + \frac{t}{kA} + \frac{1}{h_2 A}} + \dot{m}(h_{hot} - h_{cold}) \quad (11)$$

The wall temperature is determined by approximating the heat transfer from the heating elements through the wall as one-dimensional, yielding:

$$\dot{Q}_{ele,wall} = H \left[ hA(T_{wire} - T_{air}) + \frac{kA(T_{wire} - T_{\infty})}{t} \right] \quad (12)$$

This equation provides a relationship between the power output of the heating elements and the resulting wall temperature:

Table 11: Heater power and resultant estimated heating element temperature.

$\dot{Q}_{gen}$ (W)	0	100	200	300	400	500
$T_w$ (°C)	168	324	480	635	791	947

Heat loss from air escaping through holes for plumbing instrumentation and grips into the chamber was calculated. In order to determine if the heat loss was a concern, the control volume calculation was performed below was performed with the following assumptions.

- Mass flow rates of air estimated from assuming  $1 \frac{cm^3}{s}$  of air through the gaps
- Air temperature inside assumed to be 200°C
- Air temperature outside assumed to be 20°C

Additionally, the enthalpy values were determined from the assumed air temperatures via linear interpolation [28].

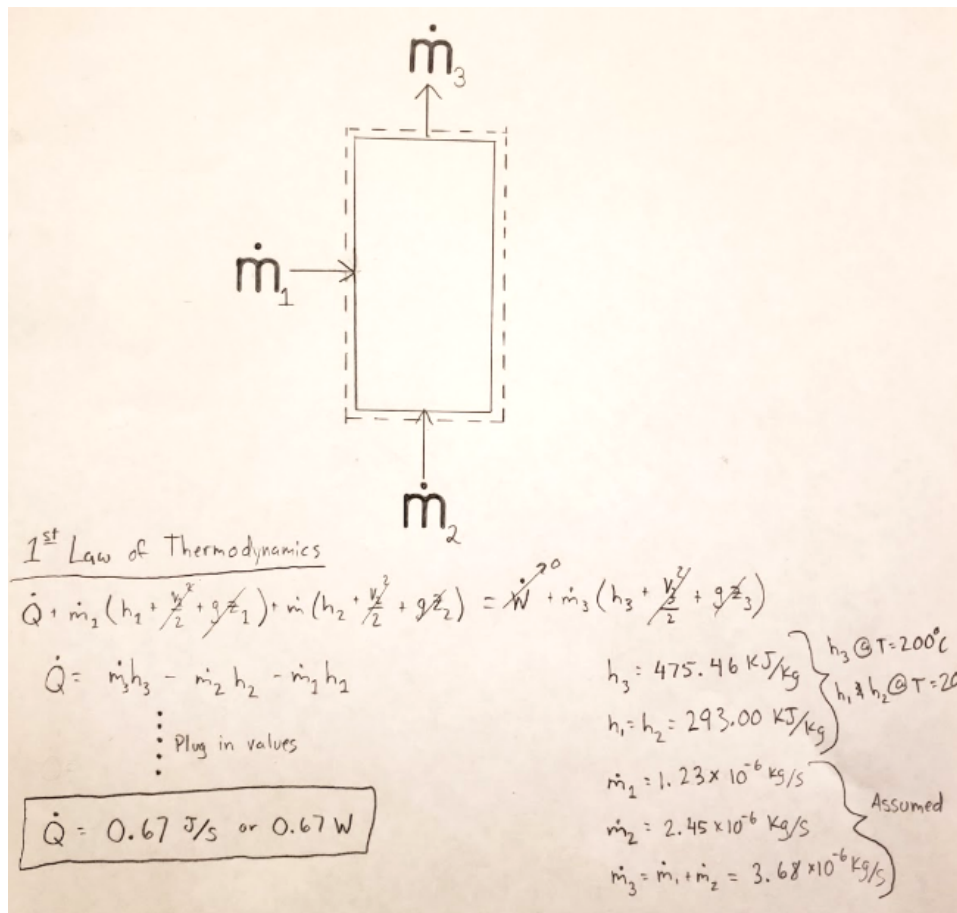


Figure 52: Sketch of control volume calculation for heat loss from escaping air.

The calculated loss of 0.67 W was not a concern because the power input was expected to be three orders of magnitude higher.

Natural convection coefficients for a cylindrical surface surrounded by a fluid are calculated with the following spreadsheet [29]:

Inputs			Calculations		
Fluid Temp, $T_a =$	200	$^{\circ}\text{C}$	Temp Diff, $\Delta T =$	150	$^{\circ}\text{C}$
Surface Temp, $T_s =$	350	$^{\circ}\text{C}$	Abs. Film Temp, $T_f =$	548	$^{\circ}\text{K}$
Film Temp., $T_f =$ [ $T_s = (T_a + T_s)/2$ ]	275	$^{\circ}\text{C}$	Prandtl Number, $Pr =$	0.6	
Cylinder Diam., $D =$	0.2	m	Grashof Number, $Gr =$	9.22E+07	
Fluid Density, $\rho =$	1.225	kg/m <sup>3</sup>	Rayleigh No., $Ra =$	5.12E+07	
Fluid viscosity, $\mu =$	1.87E-05	N-s/m <sup>2</sup>			
Fluid Sp. Heat, $C_p =$	1	J/g- $^{\circ}\text{K}$	$Nu =$	44	
Fluid Sp. Heat, $C_p =$	1000	J/kg- $^{\circ}\text{K}$	$h =$	7.49	W/m <sup>2</sup> -K
Fluid Thermal Conductivity, $k =$	0.03365	J/s-m-K			
Fluid Thermal Expans. Coeff, $\beta =$	0.001824	$^{\circ}\text{C}^{-1}$			

$$Nu = \left\{ 0.60 + \frac{0.387 Ra^{1/6}}{[1 + (0.559/Pr)^{9/16}]^{8/27}} \right\}^2$$

$$Gr = \frac{D^3 \rho^2 g \Delta T \beta}{\mu^2} \quad Nu = \frac{h D}{k} \quad Pr = \frac{\mu C_p}{k}$$

for  $Ra \leq 10^{12}$  ( $Ra = Gr Pr$ )

Natural Convection Heat Transfer from an Isothermal Horizontal Cylinder

Figure 53: Spreadsheet used for natural convection coefficient calculations [29].

# Appendix B: Parts and Assembly Drawings

## Chamber Drawings

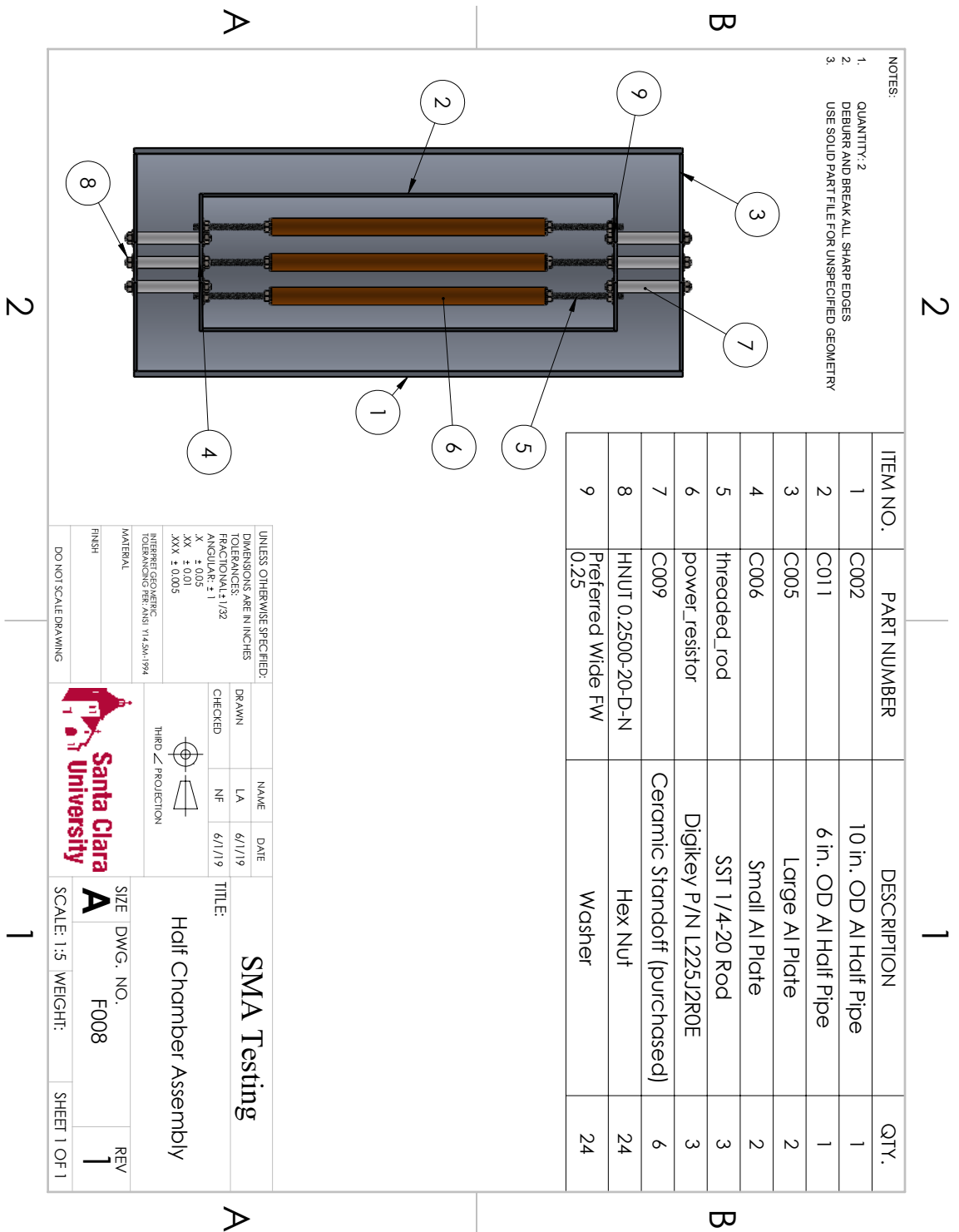


Figure 54: Drawing of a chamber assembly half.

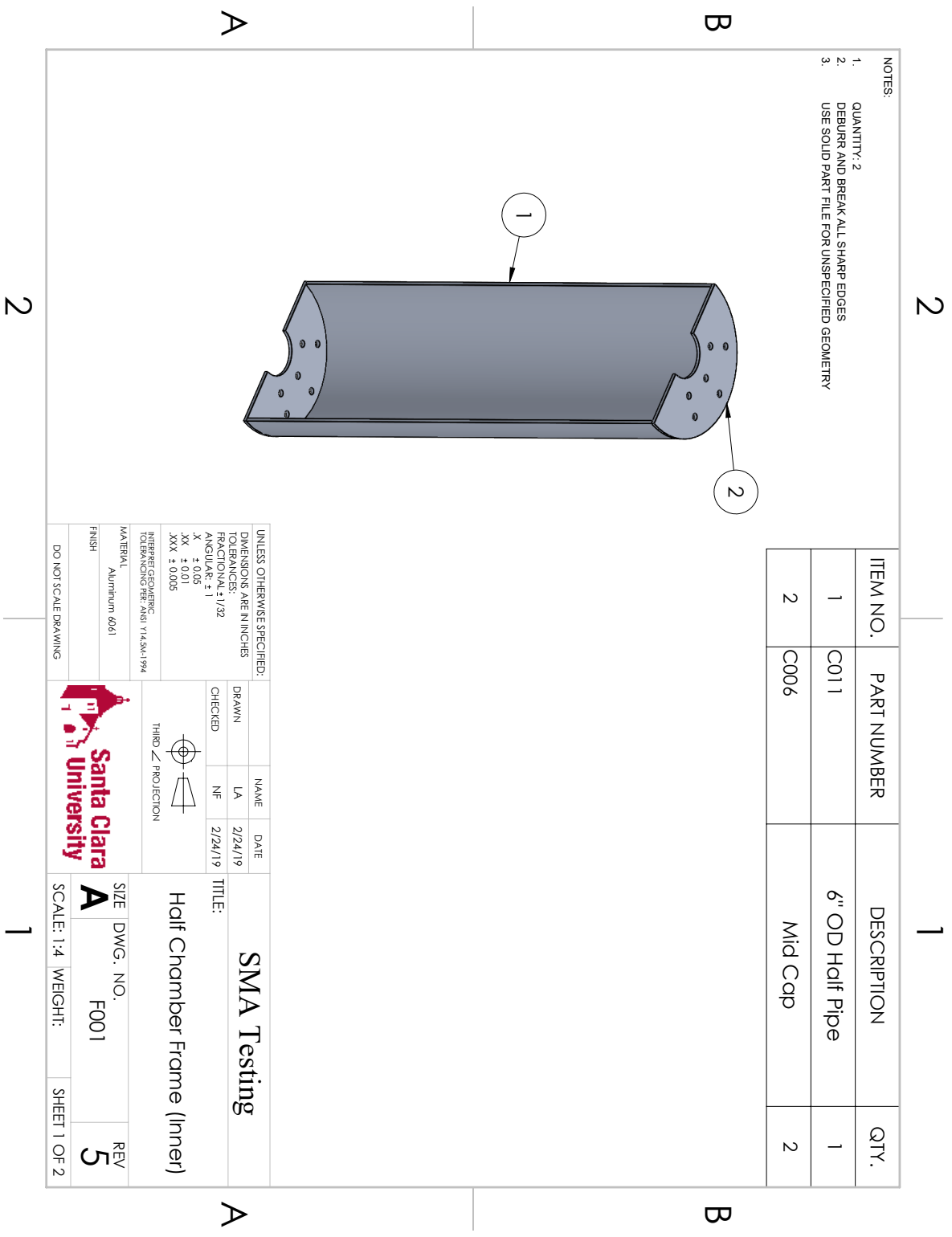


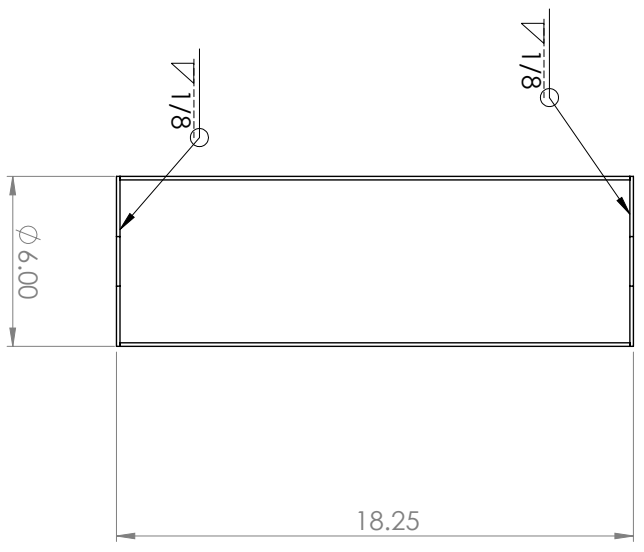
Figure 55: Drawing of the inner chamber frame.

2

1

NOTES:

- 1. QUANTITY: 2
- 2. DEBURR AND BREAK ALL SHARP EDGES
- 3. USE SOLID PART FILE FOR UNSPECIFIED GEOMETRY



2

1

UNLESS OTHERWISE SPECIFIED: DIMENSIONS ARE IN INCHES TOLERANCES: FRACTIONAL: ± 1/32 ANGULAR: ± 1° X ± 0.05 XX ± 0.01 XXX ± 0.005		DRAWN LA	NAME LA	DATE 2/24/19	 THIRD ANGLE PROJECTION	<b>SMA Testing</b>  TITLE: Half Chamber Frame (Inner)
INTERFEROMETRIC DIMENSIONS: 95% (AS) Y14.5M-1.194 MATERIAL Aluminum 6061 FINISH DO NOT SCALE DRAWING		CHECKED NF	DATE 2/24/19	SIZE <b>A</b>		
				SCALE: 1:5 WEIGHT:	SHEET 2 OF 2	

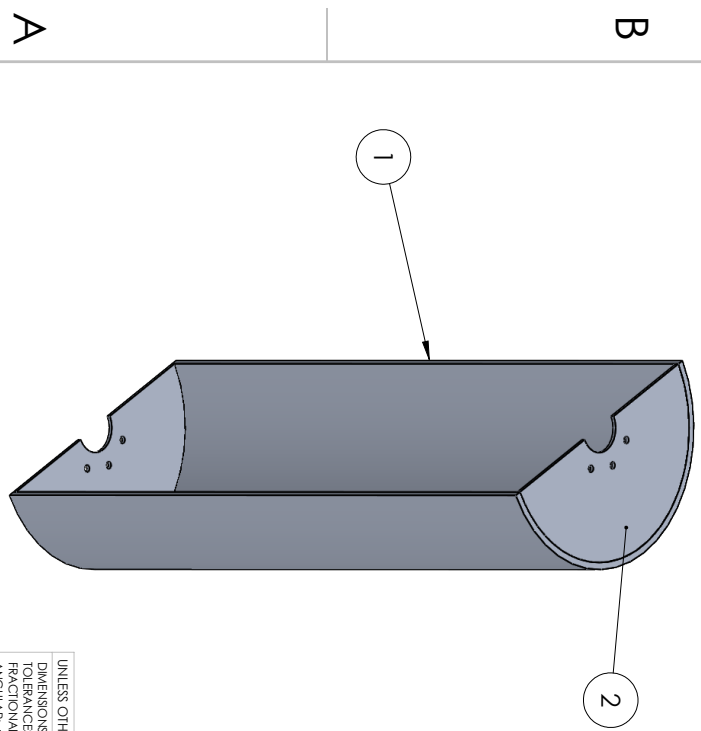


2

1

- NOTES:
1. QUANTITY: 2
  2. DEBURR AND BREAK ALL SHARP EDGES
  3. USE SOLID PART FILE FOR UNSPECIFIED GEOMETRY

ITEM NO.	PART NUMBER	DESCRIPTION	QTY.
1	C002	10" OD Half Pipe	1
2	C005	End Cap	2



2

1

UNLESS OTHERWISE SPECIFIED: DIMENSIONS ARE IN INCHES TOLERANCES: FRACTIONAL ± 1/32 ANGULAR ± 1° X ± 0.05 XX ± 0.01 XXX ± 0.005				DRAWN LA	NAME NF	DATE 2/24/19	 THIRD ANGLE PROJECTION	TITLE: <b>SMA Testing</b>  Half Chamber Frame (Outer)
INTERFEROMETRIC DIMENSIONS: 95% (AS) Y14.5M-1994				CHECKED				
MATERIAL Aluminum 6061		FINISH				SIZE <b>A</b>	DWG. NO. F002	REV <b>4</b>
DO NOT SCALE DRAWING				SCALE: 1:5		WEIGHT:		SHEET 1 OF 2

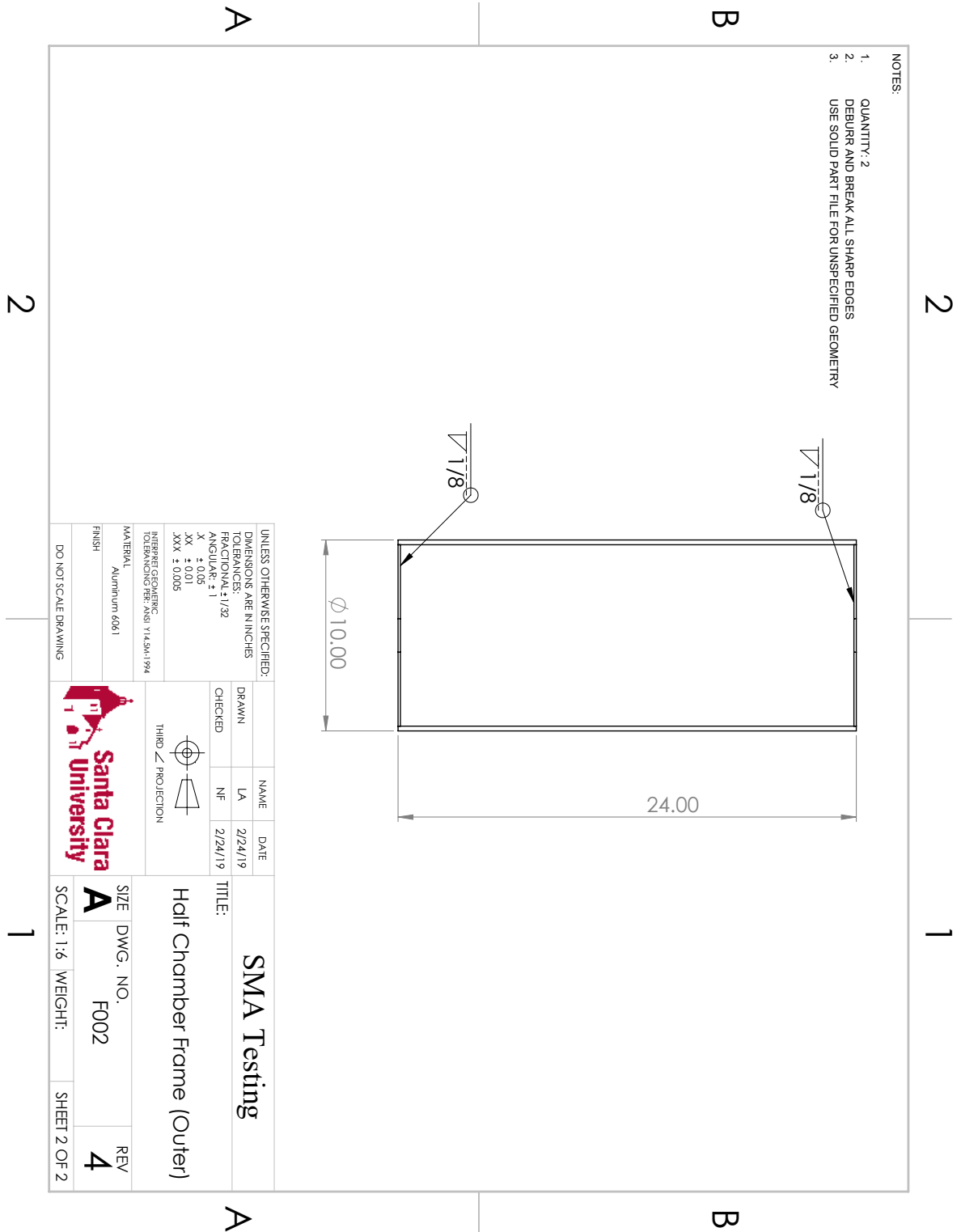


Figure 56: Drawing of the outer chamber frame.

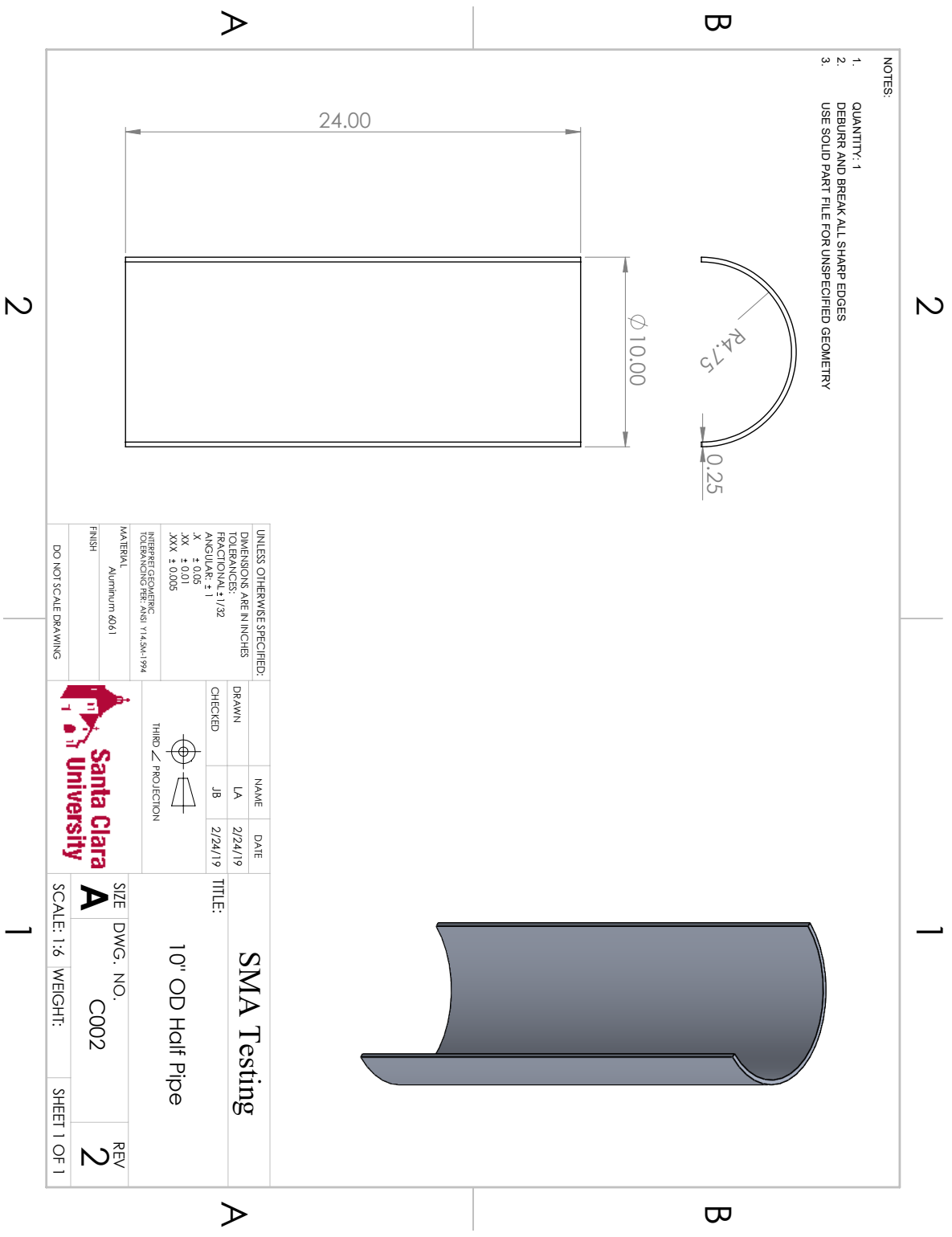


Figure 57: Drawing of the 10 in. OD pipe split in half.

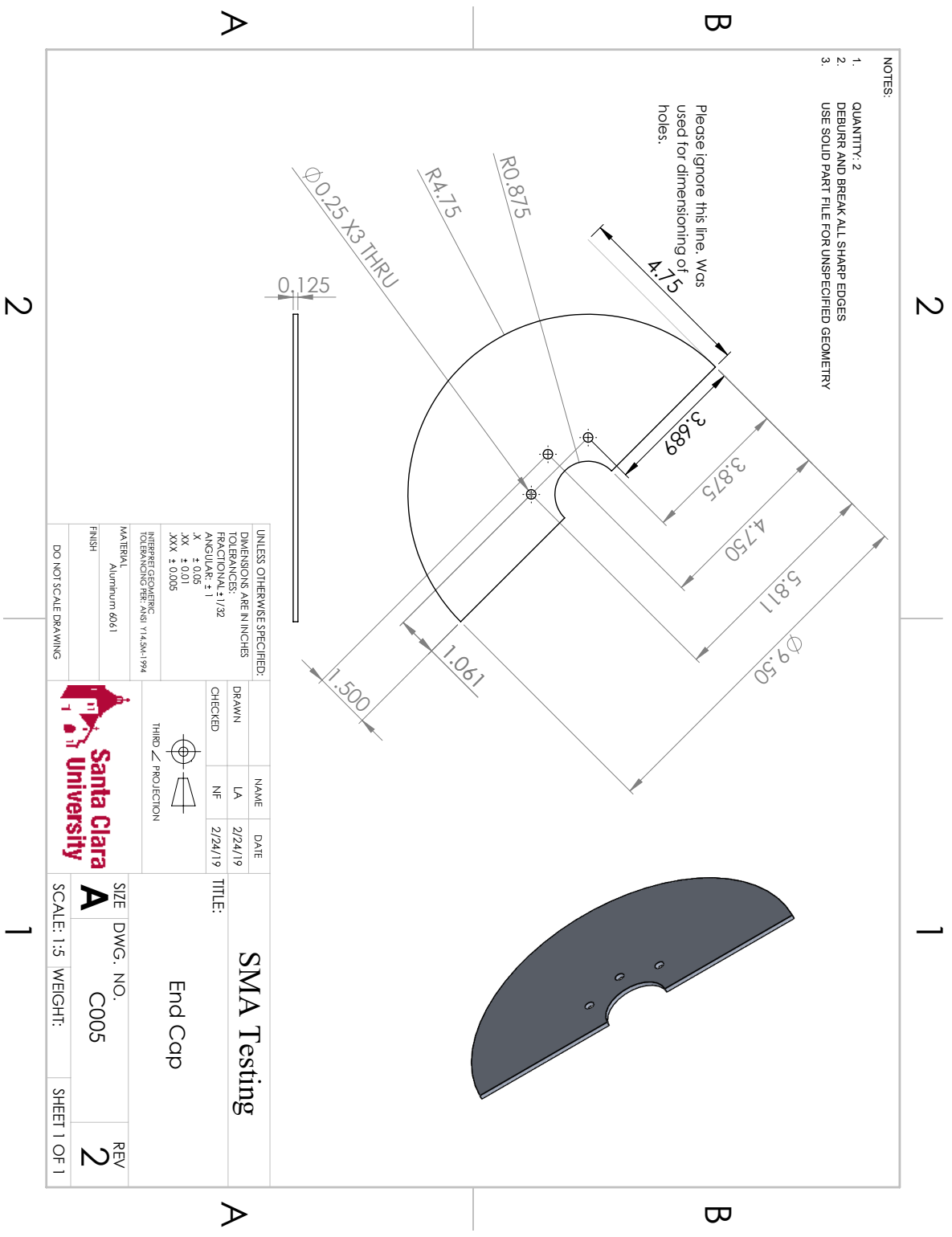


Figure 58: Drawing of aluminum end cap for the outer wall.

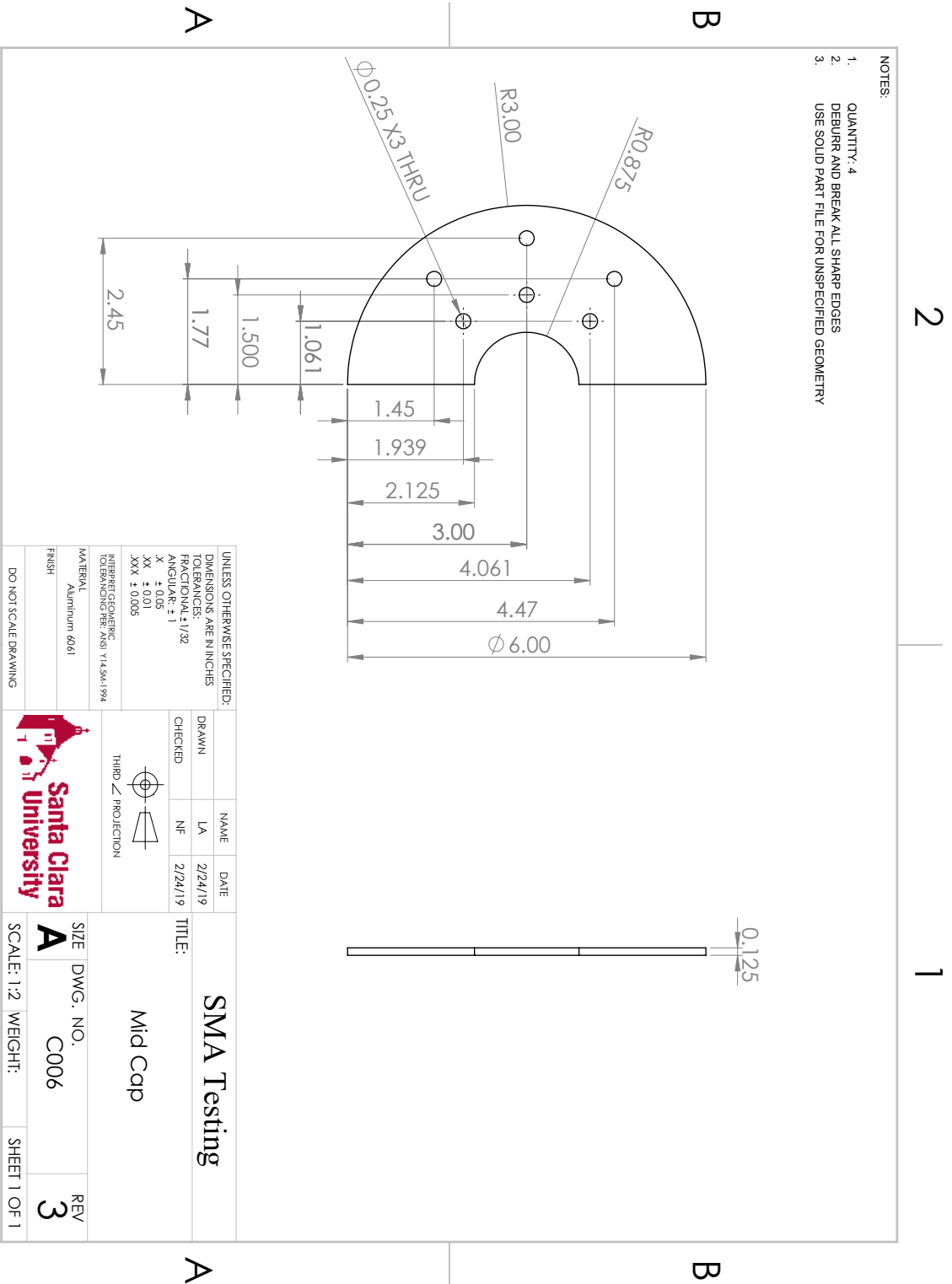


Figure 59: Drawing of the end cap for the inner wall.

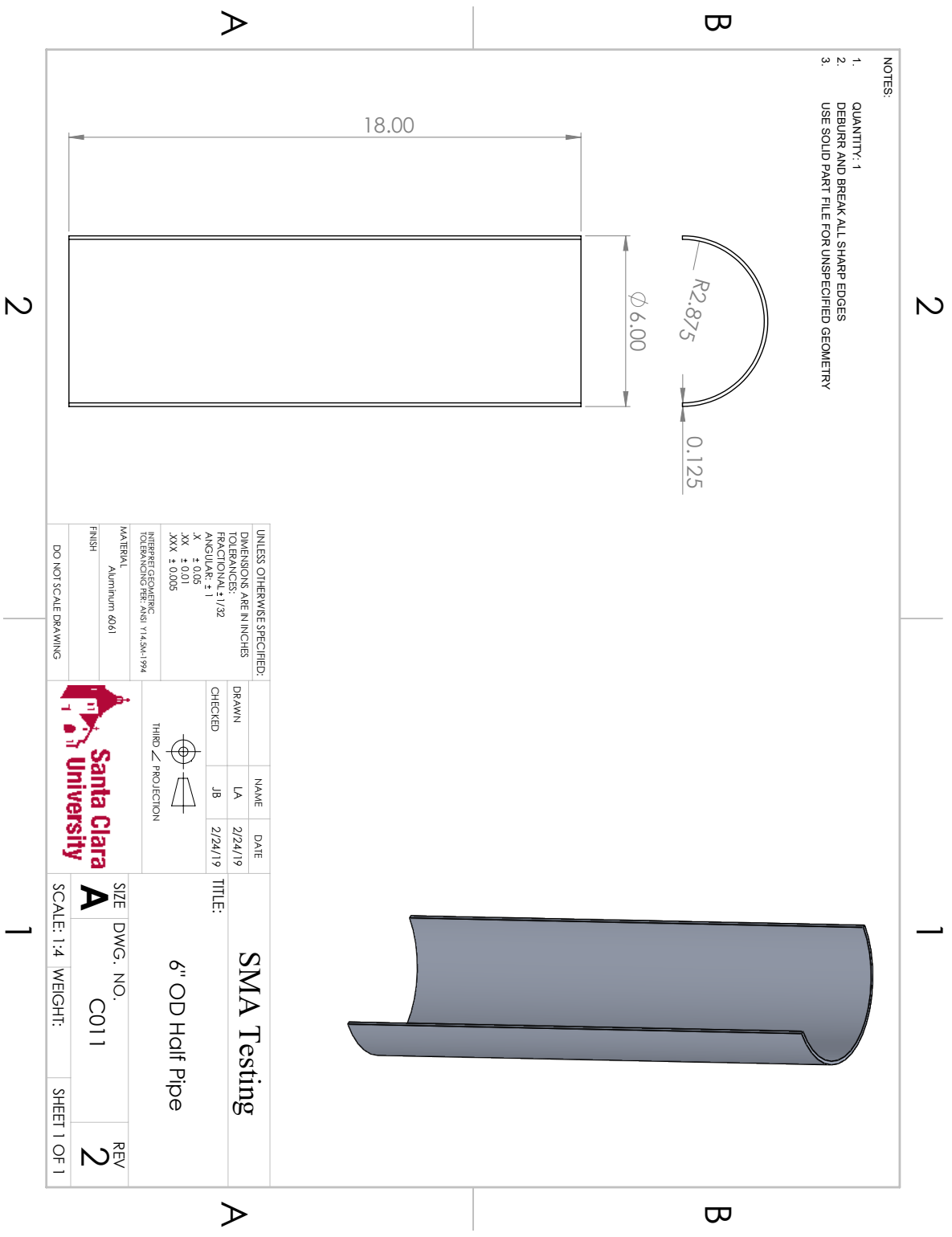


Figure 60: Drawing of the 6 in. OD pipe split in half.

# Base/Fixturing Drawings

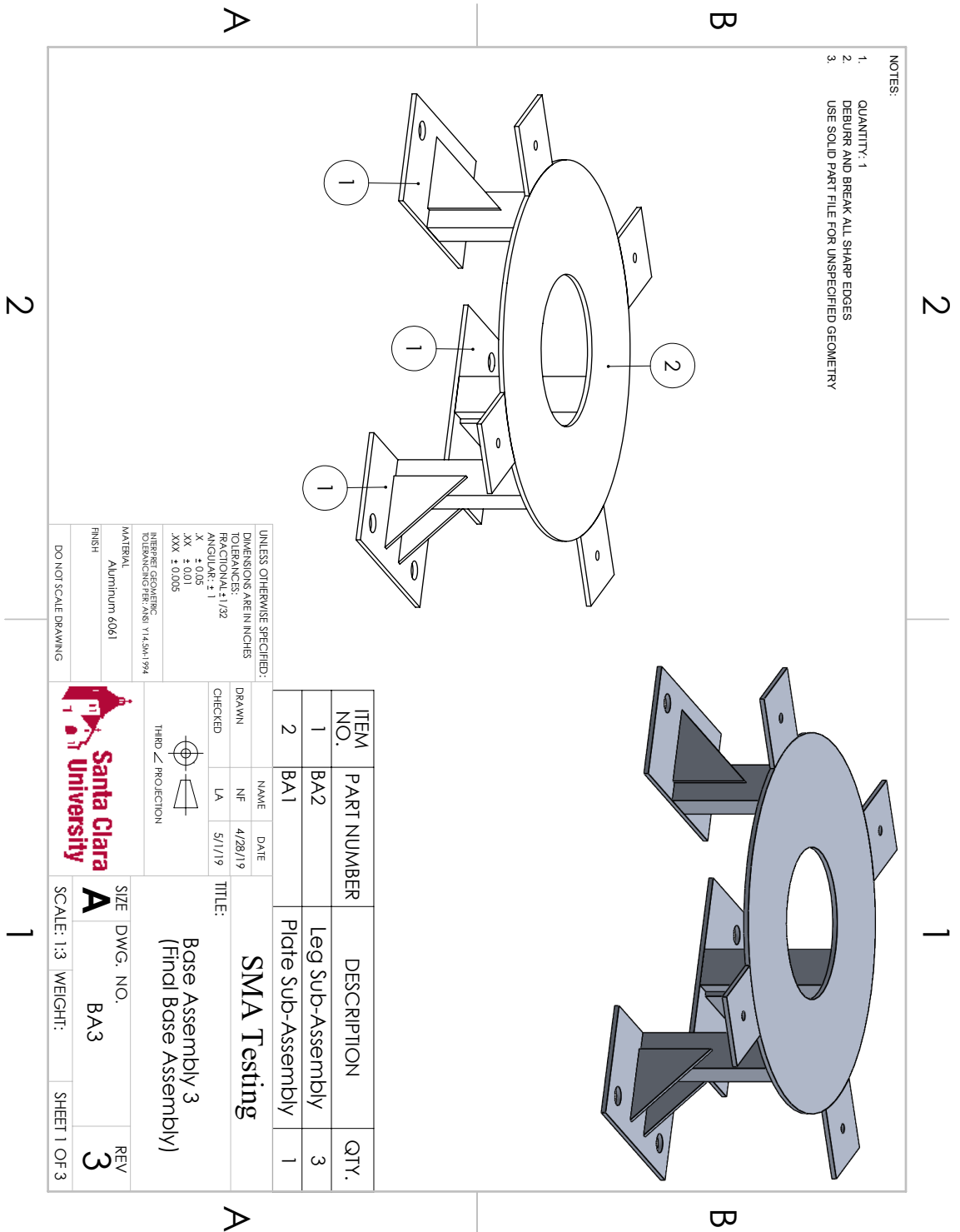
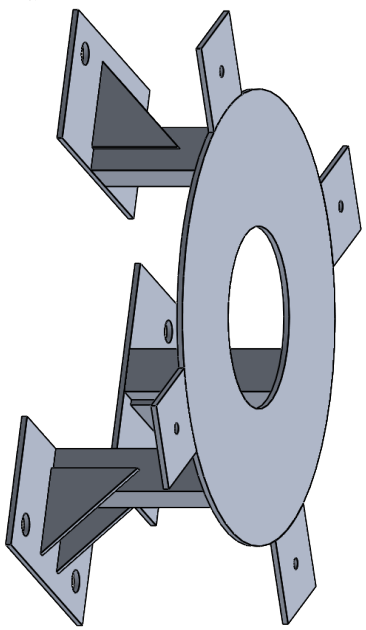
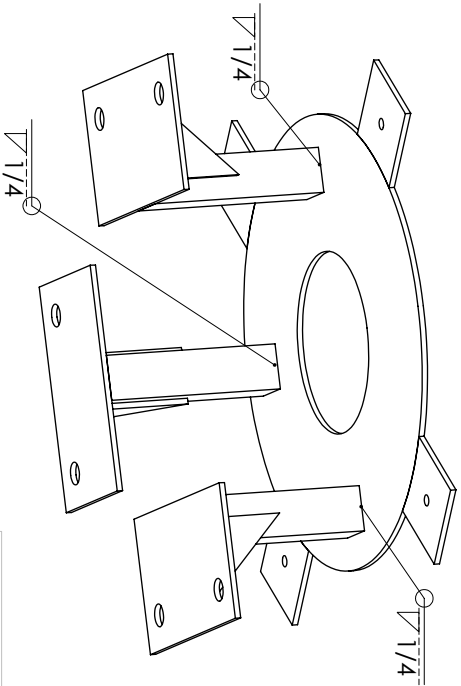


Figure 61: Drawing of base assembly.

2

1

- NOTES:
1. QUANTITY: 1
  2. DEBURR AND BREAK ALL SHARP EDGES
  3. USE SOLID PART FILE FOR UNSPECIFIED GEOMETRY



2

1

UNLESS OTHERWISE SPECIFIED: DIMENSIONS ARE IN INCHES TOLERANCES: FRACTIONAL: ± 1/32 ANGULAR: ± 1° XX ± 0.01 XXX ± 0.005		DRAWN	NAME	DATE	<b>SMA Testing</b>  Base Assembly 3 (Final Base Assembly)
INTERPRET GEOMETRIC TOLERANCING PER: ASME Y14.5M-1994		CHECKED	LA	5/1/19	
MATERIAL: Aluminum 6061		 THIRD ANGLE PROJECTION		SIZE	REV
FINISH: DO NOT SCALE DRAWING				DWG. NO.	BA3
				SCALE: 1:3	WEIGHT:
				SHEET 2 OF 3	

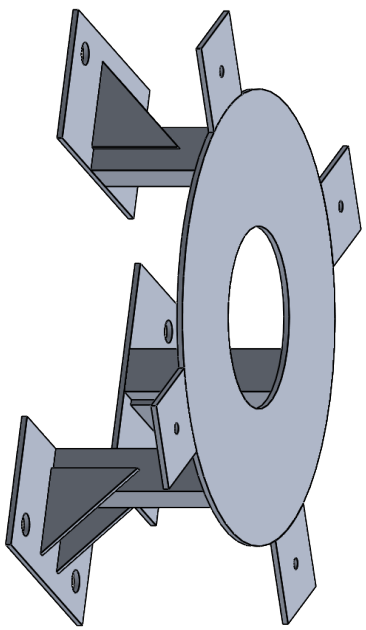
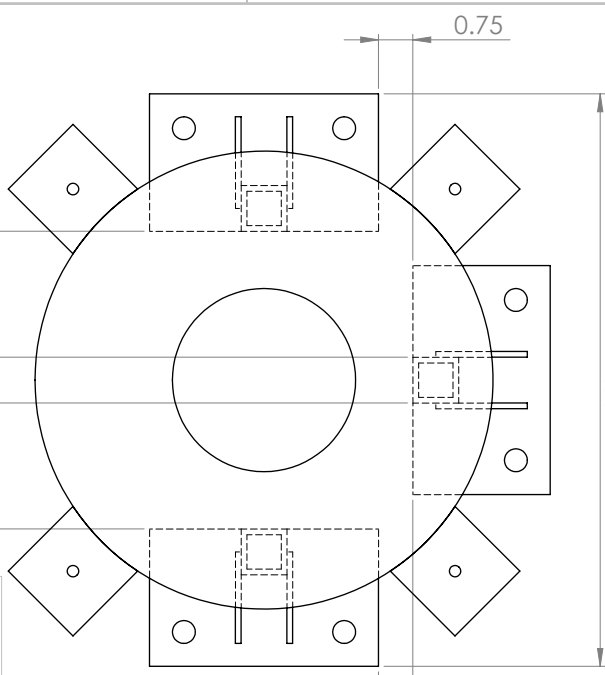


2

1

- NOTES:
1. QUANTITY: 1
  2. DEBURR AND BREAK ALL SHARP EDGES
  3. USE SOLID PART FILE FOR UNSPECIFIED GEOMETRY

Top View



A

B

A

B

2

1

UNLESS OTHERWISE SPECIFIED:  
 DIMENSIONS ARE IN INCHES  
 TOLERANCES:  
 FRACTIONAL: ± 1/32  
 ANGULAR: ± 1°  
 XX ± 0.01  
 XXX ± 0.005

INTERPRET GEOMETRIC TOLERANCING PER: AS Y14.5M-1994

MATERIAL: Aluminum 6061

FINISH:

DO NOT SCALE DRAWING

NAME	DATE
DRAWN	4/28/19
CHECKED	5/1/19

THIRD ANGLE PROJECTION

TITLE:		SIZE	DWG. NO.	REV
SMA Testing		A	BA3	3
(Final Base Assembly)		SCALE: 1:3	WEIGHT:	SHEET 3 OF 3



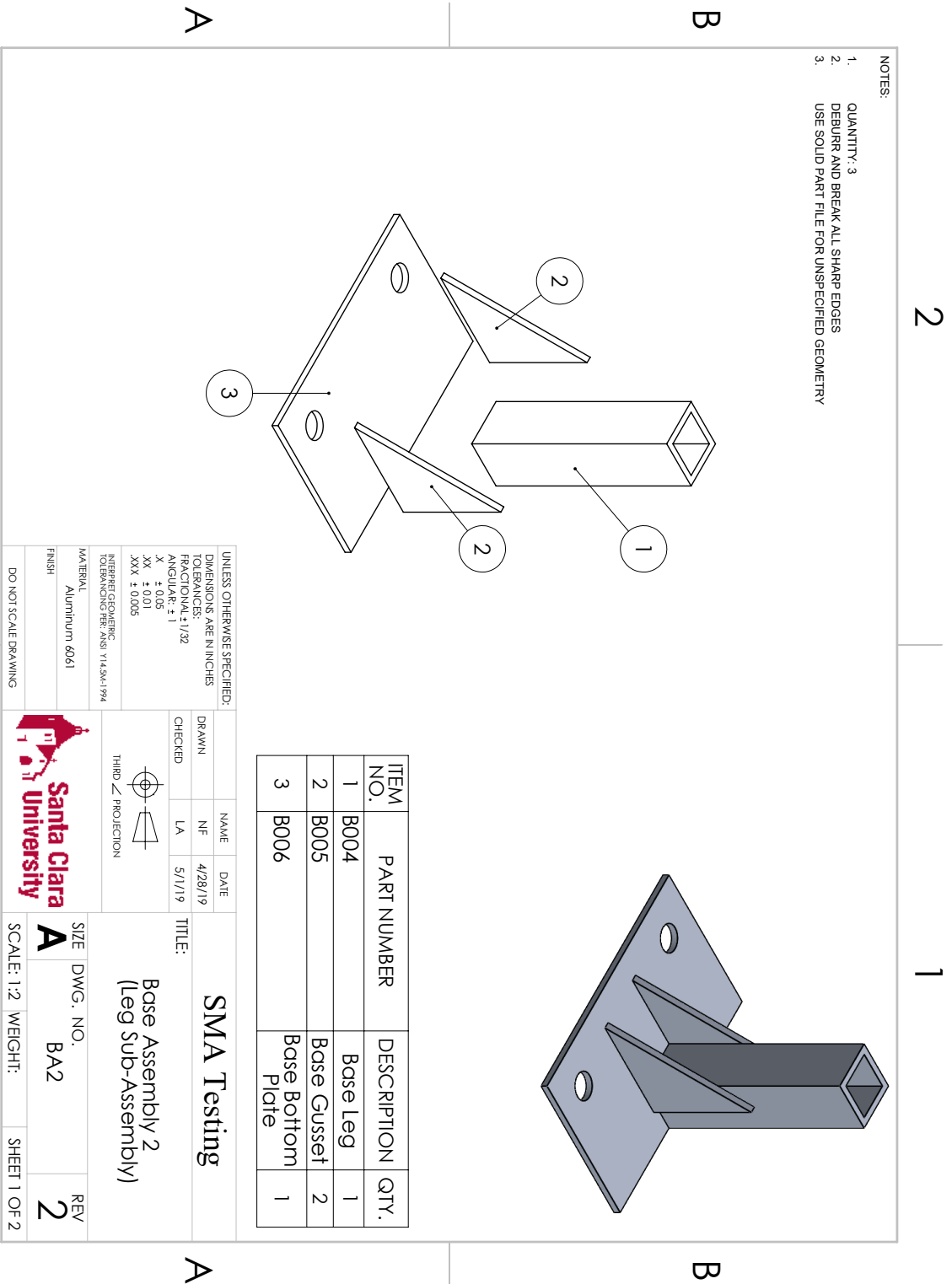
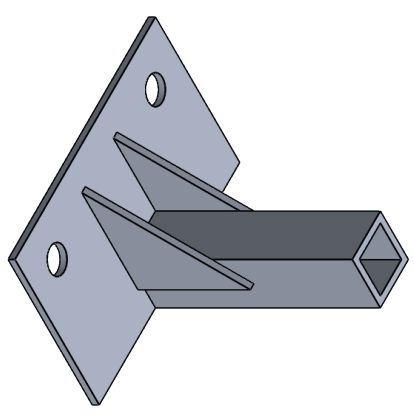
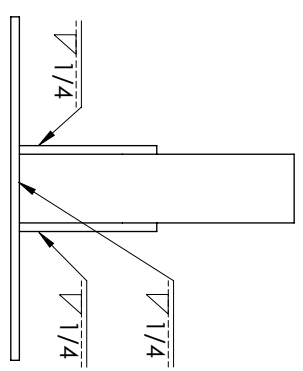
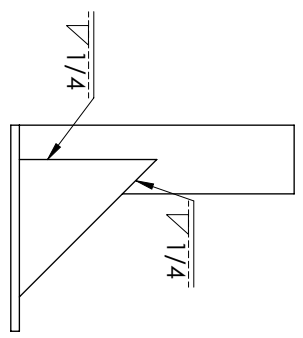


Figure 62: Drawing of the leg assembly.

2

1

- NOTES:
1. QUANTITY: 3
  2. DEBURR AND BREAK ALL SHARP EDGES
  3. USE SOLID PART FILE FOR UNSPECIFIED GEOMETRY



B

B

A

A

2

1

UNLESS OTHERWISE SPECIFIED: DIMENSIONS ARE IN INCHES TOLERANCES: FRACTIONAL ± 1/32 ANGULAR ± 1° XX ± 0.01 XXX ± 0.005		DRAWN	NAME	DATE	<b>SMA Testing</b>  TITLE: Base Assembly 2 (Leg Sub-Assembly)
INTERPRET GEOMETRIC TOLERANCING PER: AS Y14.5M-1994		CHECKED	LA	5/1/19	
MATERIAL Aluminum 6061		 THIRD ANGLE PROJECTION		SIZE	REV
FINISH		 Santa Clara University		A	2
DO NOT SCALE DRAWING		SCALE: 1:2		WEIGHT:	SHEET 2 OF 2

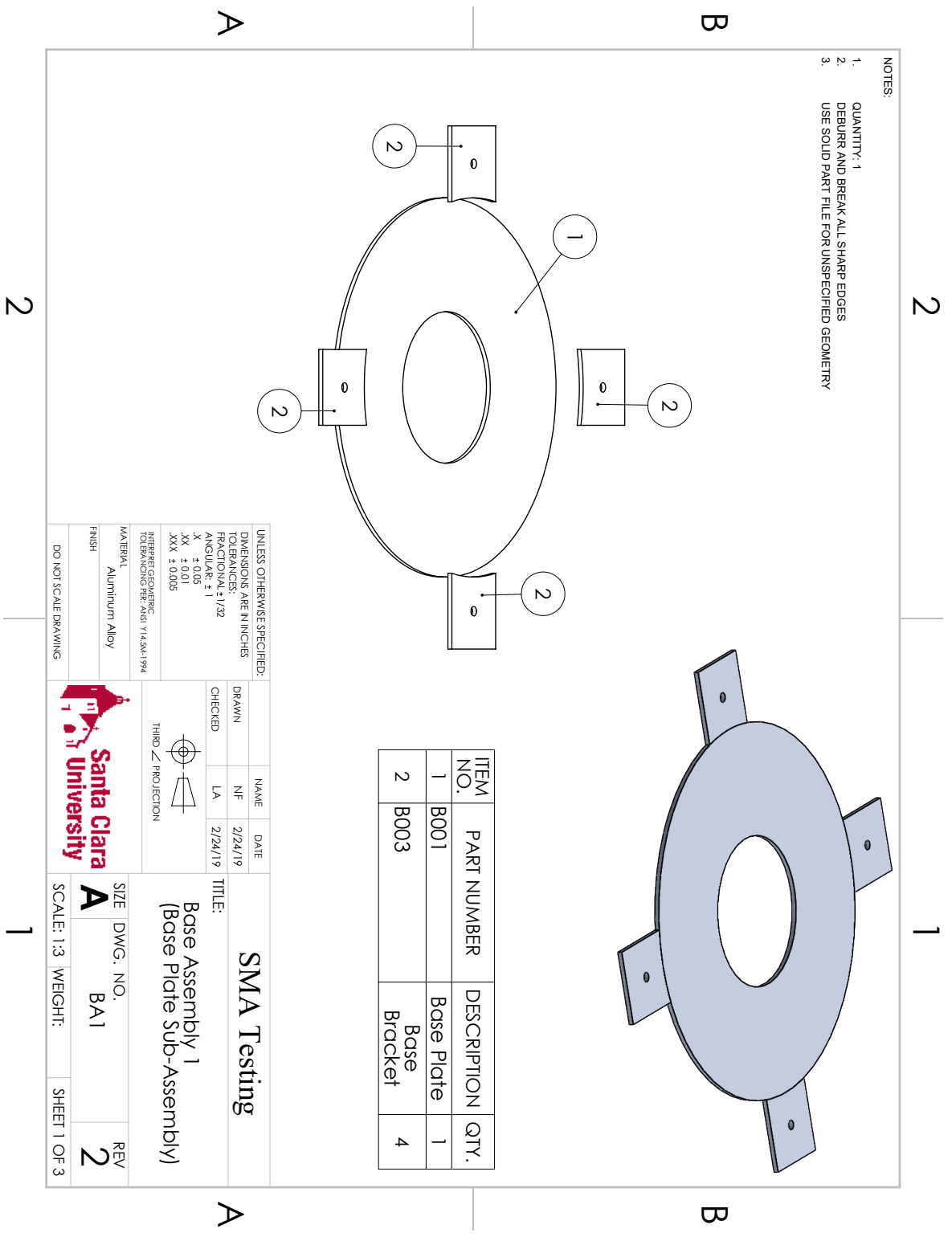
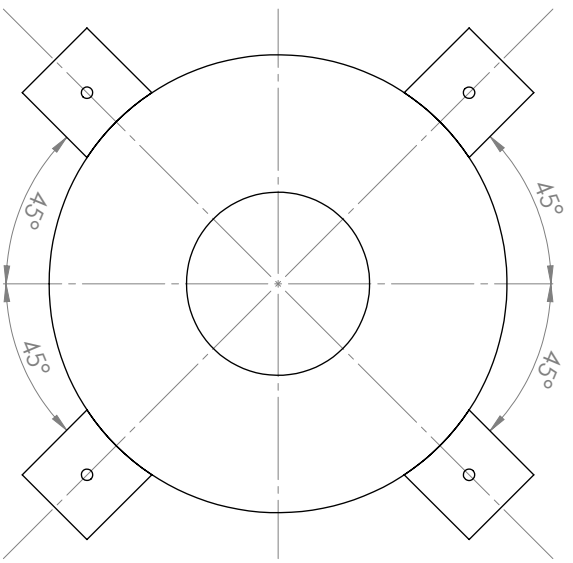
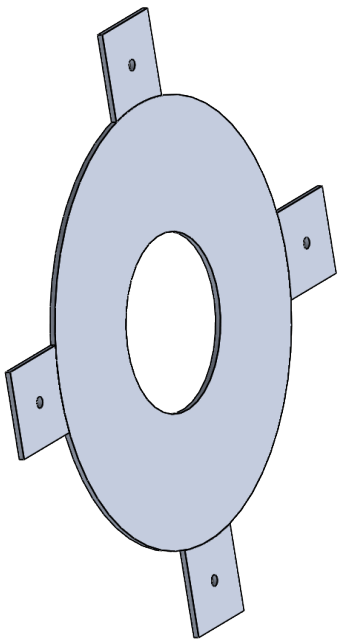


Figure 63: Drawing of the base plate assembly.

2

1

- NOTES:
1. QUANTITY: 1
  2. DEBURR AND BREAK ALL SHARP EDGES
  3. USE SOLID PART FILE FOR UNSPECIFIED GEOMETRY



Top View

2

1

UNLESS OTHERWISE SPECIFIED: DIMENSIONS ARE IN INCHES TOLERANCES: FRACTIONAL: ± 1/32 ANGULAR: ± 1° XX ± 0.01 XXX ± 0.005		DRAWN	NAME	DATE
INTERPRET GEOMETRIC TOLERANCING PER: AS Y14.5M-1994		CHECKED	LA	2/24/19
MATERIAL: Aluminum Alloy		 THIRD ANGLE PROJECTION		
FINISH: DO NOT SCALE DRAWING				
TITLE:		SMA Testing		
SIZE: A		DWG. NO.: BA1		
SCALE: 1:3		WEIGHT:		
REV: 2		SHEET 2 OF 3		

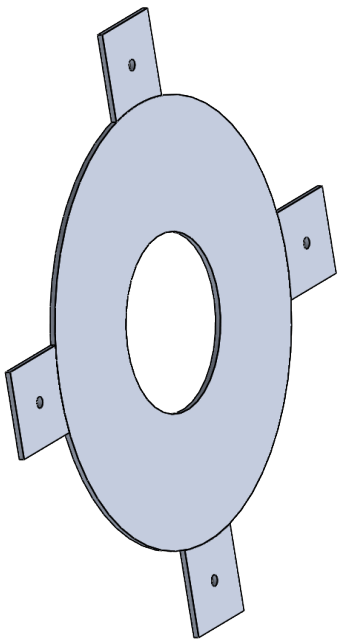
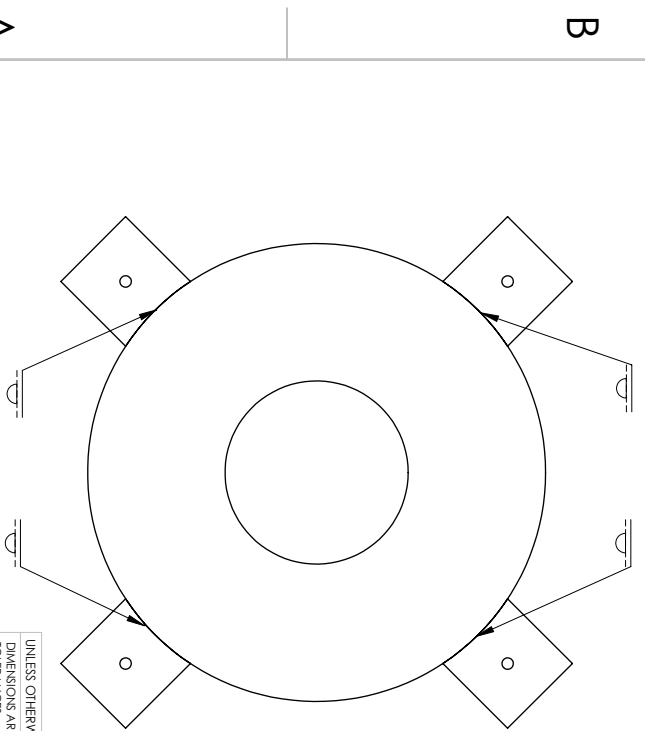
Base Assembly 1  
(Base Plate Sub-Assembly)



2

1

- NOTES:
1. QUANTITY: 1
  2. DEBURR AND BREAK ALL SHARP EDGES
  3. USE SOLID PART FILE FOR UNSPECIFIED GEOMETRY



Bottom View  
 Note: weld only on bottom face of assembly

2

1

UNLESS OTHERWISE SPECIFIED: DIMENSIONS ARE IN INCHES			
TOLERANCES:			
FRACTIONAL: ± 1/32			
ANGULAR: ± 1°			
XX ± 0.01			
XXX ± 0.005			
INTERPRET GEOMETRIC TOLERANCING PER: AS Y14.5M-1994			
MATERIAL: Aluminum Alloy			
FINISH: DO NOT SCALE DRAWING			
DRAWN	NAME	DATE	
CHECKED	NF	2/24/19	
	LA	2/24/19	
THIRD ANGLE PROJECTION			
TITLE:			REV
SMA Testing			2
Base Assembly 1 (Base Plate Sub-Assembly)			
SIZE	DWG. NO.		
A	BA1		
SCALE: 1:3	WEIGHT:	SHEET 3 OF 3	



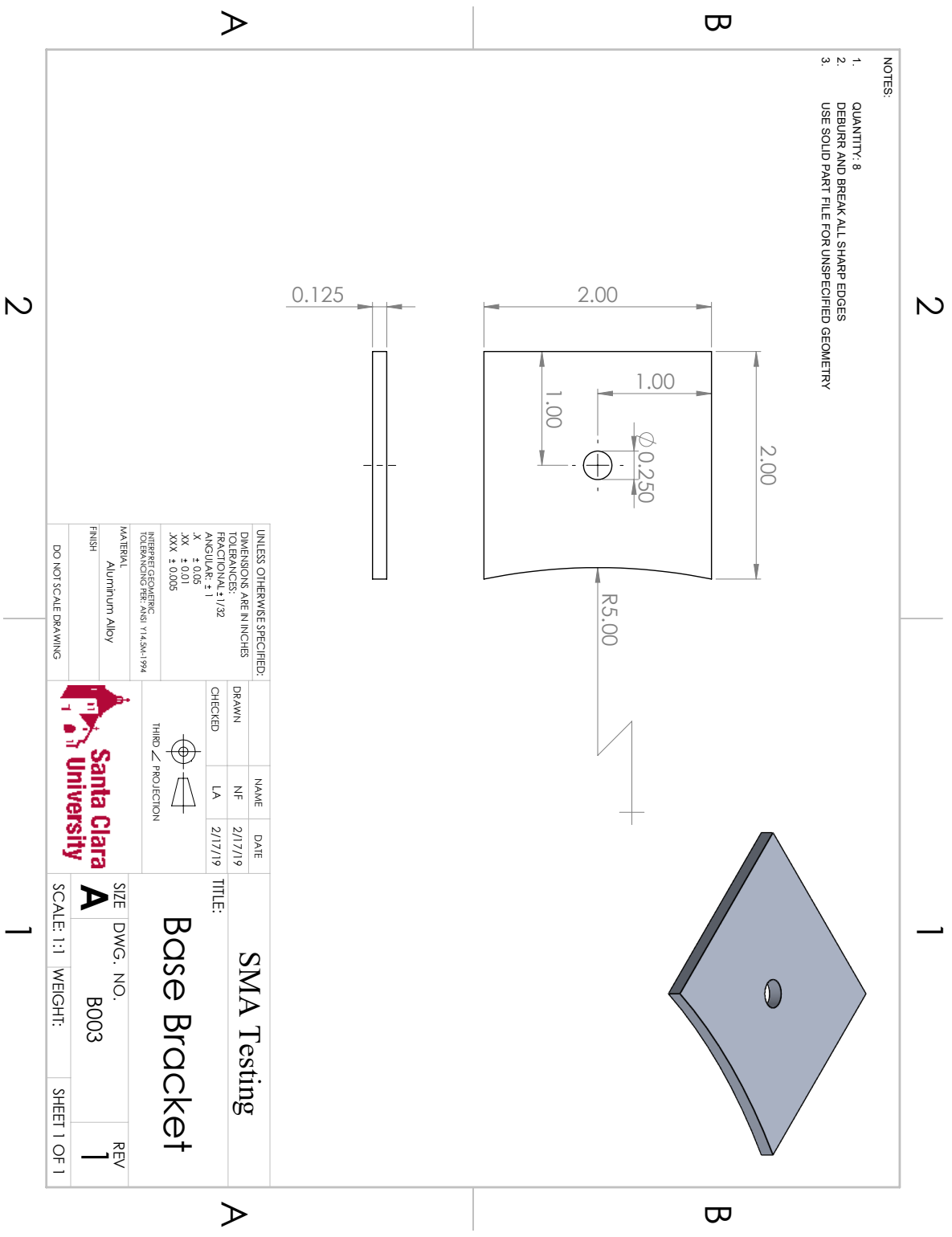


Figure 64: Drawing of the brackets used to fix the chamber.

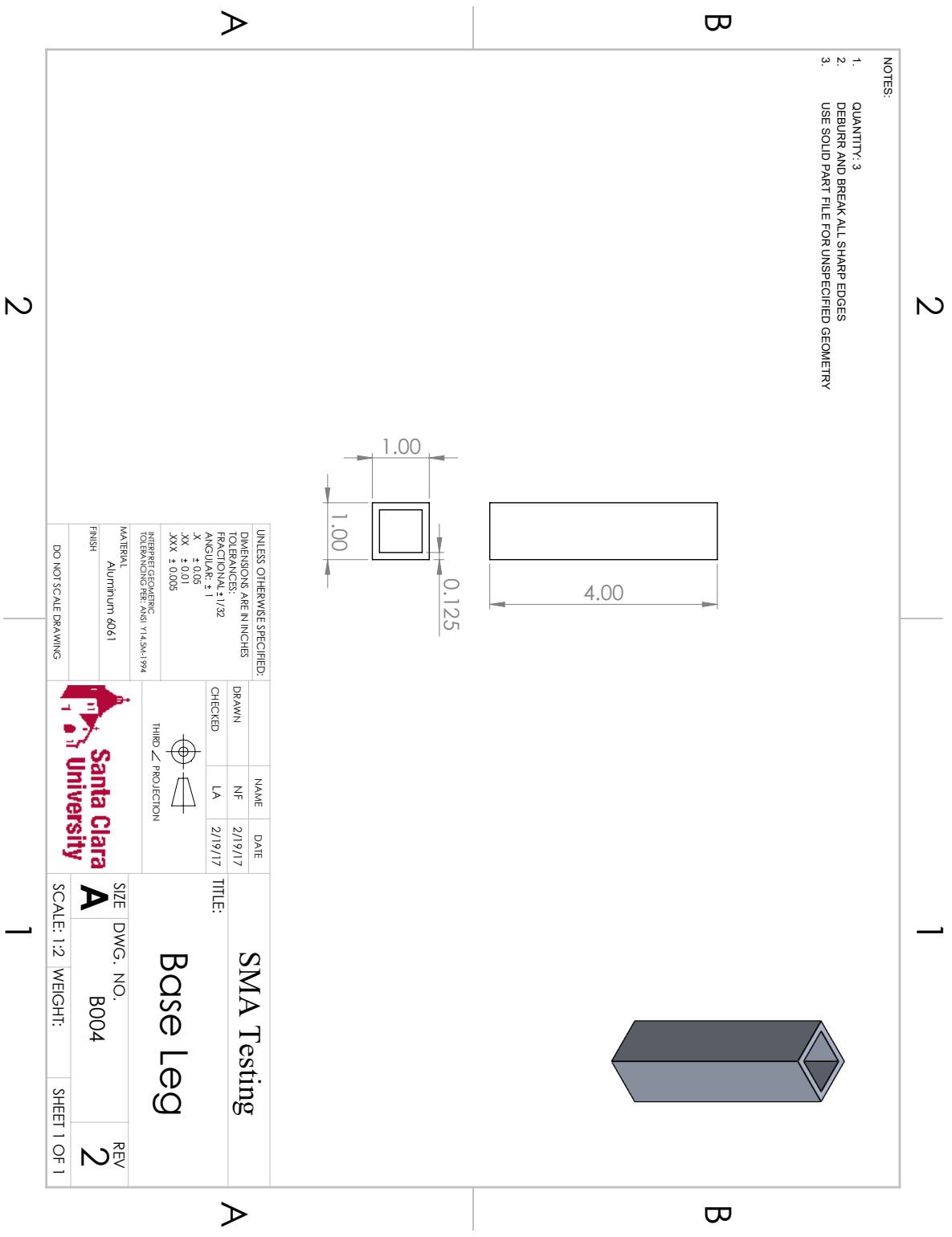


Figure 65: Drawing of tube used for the base legs.



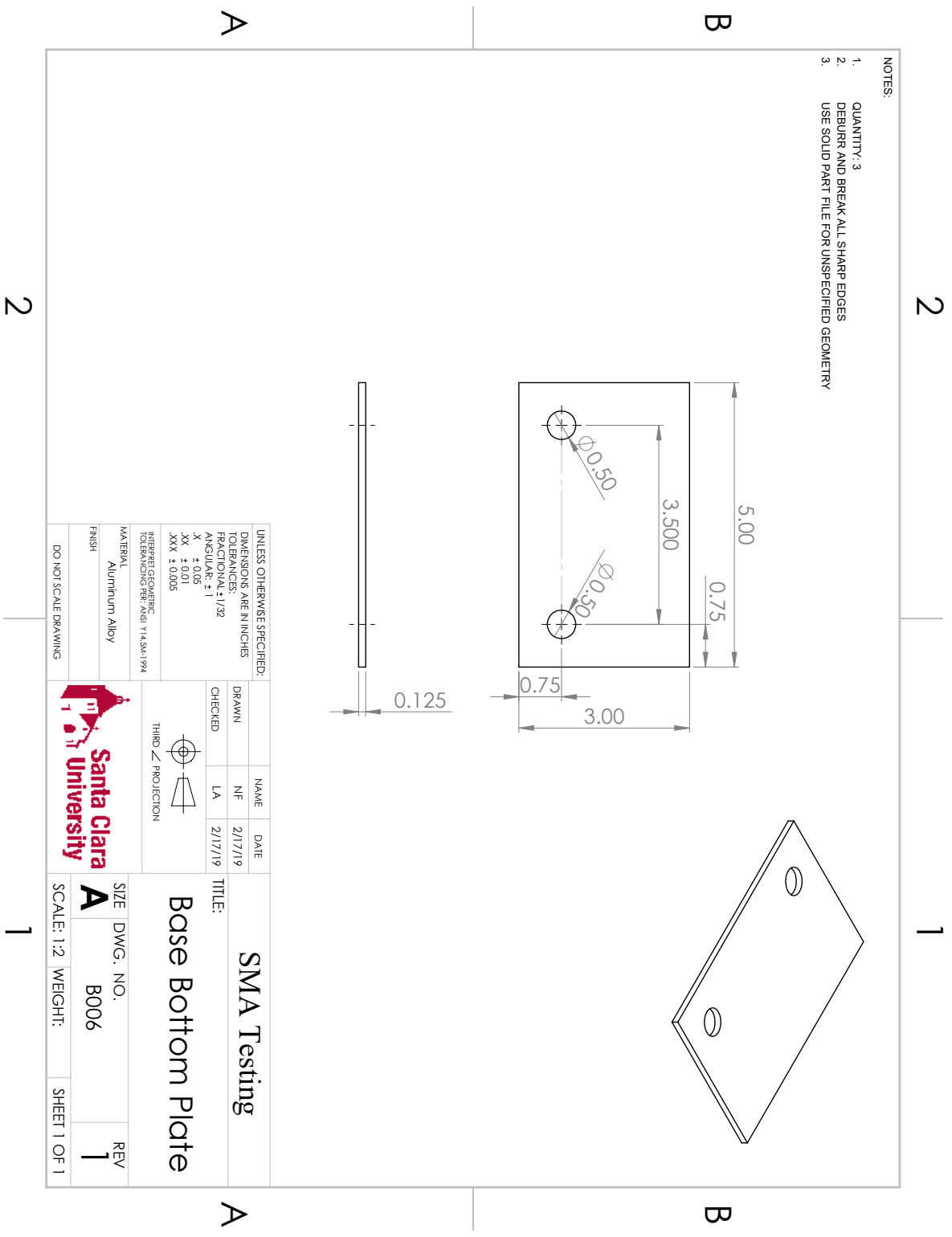


Figure 66: Drawing of the plates used at the ends of the legs.

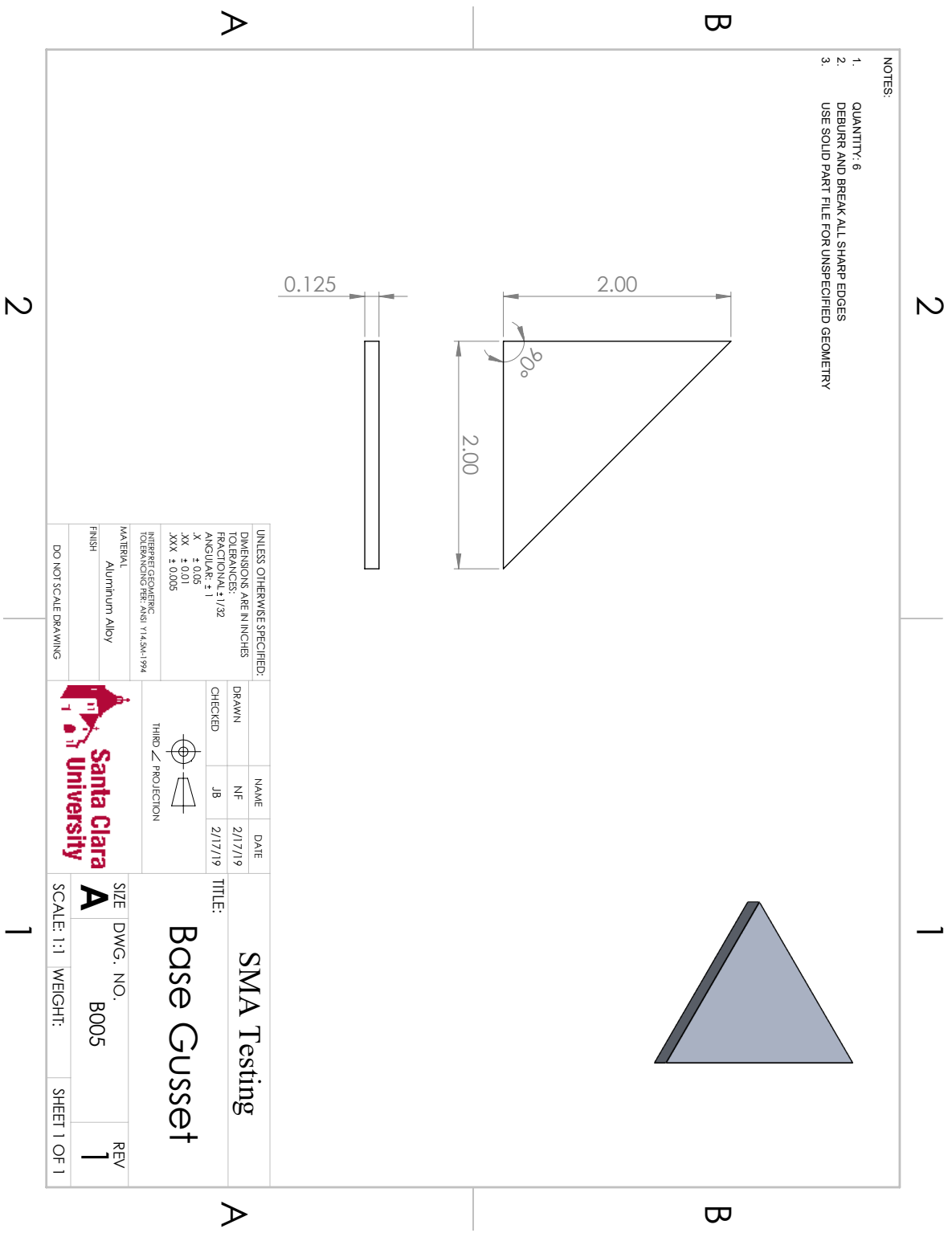


Figure 67: Drawing of the gusset used for the legs.

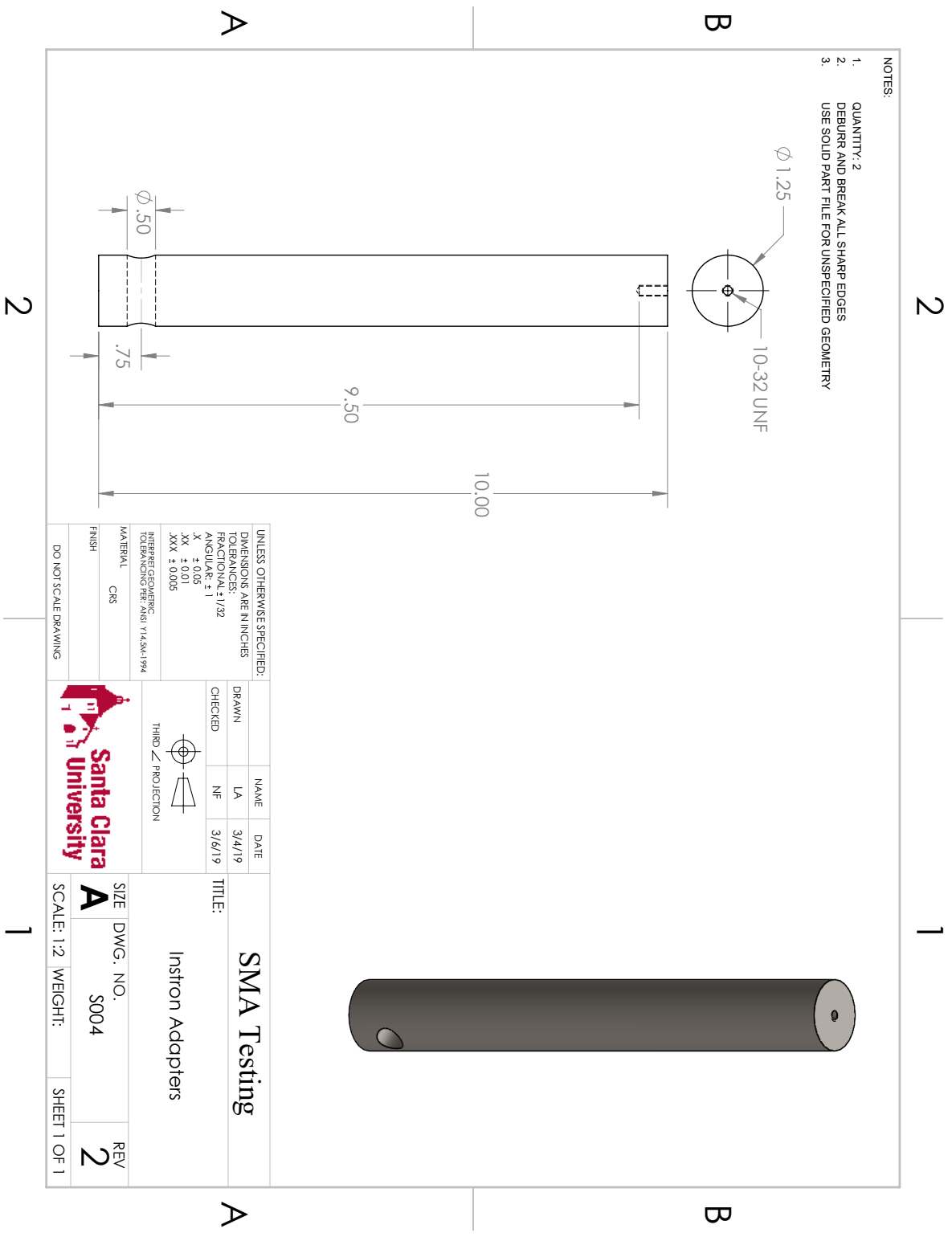


Figure 68: Drawing of the threaded grip.

## Appendix C: Thermal Simulations

Provided below are plotted temperature distributions associated with the FEA thermal simulations conducted in SolidWorks for the two primary iterations (based on heating element type) of the environment chamber design.

### Simulation with Wire Heating Elements

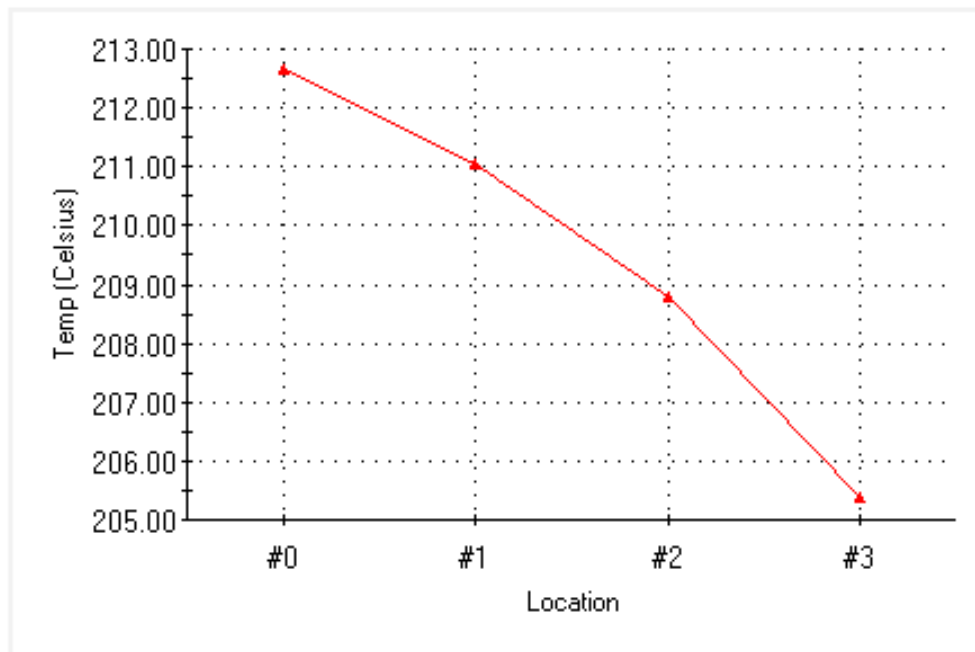


Figure 69: Plot of temperature distribution along specimen length, from the mid-length (Location 0) to one end (Location 3).

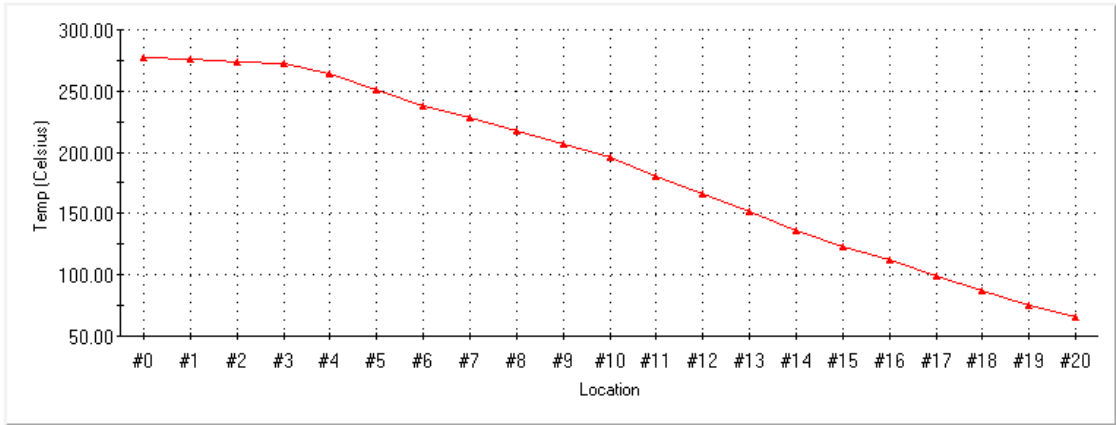


Figure 70: Insulation temperature variation. Probed from the heating element contact point (Location 0) to the outer wall contact point (Location 20).

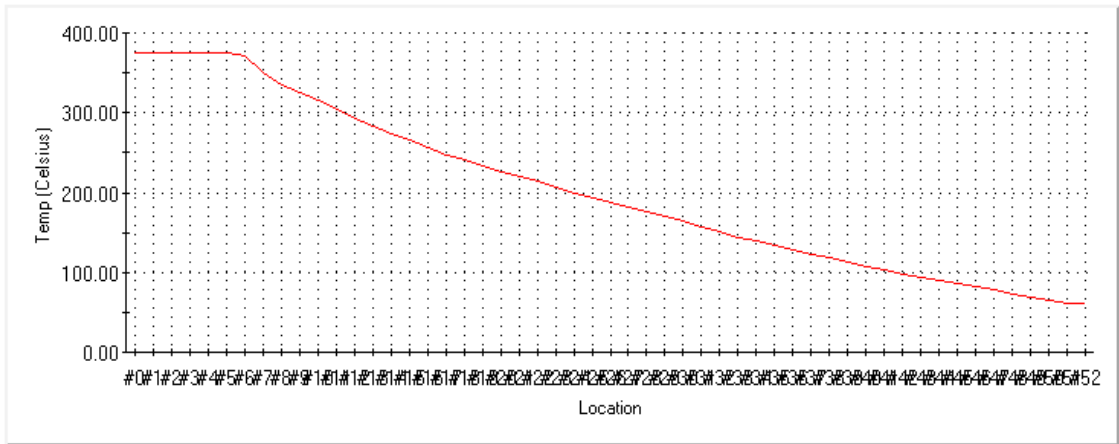


Figure 71: Temperature variation from heating element (Location 0) to outside edge of chamber (Location 52).

## Simulation with Power Resistors

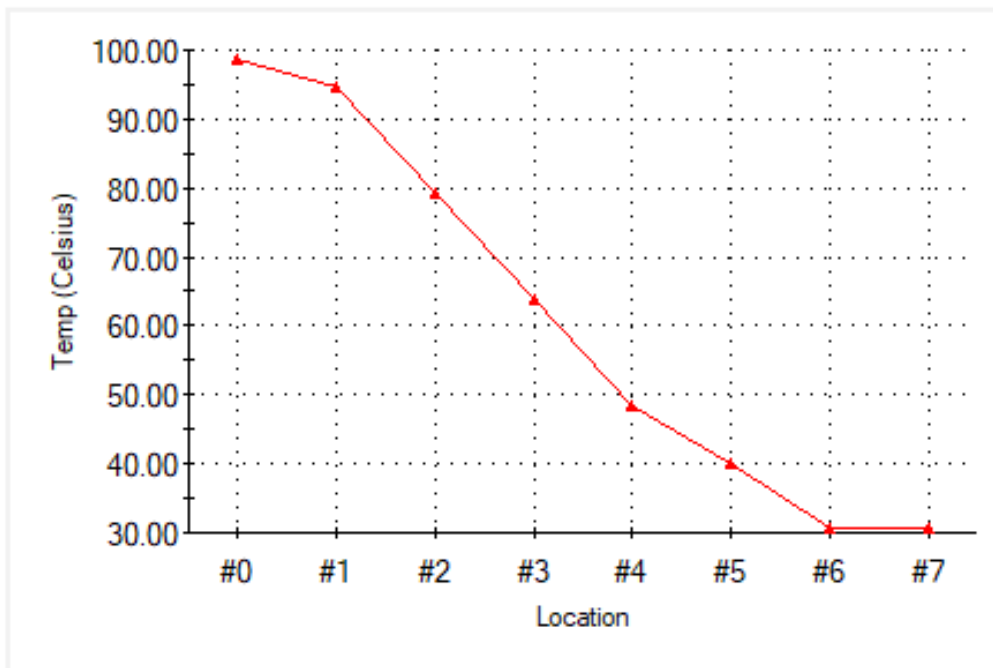


Figure 72: Temperature distribution plot from the inner wall (Location 0) to the outer wall (Location 7) of the chamber.

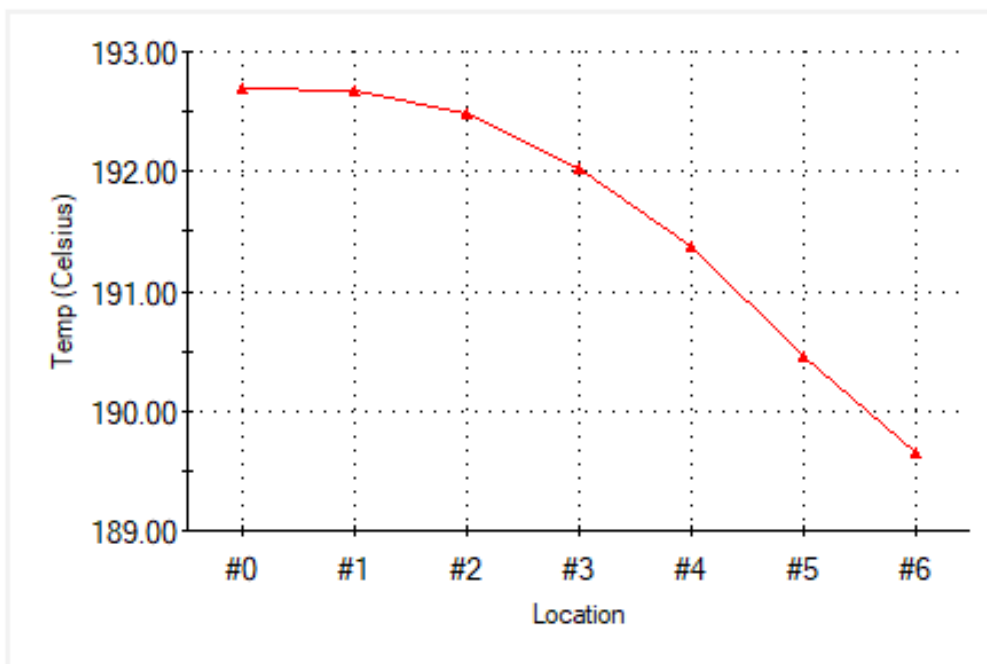


Figure 73: Temperature distribution plot of the specimen from mid-length (Location 0) to one end (Location 6).

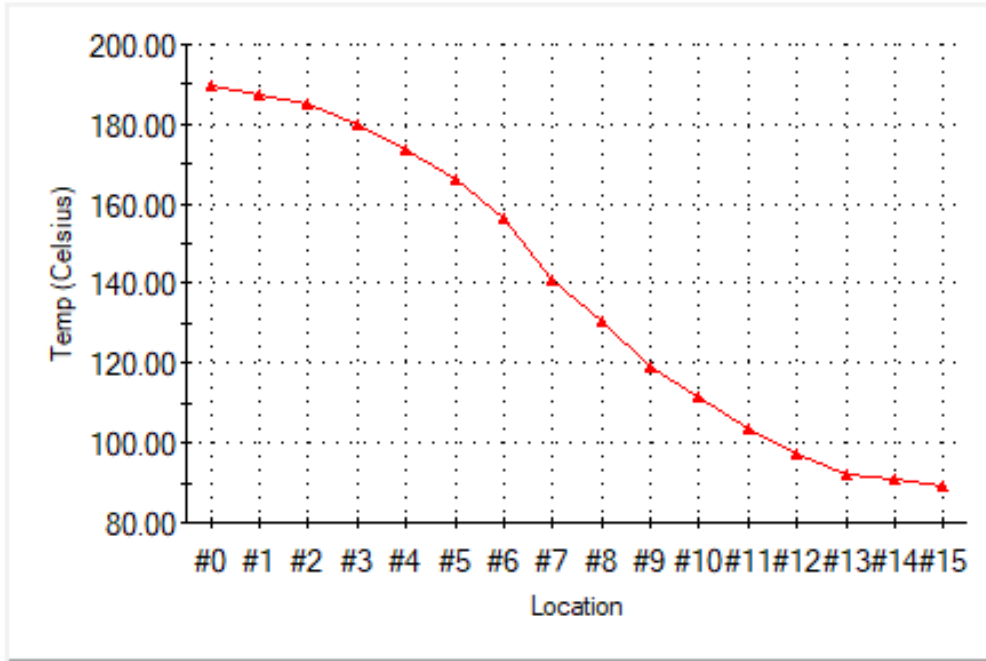


Figure 74: Temperature distribution plot along the length of the grip. Probed from the specimen contact point (Location 0) to the protruding end (Location 15).

## Appendix D: SMA Compositional Analysis

Compositional analysis was performed through a combination of scanning electron microscopy (SEM) and energy-dispersive spectroscopy (EDS). This process entails placing a specimen under a focused beam of electrons, in order to illuminate it for high-resolution imaging (resolution of 1-2 nm) of surface topography, as well as to produce various energy emissions that can be used for composition and phase mapping [30]. Interaction between the beam and the specimen involves excitation of the specimen's electrons, causing some to be ejected (ionization) and others to move around within the electron shells around the nucleus of each atom affected by the beam [31]. When an electron moves from a higher energy shell to a lower one, the energy difference is emitted as an X-ray, which can then be measured by a spectrometer [31]. As each element has a unique atomic structure, a unique electromagnetic emission spectrum profile can then be observed for each element [32]. This principle allows for an observer to take the characteristics and number of X-rays emitted by an alloy sample under an electron microscope, produce an EDS emission spectrum, and then accurately quantify the alloy's composition.

Two first-year students, Jake Taylor and Ryan Konrath, working with our project advisor Dr. Robert Marks, as well as Dr. Ashley Kim and Shaun Snyder, respectively the director and the laboratory manager of the Santa Clara University Center for Nanostructures, performed this analysis on the SMA being studied for this project. Prior to their work, it was only known that the alloy was some combination of Cu-Al-Ni, with the primary element being copper. The EDS spectrum they produced can be seen in the figure below. Converting weight ratios to atomic ratios, it was determined that the alloy's composition is 71.9 at% Cu, 23.9 at% Al, 4.2 at% Ni.



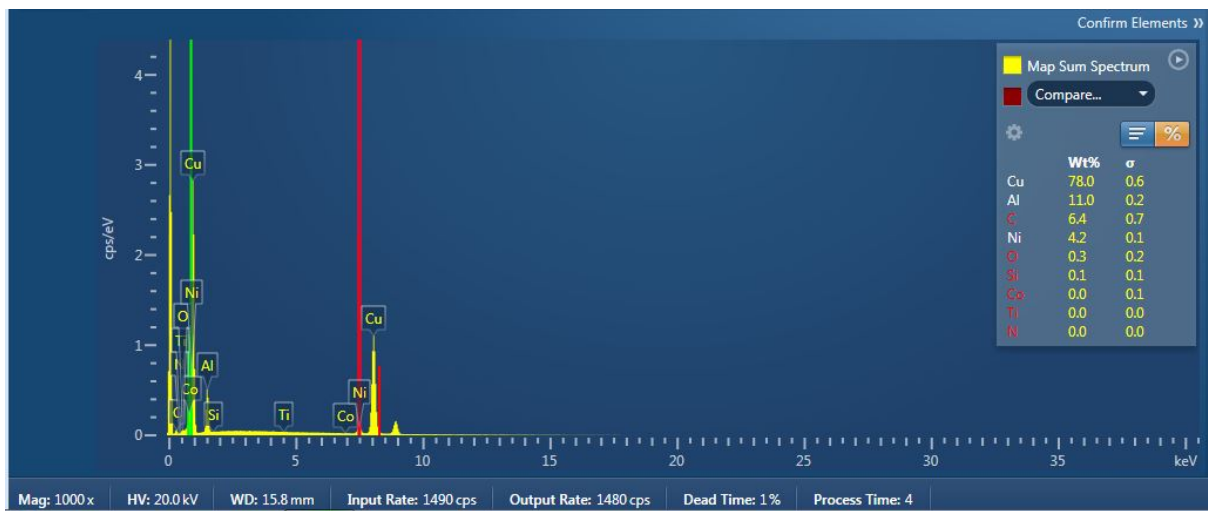


Figure 75: EDS spectrum showing composition (by weight percent) of the Cu-Al-Ni SMA. Provided by A. Kim, S. Snyder, R. Marks, J. Taylor, and R. Konrath. Reproduced with permission.

## Appendix E: Subsystem Concept Scoring

These are the concept scoring matrices used to determine the most viable options for implementation of each major subsystem. The spreadsheet modules used were provided by Dr. Gaetano Restivo.

For different subsystems, a variety of options were considered and scored on relevant criteria. It is important to note that the first ranking choice was not always chosen, as it often became clearer during the design process that other options were more viable in terms of cost or manufacturability. For instance, we elected to use aluminosilicate ceramic fiber for the insulation instead of calcium silicate, as the former is commonly available in sheets and blankets that are very easy to cut and shape. Another example would be the grips, where we had to design and machine custom threaded grips due to the inability of collets to grip specimens under tensile load.

	TARGET	DESIGN IDEAS							
	or								
CRITERIA	FACTOR	1 = Baseline	Box		Tube		Sphere		
Time – Design	3	3		3		3		4	
Time – Build	4	4		4		6		10	
Time – Test	2	2		2		2		2	
<b>Time weighting</b>	<b>15</b>		<b>15</b>		<b>15.00</b>		<b>17.50</b>		<b>24.17</b>
Cost – Prototype	\$ 75.00	\$ 75.00		\$ 75.00		\$ 125.00		\$ 125.00	
Cost – Production	\$ 100.00	\$ 100.00		\$ 100.00		\$ 150.00		\$ 150.00	
<b>Cost weighting</b>	<b>15</b>		<b>15</b>		<b>15.00</b>		<b>23.75</b>		<b>23.75</b>
Weight	20	3	60	3	60	3	60	3	60
Size	15	3	45	3	45	3	45	4	60
Ease of Installation	30	3	90	5	150	4	120	1	30
Ease of Storage	5	3	15	5	25	4	20	2	10
	<b>TOTAL</b>		<b>210.0</b>		<b>280.0</b>		<b>233.8</b>		<b>142.1</b>
	<b>RANK</b>		<b>3.0</b>		<b>1.0</b>		<b>2.0</b>		<b>4.0</b>
	<b>% MAX</b>		<b>75.0%</b>		<b>100.0%</b>		<b>83.5%</b>		<b>50.7%</b>
	<b>MAX</b>		<b>280.0</b>						

Figure 76: Detailed scoring matrix showing the considered options for the chamber geometry.

CRITERIA	TARGET	DESIGN IDEAS									
	FACTOR	Baseline	S2 Glass Fibre	Mineral Fibre	Calcium Silicate	HT Glass Cellular	Perlite	Ceramic Fibre	Thermal Cements		
Time – Design	8	8	10	10	10	10	10	10	10	10	
Time – Build	8	8	4	7	12	6	8	4	9		
Time – Test	8	8	10	10	10	10	10	10	10		
<b>Time weighting</b>	5	5	5.00	5.63	6.67	5.42	5.83	5.00	6.04		
Cost – Prototype	\$ 100.00	\$100.00	\$120.00	\$80.00	\$80.00	\$90.00	\$80.00	\$130.00	\$50.00		
Cost – Production	\$ 100.00	\$100.00	\$120.00	\$80.00	\$80.00	\$90.00	\$80.00	\$130.00	\$50.00		
<b>Cost weighting</b>	5	5	6.00	4.00	4.00	4.50	4.00	6.50	2.50		
Weight	5	4	20	4	20	3	15	4	20	1	
Cost to Produce	5	4	20	2	10	3.5	17.5	3	15	3	
Time to Produce	5	4	20	4	20	4	20	4	20	4	
Size	5	4	20	4	20	3	15	4	20	2.5	
Thermal Resistance	35	4	140	5	175	5	175	4	140	5	
Ease of shaping	8	4	32	4	32	5	40	0	0	0	
Shape Holding (firmness)	8	4	32	2	16	2	16	5	40	4	
Max. Temperature	19	4	76	4	76	3	57	3.5	66.5	1	
<b>TOTAL</b>		360.0	368.0	365.9	345.8	266.1	277.7	364.5	183.0		
<b>RANK</b>		4.0	1.0	2.0	5.0	7.0	6.0	3.0	8.0		
<b>% MAX</b>		97.8%	100.0%	99.4%	94.0%	72.3%	75.5%	99.0%	49.7%		
<b>MAX</b>		368.0									

Figure 77: Detailed scoring matrix showing the considered options for insulation materials.

CRITERIA	TARGET	DESIGN IDEAS					
	FACTOR	Baseline	Resistive - Parallel	Resistive - Waved	Resistive - Helix	Radiative	
Time – Design	10	10	8	10	16	10	
Time – Build	10	10	5	8	14	20	
Time – Test	15	15	15	15	15	15	
<b>Time weighting</b>	5	5	3.83	4.67	6.67	6.67	
Cost – Prototype	\$ 100.00	\$100.00	\$ 50.00	\$70.00	\$90.00	\$ 300.00	
Cost – Production	\$ 100.00	\$100.00	\$ 50.00	\$70.00	\$90.00	\$ 300.00	
<b>Cost weighting</b>	10	10	5.00	7.00	9.00	30.00	
Max. Temperature	15	4	60	4	60	4	75
Heat Transfer	30	4	120	3	90	4	150
Shape Manipulation	15	4	60	4	60	4	75
Power Controllability	15	4	60	5	75	5	45
<b>TOTAL</b>		300.0	291.2	318.3	329.3	263.3	
<b>RANK</b>		3.0	4.0	2.0	1.0	5.0	
<b>% MAX</b>		91.1%	88.4%	96.7%	100.0%	80.0%	
<b>MAX</b>		329.3					

Figure 78: Detailed scoring matrix showing the considered options for the heating elements.

	TARGET or FACTOR	DESIGN IDEAS											
CRITERIA		1 = Baseline	Collet - Wide		Collet - Narrow		Chuck - Wide		Chuck - Narrow		Grip		
Time - Design	5	5	5	5	6	5	6	5	6	10			
Time - Build	5	5	5	5	6	5	6	5	6	10			
Time - Test	5	5	1	1	1	1	1	1	1	1			
Time weighting	5	5	3.67	3.67	4.33	4.33	3.67	3.67	4.33	7.00			
Cost - Prototype	\$ 80.00	\$ 80.00	\$ 80.00	\$ 60.00	\$ 140.00	\$ 140.00	\$ 120.00	\$ 120.00	\$ 150.00	\$ 150.00			
Cost - Production	\$ 80.00	\$ 80.00	\$ 80.00	\$ 60.00	\$ 140.00	\$ 140.00	\$ 120.00	\$ 120.00	\$ 150.00	\$ 150.00			
Cost weighting	5	5	5.00	3.75	8.75	8.75	7.50	7.50	9.38	9.38			
Weight	10	4	40	4	40	5	50	1	10	2	20	1	10
Load Distribution	40	4	160	5	200	5	200	4	160	4	160	1	40
Ease of Specimen Replacement	10	4	40	3	30	3	30	4	40	4	40	5	50
Heat Loss	10	4	40	3	30	5	50	3	30	5	50	3	30
Reliability	20	4	80	5	100	3	60	4	80	2	40	2	40
	TOTAL		360.0		401.3		391.9		317.6		308.2		163.6
	RANK		3.0		1.0		2.0		4.0		5.0		6.0
	% MAX		89.7%		100.0%		97.7%		79.1%		76.8%		40.8%
	MAX		401.3										

Figure 79: Detailed scoring matrix showing the considered options for the specimen fixturing.

# Appendix F: Project Timelines

Provided below are Gantt charts and a task dependency flowchart, which were used to organize and manage the tasks and timelines for this project. The Gantt charts are, in order: an initial tentative chart for the year, and revised versions for the Winter Quarter and Spring Quarter that better reflected expectations for milestones based on our progress.

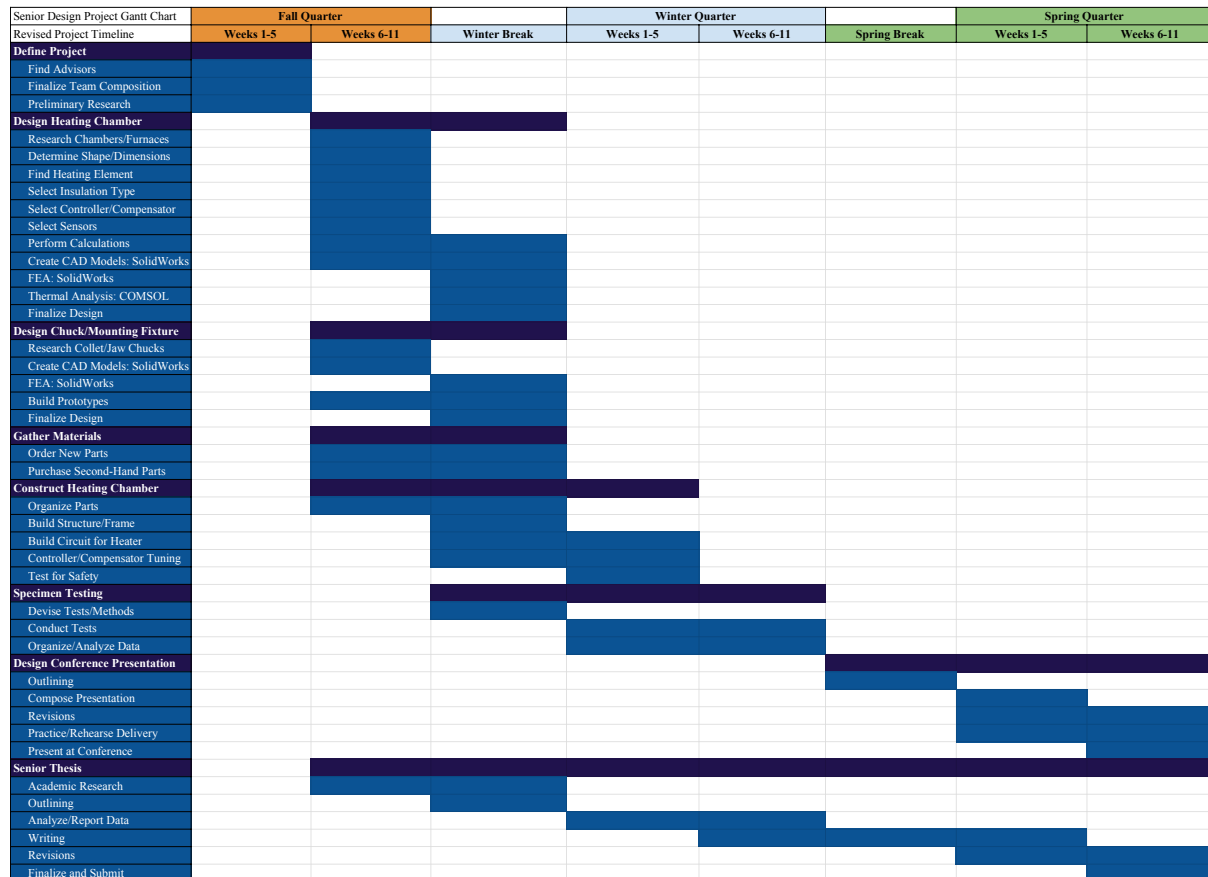


Figure 80: Initial Gantt chart showing project timeline and tasks for the duration of the project.

Senior Design WINTER Gantt Chart	Winter Break	Weeks 1-2	Weeks 3-4	Weeks 5-6	Weeks 7-8	Weeks 9-10	Finals Week
<b>Environment Chamber</b>							
Order Metal Stock							
Order Heating Elements							
Order Insulation							
Order Temp. Controller							
Order Misc. Parts (Adhesive, Wires, Fasteners, etc.)							
Redo Calculations for Revised Design							
Revise CAD Models: SolidWorks							
Create Technical Drawings							
Redo FEA: SolidWorks							
Finalize Design							
<b>Chuck/Mounting Fixture</b>							
Buy Collets							
Acquire or Make Tool Holder/Adapters							
<b>Assemble Heating Chamber</b>							
Build Structure/Frame							
Build Heating Circuitry							
Program Temp. Controller							
Test for Safety							
<b>Specimen Testing</b>							
Devise Tests/Methods							
Conduct Tensile/Basic Tests							
Organize/Analyze Data							
<b>Senior Thesis</b>							
Outlining							
Analyze/Report Data							
Writing							

Figure 81: Revised Gantt chart for the winter quarter.

Senior Design - Spring Gantt Chart	Spring Quarter											
SMA Testing / Environ. Chamber	Spring Break	Week 1	Week 2	Week 3	Week 4	Week 5	Week 6	Week 7	Week 8	Week 9	Week 10	Finals Week
<b>Gather Final Materials</b>												
Heating System Components												
Misc. Assembly Components												
<b>Finish Building Chamber</b>												
Weld Structure/Frame												
Weld Base/Stand												
Build Circuit for Heater												
Validate Performance/Safety												
<b>Specimen Testing</b>												
Conduct Tests												
Organize/Analyze Data												
<b>Design Conference Presentation</b>												
Outlining												
Compose Presentation												
Revisions												
Practice/Rehearse Delivery												
Present at Conference												
<b>Senior Thesis</b>												
Continue Academic Research												
Outlining												
Analyze/Report Data												
Writing/Revisions/Feedback												
Finalize and Submit												
<b>Course Assignments</b>												
Thesis TOC/Intro Drawings												
Resume + Community Service												
Experimental Protocol + PDS												
Societal/Environmental Impact												
Design Conference Presentation												
Thesis Draft												
Patent Search OR Business Plan												
Surveys/Questionnaires												
Open House + Hardware												
Thesis Final Version												

Figure 82: Revised Gantt chart for the spring quarter, also showing key assignments and Senior Design course-related deadlines.

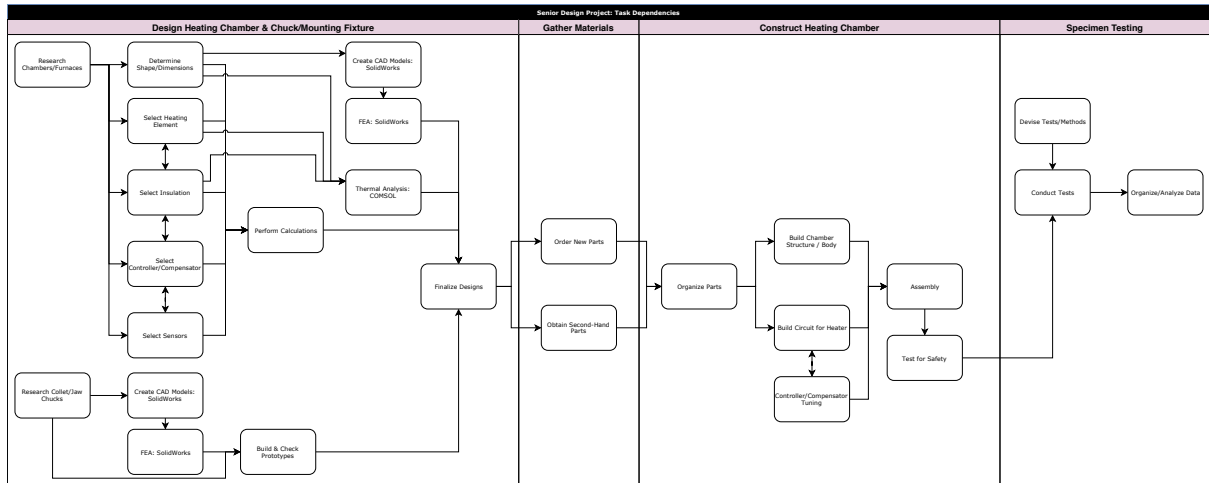


Figure 83: Task dependency flowchart used to aid in organizing order and progression of tasks for the project.

## Appendix G: SMA Tensile Testing

Prior to completing the chamber, room temperature tensile testing was performed on the Cu-Al-Ni SMA. The 12 in. long specimen was cut into 2 in., 4 in., and 6 in. sections so that force vs. displacements plots could be created for each. These plots were necessary so that a new plot that used the inverse slopes and original length-to-area ratio of each specimen could be made. Optical extensometry was not used, because the chamber does not feature a window, resulting in the need to refine the data recorded by the test machine to account for load-train displacement.

Once tensile test data was obtained for each length, it was refined to eliminate any load-train displacement (in the crosshead, grips/adapters, etc.) that was picked up in measurements [33]. Doing so was possible since the displacements of the mechanical components are reversible and were assumed to be linear-elastic [33]. Furthermore, the entire displacement was modeled with the following equation:

$$\Delta x_{total} = \Delta x_{specimen} + \Delta x_{machine} = \frac{1}{E} \left( \frac{\Delta F L_o}{A_o} \right) + \frac{\Delta F}{k_{machine}} \quad (13)$$

where  $E$  is the SMA's elastic modulus,  $F$  is the force,  $L_o$  is the initial length of the specimen,  $A_o$  is the the specimens original cross-sectional area, and  $k_{machine}$  is the machines spring constant [34]. This equation is in the slope-intercept form of  $y = mx + b$ , where  $y$  is  $\frac{\Delta x_{total}}{\Delta F}$ ,  $x$  is  $\frac{L_o}{A_o}$  and the slope is  $\frac{1}{E}$  [34]. With this information, we were able to determine the specimen's elastic modulus.



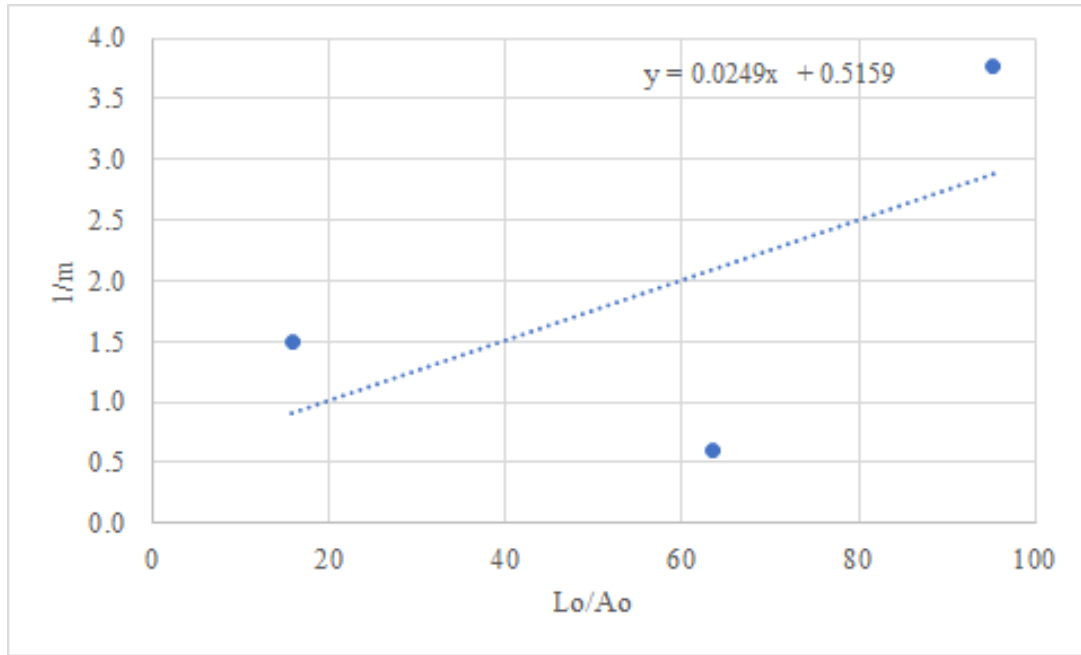


Figure 84:  $\frac{L_o}{A_o}$  vs.  $\frac{1}{m}$  plot of the refined data from room temperature tensile testing, used to determine the elastic modulus of the SMA.

We were told by the supplier that the specimen was a Cu-based alloy, meaning the expected elastic modulus might be within the realm of 97-150 GPa [35] . After obtaining the slope of the refined plot (0.0249) and taking its inverse, the elastic modulus was calculated to be 40.16 GPa. This indicated that the alloy consisted of copper and other more ductile metals.

## Appendix H: Using the Controller

The key processes for setting up the controller for the heating tests conducted for this project, specifically defining a temperature setpoint and modifying PID gains, are given step-by-step below. Full details on these processes, and instructions on how to perform more complex operations with the controller can be found in the Omega CN1500 Series Multi-Zone Ramp & Soak Controller User's Guide [36]. The print copy of this guide supplied with the controller will be provided to the Materials Laboratory along with the environment chamber, thermocouples, and power supply. Please note, the controller has a security passcode that needs to be entered using the front panel keys; this passcode is 3254.

Users may choose any or all of the 4 controller channels available, as needed for the desired application. Channels can be set-up for simple start-stop, more complex ramp-soak, or indefinite-hold-at-setpoint (what we used) processes.

### Programming a Set-point Temperature

1. Verify which controller(s) is receiving input by checking the connectors on the backside. Refer to page 24 of the user guide [36] for connector numbers and their corresponding controller.
2. Press the "CTR SEL" button until the desired controller number appears.
3. Once the desired controller number is on the screen, maintain the "CTR SEL" button pressed and simultaneously press the "SETPT" button. The screen will now accept a temperature set-point value in degrees Celsius.
4. The "SETPT" button has left & right arrows below it. These serve to adjust the digit that is desired.
5. The "RUN/STP" button has up & down arrows below it to indicate that a value can be incremented by pressing this. In order to increase the number, press and hold this button until the desired number appears. Please note, if pressed and immediately released, the value will decrease.

6. Once the correct number is entered, press the “CTR SEL” to save the set-point.
7. This controller is now ready.

## PID Tuning

1. Verify which controller(s) is receiving input by checking the connectors on the back-side. Refer to page 24 of the user guide [36] for connector numbers and their corresponding controller.
2. Press the “CTR SEL” button until the desired controller number appears on the screen.
3. Hold the “CTR SEL” button until the unit displays “EntEr PASSCOdE”. Enter the passcode to proceed.
4. The “CTR SEL” can be pressed to choose the mode. Press the button until “tun-inG” is on the screen.
5. Press the “PROG” button. Afterwards, select the desired controller (Cntr 1, 2, etc.) by using the “RUN/STP” button.
6. The proportional band (equivalent to proportional gain) will be the first adjustable parameter. Set the value by using the “SETPT” and “RUN/STP” buttons. Save the value by pressing “PROG”.
7. “Reset” will be the next adjustable parameter and corresponds to the integral gain. Adjust accordingly. Save the value by pressing “PROG”.
8. “Rate” will be the last adjustable parameter and corresponds to the derivative gain. Adjust accordingly. Save the value by pressing “PROG”.

The controller has been fitted with an emergency shutoff switch. To begin heating, rotate it clockwise to disengage, thus closing the circuit between the controller and power supply. Afterwards, flip the power switch on the power supply to its “on” position. this switch is circled in blue in Figure 85. At any time the user can depress the shutoff switch to break the circuit, thus causing the power supply to send 0 W to the chamber’s heating elements.

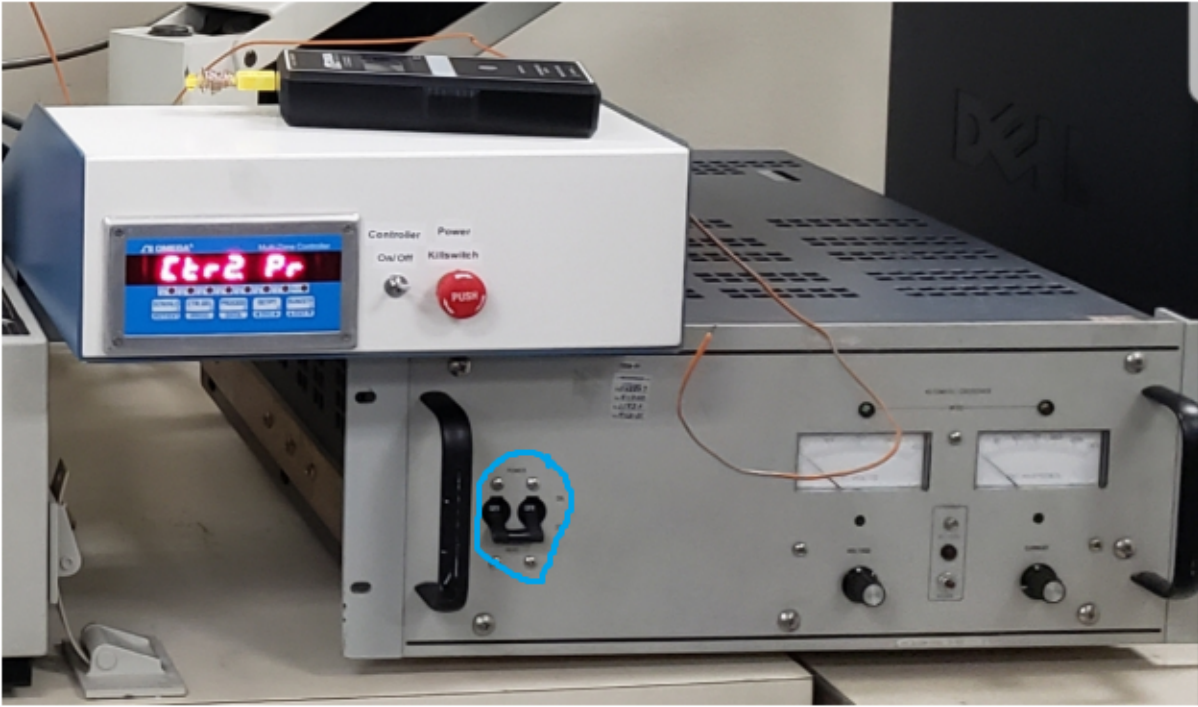



Figure 85: Controller and power supply switched on but not supplying power to the chamber.

# Appendix I: Design Conference Presentation Slides

SANTA CLARA UNIVERSITY




## Environment Chamber for Shape Memory Alloy Testing

**Luis Acevedo, Joseph Bodo, Nick Fernandes**  
Undergraduate Design Project, Mechanical Engineering

www.scu.edu Department of Civil & Environmental Engineering Santa Clara University

SANTA CLARA UNIVERSITY


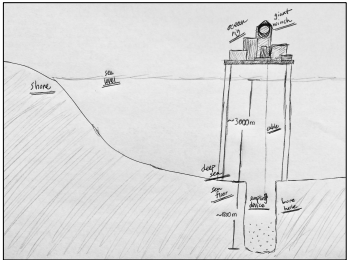


## Overview

1. Project Description & Background
2. Ideation and Design Stages
3. Design Validation
4. Implementation: Manufacture and Assembly
5. Future Work

Santa Clara University

SANTA CLARA UNIVERSITY

## Motivations

I. Searching for Life Below the Seafloor

Santa Clara University

SANTA CLARA UNIVERSITY




## Key Project Participants & Roles

- = **Dr. Geoff Wheat**
  - Marine geochemist heading the project
- = **Dr. Christopher Kitts**
  - Director of SCU Robotics Systems Laboratory
- = **Rachel Stolzman**
  - Graduate student designing a water collection device actuated by a shape memory alloy (SMA)
- = **This Team**
  - Studying novel SMA blends to assist in the design of the sampling device

Santa Clara University

SANTA CLARA UNIVERSITY




## Background: Shape Memory Alloys

- = Alloys revert to predetermined shape
  - Shape set during manufacture, can be altered
- = Inelastic deformation can be recovered by heating and/or unloading
  - Activation/transition temperature
- = Shape recovery occurs due to transition between microstructure phases

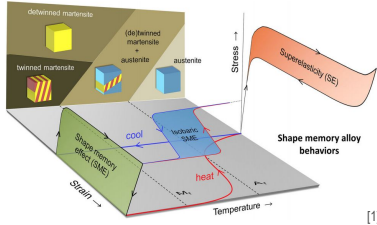
[1][2][3]

Santa Clara University

SANTA CLARA UNIVERSITY



## Background: Shape Recovery



Shape memory alloy behaviors

[1]

Santa Clara University

SANTA CLARA UNIVERSITY



**Motivations**

II. Provide a Research Tool for SCU

- = Expand scope of materials science research at SCU
  - Tensile tests can only be conducted at room temperature
    - = Limits scope of materials testing, cannot study deformation behavior at elevated temperatures
  - Different capacity load cells on available machines
    - = Each testing machine in the Materials Science Laboratory has different testing ranges/capabilities
  - = Would need to buy environment chambers for all machines, or only one and be limited in testing capability



SANTA CLARA UNIVERSITY




**Objective**

A Solution to Address Both Motivations

- = Design and build an environment chamber
  - Chamber will be compatible with tensile testing machines in the Materials Science Laboratory
    - = Eliminate need to buy multiple environment chambers
    - = Provides School of Engineering with a convenient, low-cost tool for research
  - Allow for material testing and studies at elevated temperatures
    - = Can determine transition temperature of SMA
    - = Can observe deformation and shape recovery
    - = Measure force exerted by shape memory effect




SANTA CLARA UNIVERSITY



**Design Specifications & Constraints**

- = Temperature
  - Max. operating temp. = 250°C
  - Max. temp. variation along specimen = ±5°C
  - Safe exterior wall temp. = 40°C [4]
- = Circuitry
  - Max. power consumption: 1kW
  - Max. voltage through circuit: 50V
- = Shape & Weight
  - Outer diameter: 10 in.
  - Height: 24 in.
  - Max. weight = 60 lb.



SANTA CLARA UNIVERSITY




**Chamber Design**

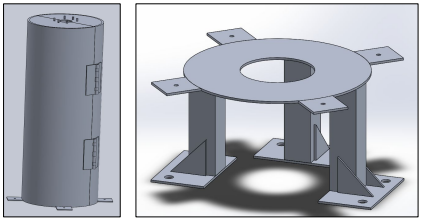





SANTA CLARA UNIVERSITY



**Chamber Fixturing**






SANTA CLARA UNIVERSITY



**Assembly Components & Materials**

- = Chamber Body
  - 6061 Al tubes and flat plates
- = Thermal Insulation
  - Aluminosilicate ceramic fiber blanket
  - Ceramic standoffs and tubing
  - Silicone rubber sheets
- = Heating
  - Vitreous enameled power resistors
  - PID temperature controller
  - DC power supply





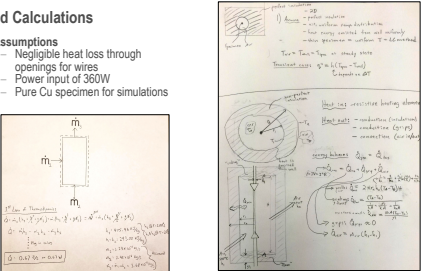
**SANTA CLARA UNIVERSITY**

### Steady-State Thermal Analysis

**Hand Calculations**

**Assumptions**

- Negligible heat loss through openings for wires
- Power input of 360W
- Pure Cu specimen for simulations



**SANTA CLARA UNIVERSITY**

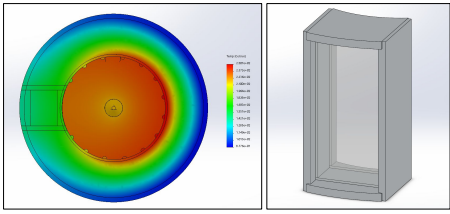
### SolidWorks Thermal Simulations

- = 36V / 30A max
- = (6x) 225W heating elements
- = Energy balance (below) relates power input to temperature
- = Natural convection - iterative process

Unit	Equation	Value
Power Input	$P = IV$	360 W
Heat Transfer Coefficient	$h = \frac{k}{L} \ln\left(\frac{r_2}{r_1}\right)$	111.08 W/m <sup>2</sup> ·K
Nusselt Number	$Nu = \frac{hD}{k_f}$	111.08
Prandtl Number	$Pr = \frac{\mu c_p}{k_f}$	0.707
Rayleigh Number	$Ra = \frac{g\beta(T_w - T_\infty)L^3}{\nu\alpha}$	1.11e+05
Grashof Number	$Gr = \frac{g\beta(T_w - T_\infty)L^3}{\nu^2}$	1.11e+05

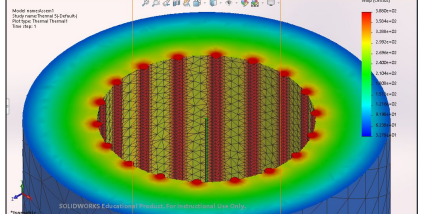
$$P = IV = I^2 R = \frac{HkA_s(T_w - T_2)}{L} = \frac{2\pi r_2(T_A - T_B)H}{r_1 r_2} + \frac{1}{r_1^2} \ln\left(\frac{r_2}{r_1}\right) + \frac{1}{r_2} + \frac{2(T_A - T_B)}{h_1 A + h_2 A} + \dot{m}(h_{hot} - h_{cold})$$

**SANTA CLARA UNIVERSITY**



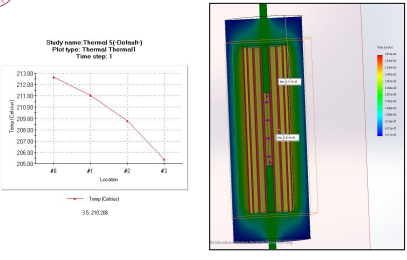
**Simulation Results: With a Window**

**SANTA CLARA UNIVERSITY**



**Simulation Results (Without Window)**

**SANTA CLARA UNIVERSITY**



**Simulation Results: SMA Wire Specimen**

**SANTA CLARA UNIVERSITY**

### Manufacturing Processes

- = Bandsaw & Waterjet Cutting
- = Milling
- = Drilling
- = Welding
- = Grinding, Sanding, Polishing
- = Wiring, Soldering

SANTA CLARA UNIVERSITY




### Cutting & Machining Parts





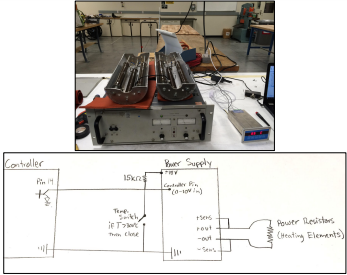
SANTA CLARA UNIVERSITY

### Heating Elements: Power Resistors







SANTA CLARA UNIVERSITY

### Temperature Control System



The schematic diagram shows a control loop. A 'Controller' is connected to a 'Power Supply' (150W) and a 'Power Resistor (Heating Element)'. The power supply is connected to the resistor. The resistor is connected to a 'Temperature Sensor' (RTD) which provides feedback to the controller. The controller is also connected to a 'Power Supply' (150W) and a 'Power Resistor (Heating Element)'.

SANTA CLARA UNIVERSITY

### Chamber Assembly







SANTA CLARA UNIVERSITY

### Performance Validation

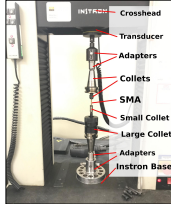


- = Ran heating test to 200°C interior temperature
  - Time to reach setpoint was 32 min
  - Exterior wall temp. = 21°C
- = Ongoing process
  - Will be conducting further testing to verify operating temp., steady-state error, exterior wall temp.

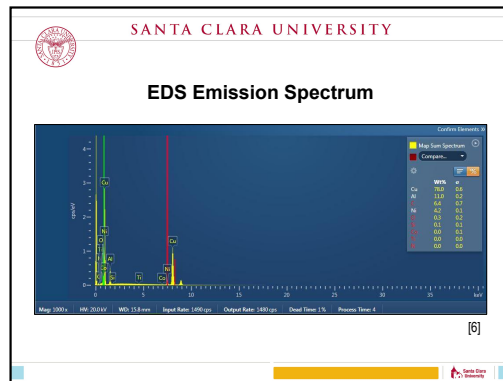
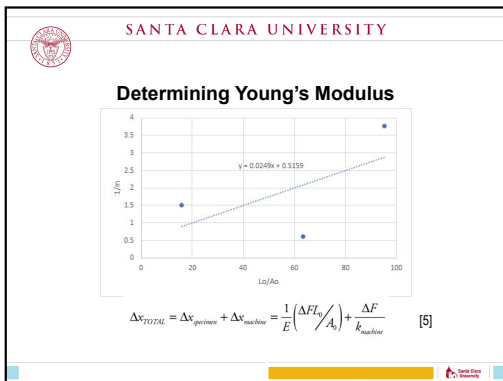
SANTA CLARA UNIVERSITY

### Specimen Tests Performed So Far

- = Tensile tests on various lengths
  - 2 in., 4 in., and 6 in. specimen sections tested
- = Load vs. Displacement plots [5]
  - Data refined to account for load-train displacement
  - Elastic modulus = ~40 GPa
- = Compositional Analysis [6]
  - Identified alloy composition to be 71.9at% Cu, 23.9at% Al, 4.2at% Ni
  - Working on imaging of microstructures





SANTA CLARA UNIVERSITY

### Approximate Cost to Produce

Undergraduate Programs Senior Design Grant	\$1500	
Approximate Costs	Paid from Budget	Sponsorship & Donations
Materials & Components	\$890	\$400
Manufacturing	\$390	\$800
Cost to Produce	\$2500	

SANTA CLARA UNIVERSITY

### Future Work

- = Performance Validation
- = Shape Memory Alloy Tests

SANTA CLARA UNIVERSITY

### Shape Memory Alloy Testing

- = Finish assembling chamber base
- = Thread ends of specimen so they can be screwed into custom grips
  - Properly secure specimens during tensile testing
- = Assess suitability of SMA blends for use in water sampling device
  - Verify alloy transition temperatures
  - Determine max. recoverable strain
  - Measure force exerted by shape memory effect

SANTA CLARA UNIVERSITY

### References

- P. Chowdhury, "Frontiers of Theoretical Research on Shape Memory Alloys: A General Overview," *Shape Memory and Superelasticity*, vol. 4, no. 1, pp. 26-40, Mar. 2018. doi: 10.1007/s40830-018-0161-4. [Accessed: 1 Oct. 2018].
- R. Deshpande, "A look into Cu-based shape memory alloys: Present scenario and future prospects," *Journal of Materials Research*, vol. 29, no. 16, pp. 1681-1698, Aug. 2014. doi: 10.1537/jmr.2014.169. [Accessed: 23 Oct. 2016].
- M. Bagepouz, A. Shokoufar, A. Zohraseni, and A. F. Bahelgerdy, "Effect of Severe Plastic Deformation on Shape Memory and Mechanical Properties of Nanostructured Cu-Zn-Al Alloy," *Journal of Nano- and Electronic Physics*, vol. 9, no. 1, pp. 01008-1-01008-6, Feb. 2017. doi: 10.21272/jnep.9(1)01008. [Accessed: 5 Nov. 2018].
- E. Unger and K. Stroud, "A New Approach to Defining Human Touch Temperature Standards," in *Proc. of the 40th Int. Conf. on Environmental Systems*, 11-15 July 2010, Barcelona, Spain [Online], doi: 10.2514/6.2010-6310. [Accessed: 14 Nov. 2018].
- R. Marks, "Appendix VI: Refining Uniaxial Tensile Test Data when Total Load-Train Displacement is Measured," *MSCof FEA Lab Handout*. [Accessed: 17 Oct. 2018].
- Compositional analyses by A. Kim, S. Snyder, R. Marks, J. Taylor, and R. Konrath

**SANTA CLARA UNIVERSITY**




## Acknowledgements

<b>Project Advisors</b>	<b>SCU School of Engineering</b>
Dr. Robert Marks	Dr. Parithea Soghehrband
Dr. Christopher Kitts	Dr. Tim Hight
<b>SMA Research Project</b>	Dr. Tony Restivo
Dr. Geoff Wheat	<b>SCU Machine Shop</b>
Rachel Stolzman	Don MacCubbin
Ann McGuire	Calvin Sellers
<b>SCU Center for Nanostructures</b>	Emily Takimoto
Dr. Ashley Kim	Bethany Hsu
Shaun Snyder	
Jake Taylor	
Ryan Konrath	




**SANTA CLARA UNIVERSITY**



# Thank You.

# Questions?

